



**HAL**  
open science

# Contribution to the development of a methodology to analyse the fracture phenomena in encapsulated components

Francois Leblanc

► **To cite this version:**

Francois Leblanc. Contribution to the development of a methodology to analyse the fracture phenomena in encapsulated components. Mechanics [physics.med-ph]. Université de Valenciennes et du Hainaut-Cambresis, 2004. English. NNT: . tel-00008716

**HAL Id: tel-00008716**

**<https://theses.hal.science/tel-00008716>**

Submitted on 7 Mar 2005

**HAL** is a multi-disciplinary open access archive for the deposit and dissemination of scientific research documents, whether they are published or not. The documents may come from teaching and research institutions in France or abroad, or from public or private research centers.

L'archive ouverte pluridisciplinaire **HAL**, est destinée au dépôt et à la diffusion de documents scientifiques de niveau recherche, publiés ou non, émanant des établissements d'enseignement et de recherche français ou étrangers, des laboratoires publics ou privés.

**THESE  
PRESENTEE A  
L'UNIVERSITE DE VALENCIENNES  
ET DU HAINAUT-CAMBRESIS**

**EN VUE DE L'OBTENTION D'UN  
DOCTORAT EN GENIE MECANIQUE**

**PAR**

**FRANCOIS LEBLANC**

# **CONTRIBUTION TO A METHODOLOGY FOR THE ANALYSIS OF FRACTURE PHENOMENA IN ENCAPSULATED COMPONENTS**

Le Mardi 21 Décembre 2004, devant le jury composé de:

Rapporteur	P. Davies, Habilité à Diriger des Recherches, IFREMER, Brest
Rapporteur	C. Rey, Professeur, LMT, Cachan
Examineur	B. Peseux, Professeur, Ecole Centrale de Nantes
Examineur	D. Coutellier, Professeur, ENSIAME, Valenciennes
Examineur	A. Zimmermann, Docteur, Robert Bosch GmbH, Stuttgart, Germany
Examineur	M. Watremez, Maître de conférence, ENSIAME, Valenciennes



---

# BOSCH

Corporate Research and Development  
Department Plastics Engineering  
CAE Insulation Materials

## CONTRIBUTION TO A METHODOLOGY FOR THE ANALYSIS OF FRACTURE PHENOMENA IN ENCAPSULATED COMPONENTS



LAMIH  
LABORATOIRE  
D'AUTOMATIQUE  
DE MECANIQUE ET  
D'INFORMATIQUE  
INDUSTRIELLES  
ET HUMAINES

UMR CNRS 8530

---

---

---

---

## I/ Acknowledgement

*The following study was realised in the framework of my PhD thesis. This work was a cooperation between the company Robert Bosch GmbH, corporate research and development, department plastics engineering in Waiblingen, Germany, and the L.A.M.I.H. (Laboratoire d'automatique, de mécanique et d'informatique industrielles et humaines), UMR CNRS 8530, University of Valenciennes, France.*

*My gratitude goes to Prof. Daniel Coutellier and Dr. André Zimmermann for the supervision of this work and the continuous encouragement.*

*I am grateful to Dr. Wilfried Ihl, head of the department plastic engineering, to Dr. Wolfgang Endres, former group leader, to Dr. Markus Mužic, current group leader, and to Dr. Peter Sprafke, former supervisor, for the highly interesting subject and for having placed their confidence in me.*

*I am also grateful to Mr. Alain Lecocq for the opportunity of doing my first industrial placement in the company.*

*I would also like to acknowledge the whole group of insulation materials for the possibility to carry out the research and for providing all the necessary materials to conduct the experiments as well as for the pleasant work atmosphere.*

*Valuable comments and suggestions were contributed by Dr. Olaf Wittler, Mr. Nicolas Depoorter and Mr. Julien Roger. Discussions with Prof. Dr. Dominique Leguillon are appreciated.*

*I would like to address a special thank to the members of the jury.*

*Finally, I wish to thank my friends and I would like to express thanks to my family for their support and encouragement.*

*Stuttgart*

François Leblanc



---

## II/ Abstract

The work focuses on potting materials for electronic components. A methodology to analyse the behaviour of cracks initiated in homogeneous materials or at the interface between different materials is addressed. An experimental procedure is described in order to measure the critical stress intensity factor of a homogeneous material. This procedure is then used to compare the crack behaviour in a bimaterial structure and to determine the validity of the results. Hereafter a method is proposed to determine crack growth under subcritical loading conditions. In the case of a crack at the interface of bimaterials, a methodology has been developed to measure the energy release rate necessary to let the crack propagate. With the help of numerical simulations, the corresponding stress intensity factors are computed as well as the resulting mixed mode angle. The whole work realised experimentally and the developed numerical simulations allow us to propose a methodology to analyse the behaviour of a crack placed in a multi-material structure under thermo-mechanical loads.

**Keywords:** energy release rate, stress intensity factors, fracture toughness, interface, mixed mode angle, finite element method

## III/ Zusammenfassung

Die vorliegende Arbeit befasst sich mit Vergussmassen für elektronische Erzeugnisse. Eine Vorgehensweise wird vorgeschlagen, um das Verhalten von initiierten Rissen in homogenen Materialien oder entlang der Grenzschicht zwischen verschiedenen Materialien zu analysieren. Ein experimenteller Verfahrensschritt wird beschrieben, um den kritischen Spannungsintensitätsfaktor von homogenen Materialien zu messen. Dann wird dieser Verfahrensschritt benutzt, um das Rissverhalten in verschiedenen Materialien zu vergleichen und um das Ergebnisskonfidenzintervall festzulegen. Danach wird eine Methode vorgeschlagen, um das Risswachstum des betrachteten Materials unter subkritischer Belastung festzulegen. Im Fall eines Grenzschichtrisses wird eine Vorgehensweise entwickelt, um die Energiefreisetzungsrates zu messen, die benötigt wird, um den Riss sich ausbreiten zu lassen. Mit Hilfe von numerischen Simulationen werden die entsprechenden Spannungsintensitätsfaktoren und die Modusmischungswinkel ermittelt. Die komplette experimentelle Arbeit und die entwickelte numerische Simulationen führen zu einer Methodologie, um das Verhalten von einem Riss Verbundwerkstoffen und Bauteilen unter thermischen und mechanischen Belastungen zu beurteilen.

**Schlüsselwörter:** Energiefreisetzungsrates, Spannungsintensitätsfaktoren, Bruchzähigkeit, Grenzschicht, Modusmischungswinkel, Finite Elemente Methode

---

## IV/ Résumé

*Ce travail s'articule autour de l'étude de matériaux coulés pour des composants électroniques. Une méthodologie est proposée pour analyser le comportement de fissures initiées dans des matériaux homogènes ou à l'interface entre différents matériaux. Une procédure expérimentale est décrite afin de mesurer le facteur d'intensité de contrainte critique d'un matériau homogène. Cette procédure est ensuite appliquée dans la comparaison du comportement d'une fissure d'un bimatériau et à la détermination du degré de validité des résultats. Une méthode est ensuite proposée pour déterminer la propagation de fissures dans les différents matériaux sous des chargements sous-critiques. Dans le cas d'une fissure à l'interface de bimatériaux, une méthodologie a été développée pour mesurer le taux de restitution d'énergie nécessaire à la propagation de la fissure. Les facteurs d'intensité de contraintes correspondants sont calculés à l'aide de simulations numériques, ainsi que l'angle de mode mixte résultant. L'ensemble des travaux expérimentaux réalisés et des simulations numériques développées permet de proposer une méthodologie d'analyse du comportement d'une fissure située au sein d'un composant multimatériau sollicité sous chargement thermo-mécanique.*

**Mots clés:** taux de restitution d'énergie, facteurs d'intensité de contraintes, ténacité, interface, angle de mode mixte, méthode éléments finis

---

## V/ Table of contents

<i>Acknowledgement</i>	<i>i</i>
<i>Abstract</i>	<i>iii</i>
<i>Zusammenfassung</i>	<i>iii</i>
<i>Résumé</i>	<i>iv</i>
<i>Table of contents</i>	<i>v</i>
<i>List of symbols</i>	<i>viii</i>
Latin symbols	viii
Greek symbols	ix
Acronyms	ix
<b><i>I Introduction</i></b>	<b><i>2</i></b>
<b><i>II/ Presentation of the concepts in fracture mechanics</i></b>	<b><i>6</i></b>
<b><i>II.A/ Introduction</i></b>	<b><i>6</i></b>
<b><i>II.B/ A history of fracture mechanics' development</i></b>	<b><i>7</i></b>
II.B.1/ Griffith fracture mechanics	7
II.B.2/ Energy release rate	9
II.B.3/ Linear elastic fracture mechanics	12
II.B.4/ Elastic plastic fracture mechanics	16
II.B.5/ Crack propagation	20
II.B.6/ The R-curve	21
II.B.7/ Fatigue crack growth	22
II.B.8/ Creep and visco-elastic fracture	24
<b><i>II.C/ Conclusion</i></b>	<b><i>25</i></b>
<b><i>III/ Cracks between two dissimilar materials</i></b>	<b><i>28</i></b>
<b><i>III.A/ Introduction</i></b>	<b><i>28</i></b>
<b><i>III.B/ Overview of interfacial fracture mechanics</i></b>	<b><i>29</i></b>
III.B.1/ Presentation of different concepts	29
III.B.2/ Dundurs parameters	33
III.B.3/ Stress singularity	33
III.B.4/ Mixed mode	36
III.B.5/ Energy release rate	38
III.B.6/ Interface toughness curves	38
<b><i>III.C/ Interfacial fracture toughness tests</i></b>	<b><i>40</i></b>
III.A.1/ Most common tests	40
III.C.2/ Sandwich specimen	42
III.C.3/ Experimental determination of the Energy Release Rate	42
III.C.4/ About deflection and penetration	46
<b><i>III.D/ Conclusion</i></b>	<b><i>48</i></b>

---

<b>IV/</b>	<b><i>Numerical methods available for fracture mechanics analyses</i></b>	<b>50</b>
<b>IV.A/</b>	<b>Introduction</b>	<b>50</b>
<b>IV.B/</b>	<b>Finite Element Implementation</b>	<b>51</b>
IV.B.1/	Stiffness Derivative Formulation	51
IV.B.2/	Continuum approach	52
IV.B.3/	The domain integral method	52
IV.B.4/	Mesh design	53
IV.B.5/	Zencrack	54
IV.B.6/	Calculation of the Energy Release Rate	55
IV.B.7/	Alternatives Methods	58
<b>IV.C/</b>	<b>Conclusion</b>	<b>63</b>
<b>V/</b>	<b><i>Experimental and numerical methods</i></b>	<b>66</b>
<b>V.A/</b>	<b>Introduction</b>	<b>66</b>
<b>V.B/</b>	<b>Experimental work</b>	<b>67</b>
V.B.1/	Objectives	67
V.B.2/	Preparation of specimens	67
V.B.3/	Testing devices	68
<b>V.C/</b>	<b>Numerical modelling</b>	<b>80</b>
V.C.1/	Objectives	80
V.C.2/	Cracks in homogeneous materials	80
V.C.3/	Interfacial cracks	82
<b>V.D/</b>	<b>Statistical approach</b>	<b>86</b>
V.D.1/	objectives	86
V.D.2/	Weibull distribution	86
V.D.3/	Maximum likelihood	87
V.D.4/	Bootstrap method	87
<b>V.E/</b>	<b>Conclusion</b>	<b>89</b>
<b>VI/</b>	<b><i>Experimental results</i></b>	<b>92</b>
<b>VI.A/</b>	<b>Introduction</b>	<b>92</b>
<b>VI.B/</b>	<b>Homogeneous materials</b>	<b>93</b>
VI.B.1/	Fracture toughness as a function of crack length	93
VI.B.2/	Statistical analysis	94
VI.B.3/	Simulation	98
VI.B.4/	Subcritical crack growth	101
<b>VI.C/</b>	<b>Cracks between two different materials</b>	<b>106</b>
VI.C.1/	S3PB 10mm/2mm	106
VI.C.2/	S3PB 4mm/2mm	111
VI.C.3/	S3PB 2mm/2mm	112
VI.C.4/	Angle of 0°, 2mm/2mm	113
VI.C.5/	Angle of 0°, 4mm/2mm	114
VI.C.6/	Angle of 0°, 10mm/2mm	115
VI.C.7/	Angle of 15°, 10mm/2mm	116
VI.C.8/	Angle of 30°, 10mm/2mm	117
VI.C.9/	Angle of 45°, 10mm/2mm	118
VI.C.10/	Sensitivity analysis	119
<b>VI.D/</b>	<b>Interfacial fracture energy curve</b>	<b>121</b>

---

---

<b><i>VII/ Discussion</i></b>	<b><i>124</i></b>
<b><i>VII.A/ About the fracture toughness</i></b>	<b><i>124</i></b>
Location of the crack	124
Type of mesh	124
Material parameters	125
<b><i>VII.B/ About the interface investigation</i></b>	<b><i>127</i></b>
<b><i>VIII/ Conclusion and perspectives</i></b>	<b><i>132</i></b>
<b><i>References</i></b>	<b><i>136</i></b>

---

## VII/ List of symbols

### VI.A/Latin symbols

a	Crack length
A	Crack surface
$A_I$	Material parameter for a subcritical crack growth law
$A_f$	Material parameter for the Wöhler curve
$A_n$	Material parameter for Paris law
$A_u$	Axial stiffness of a beam
B	Thickness of the body or specimen or sample
$B_u$	Coupling bending of a beam
C	Compliance
$D_i$	$i=1,2,3$ Damage variable or bending rigidity of a beam
$D_{max}$	Maximal value for damage variable
$D_u$	Bending stiffness of a beam
$E_k$	High stiffness in compression
$E_i$	$i=1,2,3$ Interface stiffness
$E'$	Effective stiffness (Young's modulus)
G	Energy release rate (ERR)
$G_c$	Critical energy release rate
h	Dimension of a beam
I	Second moment of area for a beam
J	Rice contour integral
k	Generalised stress intensity factor
K	Stress intensity factor (SIF)
$K_{IC}$	Critical Stress Intensity Factor in mode I (Fracture toughness)
[K]	Stiffness matrix
$L_i$	$i=0,1$ Fixed length
M	Moment of an applied force
$n_I$	Exponent for a subcritical crack growth law
$n_f$	Exponent for the Wöhler line
$n_n$	Exponent for Paris law
P	Applied force or measured force
[P]	Nodal force vector
Q	Hydrostatic pressure
r	Distance of a point to the origin in cylindrical system
$r_k$	Radius of the K-annulus
$r_p$	Radius of the plastic zone at crack tip
R	Fracture resistance
t	Traction vector
$t_i$	Thickness of beam i
T	T-stress in the near-tip region of a crack
$T_t$	Tangential force
$T_n$	Normal force
u	Applied displacement or measured displacement
$u_n$	Normal displacement
$u_t$	Tangential displacement
[u]	nodal displacement vector
U	Total energy of the body or system
$U_k$	Kinetic energy

---

w	Strain energy density
W	Width of the specimen or body
$W_F$	External work done by external forces
$W_p$	Potential energy of the body
$W_s$	Surface energy
Y	Geometrical factor
$Y_i$	$i=1,2,3$ Damage energy release rate

## **VI.B/Greek symbols**

$\alpha$	Dundurs parameter or coefficient of thermal expansion
$\beta$	Dundurs parameter
$\gamma_p$	Plastic energy by unit surface area
$\gamma_s$	Surface energy by unit surface area
$\Gamma$	Contour surrounding the crack tip or interfacial fracture toughness
$\delta$	Applied displacement or measured displacement
$\delta_{ij}$	Kronecker symbol
$\delta(a)$	Crack tip opening displacement
$\varepsilon$	Strain or Dundurs parameter
$[\varepsilon_i]$	Strain tensor
$\theta$	Angle in a cylindrical system
$\kappa_i$	Constant depending on plane strain or plane stress conditions
$\lambda$	Stress singularity exponent
$\mu_i$	Shear modulus
$\nu$	Poisson ratio
$\xi$	Parameter depending on the geometry
$\sigma$	Stress
$\sigma_y$	Yield stress
$\varphi$	Solid angle
$\Phi$	Stored elastic strain energy
$\psi$	Mixed Mode Angle
$\omega$	Angle of a notch

## **VI.C/Acronyms**

ADCB	Asymmetric Double Cantilever Beam
A3PB	Asymmetric 3 Points Bending
AMDR	Area Method of Data Reduction
ASTM	American Society for Testing and Materials
CT	Compact Tension
ERR	Energy Release Rate
FEM	Finite Element Method
LEFM	Linear Elastic Fracture Mechanics
LGC	Large Geometry Changes
LSY	Large Scale Yielding
MMA	Mixed Mode Angle
SIF	Stress Intensity Factors
SCCB	Symmetric Centre Cracked Beam
SSY	Small Scale Yielding

---

---

---

# **Chapter I**

## INTRODUCTION

## I/ Introduction

Reliability of industrial devices is a question which becomes more and more sensitive, especially in automotive industry. In effect, electronic components are present in every car and under so many forms that taking the inventory becomes slowly an infinite listing. And the automotive industry is very affected by a lack of reliability of components. It can happen that failure of any component may lead to catastrophic effects, especially when this component is part of a safety system. And component manufacturers improve continuously their development process to offer the customers the insurance of the best product quality. That is why a step in this direction is the component reliability.

However, while increasing the safety, more and more electronic components are introduced which are in contact with aggressive media. A major problem which can occur when devices are subjected to high stress level is failure by cracking of a component. But before the occurrence of the complete failure, it is possible that a crack may be initiated. And when a crack is discovered, for instance during an inspection in the framework of a maintenance operation, the difficulty is to judge the criticality of this crack. It is possible that the crack affects adversely the functions realised by the component. The easiest solution is simply the replacement of this component by a new one.

Besides, maintenance control and experimental methods to evaluate the reliability, the numerical simulations are another possibility which are employed during the development phase of a component, from the research and development stage to the market introduction. For instance, Finite Element Analysis (FEA) became an indispensable tool to investigate the way a component is loaded and to detect the critical zones. By this means, design variations are easier and faster modelled and results are accessible faster than by testing of prototypes. Then, some drafted variations can be directly judged as unsuitable and the testing of such versions can be avoided. This stays almost valid for existing components which failed in service. Simulations can help in the better understanding of failure mechanisms as well as in the proposal of improvement solutions.

However, the reliability of simulated results is based on the confidence of input data and techniques employed during the simulation. If the material properties and the loading conditions are not correctly considered in the simulation, the resulting conclusions will be wrong and this will lead to a wrong estimation of the reliability.

The present work will be concerned with the failure mechanism appearing in encapsulation techniques. Encapsulation is employed to protect a component from external media such as humidity, fuel, dust particles, or other chemical substances and can provide thermal and electrical isolation. Mechanical failure like cracking of the

encapsulating material can generally lead to the complete failure of the component. And this type of failure can be caused by the stresses resulting from the assembly of different materials with different coefficients of thermal expansion (Fig.I-1). Other causes can lead to failure such as the shrinkage of the material while curing or swelling by absorption of humidity. But this work is essentially concentrating on the mechanical failure mechanism.

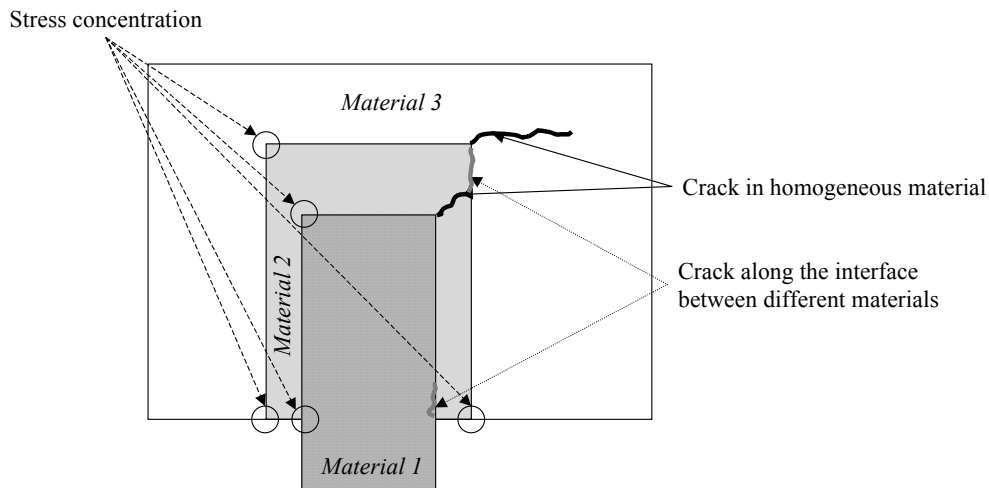


**Fig.I-1: Scheme of an encapsulated component with the critical domains for cracks and delamination**

From the assumption that a crack is already present, one has to consider that the following work takes place in the framework of the Linear Elastic Fracture Mechanics (LEFM). This theory describes the particularity of the stress state induced by a crack appearing in a bulk material or lying at the interface between two different materials. If one has to characterise a linear elastic material while cracking, classical parameters like the yield stress or the maximal tensile stress are no longer sufficient to describe efficiently what happens at the crack tip. It is such that a crack creates at the tip a stress concentration and by the way introduces in the stress state a singularity so that analytical solutions show that stresses are infinite. This phenomenon has been highlighted at the beginning of the 20<sup>th</sup> century and theories on fracture have been continuously developed and improved.

Nowadays, suitable parameters avoiding the undesirable consequence of infinite stresses are known as well as experimental procedures to measure these parameters. However, their applications in industrial environment appear slowly, and Fracture Mechanics tends to become a tool taken into account by engineers. But the nature of the stress state induced by a crack remains a problem in the domain of the numerical simulation. In this domain, too, special procedures are implemented since the past decades in order to represent and to compute the stress singularity.

These procedures need so many computational resources that they are time-consuming and by then, limited only to simple geometry such as laboratory specimens. But the continuous increase in the computational power of workstations and personal computers enables

the treatment of sufficiently complicated structures corresponding to real components. So that the need in the numerical estimation of the reliability in order to avoid failure of components corresponds to the moment where it becomes possible to simulate the processes involved in the failure.

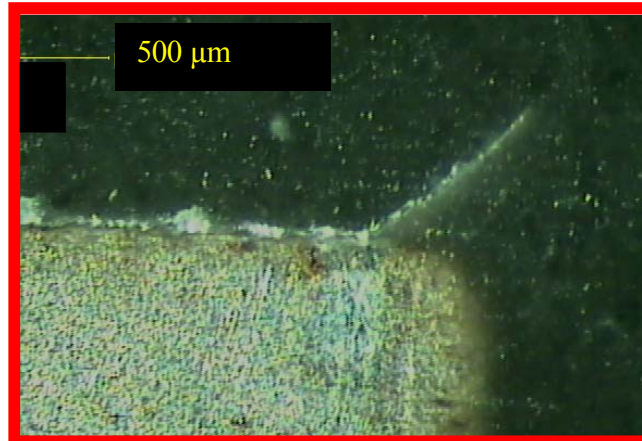


**Fig.I-2: Example of a crack located at the corner of an embedded core**

The final objective of this study is to achieve the establishment of methods in order to be able to characterise completely by means of numerical simulations the behaviour of a crack in homogeneous materials as well as at the interface between two different materials (Fig.I-2). The modus operandi of the adequate measurement methods necessary to obtain the parameters involved in the crack behaviour will be presented. Due to the industrial framework and the confidentiality of the components studied, some data are obliged to be masked.

This work will start with a description of the development of fracture mechanics theory. Researchers are acquiring continuously knowledge on the behaviour of a crack in homogeneous materials and they develop new concepts adapted to the description of the crack behaviour. The next part will present the main concepts helping to understand the different but related phenomenon of a crack between different materials. After that, a description of the complexity of the task involved in the numerical simulation of cracks will follow and some numerical methods available for these simulations will be presented. Then, the description of the experimental procedure will be presented. There exist numerous specimens to measure fracture parameters. The most important will be described and those chosen for our purpose will be highlighted as well as the methods employed to extract the results. The last part will deal with the presentation of results gathered with these methods.

---

# **Chapter II**

## **PRESENTATION OF THE CONCEPTS IN FRACTURE MECHANICS**

## **III/ Presentation of the concepts in fracture mechanics**

### **II.A/Introduction**

*The wide range of materials and the various behaviour of them lead inevitably to a large number of tests designed to investigate a given property of a given material for given processing and shape. The most studied materials are the metals and one may note the need to determine the tensile and the shear modulus for different temperatures, the coefficient of thermal expansion, the electrical conductivity, the viscosity at high temperature and so forth. The same is true for plastics and polymers which were studied as intensively as metals since they began to be widely used in engineering applications.*

*In this context, the failure of materials is a major concern when studying the reliability of products. So the pursuit of an understanding of the phenomena of fracture was needed and the grounds of the Fracture Mechanics were posed to provide a logical framework to analyse the problems.*

*We will see the fundamental notions or concepts introduced by Griffith presenting the connection between fracture stress and flaw size and the progress of Irwin due to the introduction of stress intensity factors. After that a summary of linear elastic fracture mechanics as well as elastic plastic fracture mechanics is presented, followed the consideration of the crack propagation processes.*

## **II.B/A history of fracture mechanics' development**

Historically, rock blocks used in monumental structures since the ancient time often present unexplainable cracks. Such cracks could be provoked by work imperfections and may often be the source of failure by crack propagation. Master builders of ancient time already noticed that some stones compared to others presented fracture with low energy dissipation. Later, in the eighteenth century Coulomb (1736-1806) pioneered the investigation of the fracture of stones in compression and he developed a criterion which is still currently in use. Another particular aspect regarding brittle solids is the size effect phenomenon made by Galilei (1564-1642). When visiting the venetian arsenal, he was surprised to note that workers paid more attention in the construction of big ships than in small ships. A master builder explained to him that it depended on greater brittleness of big ships compared to the smaller ones.

### **II.B.1/Griffith fracture mechanics**

This idea that small structures generally exhibit higher strengths than larger ones, was retaken by Griffith in the 1920s who studied the phenomena of rupture in glass [1920-Griffith]. He made the assumptions that every body contains a distribution of imperfections or flaws and that failure occurs at the largest of these. Larger bodies have a greater likelihood of containing bigger flaws and will, thus, fail at lower stresses. By these assumptions he introduced the fundamental notions of the new born science of Fracture Mechanics.

Nevertheless, one may note that new theories have always forerunners. For example, Inglis in 1913 considered the stresses applied near the edge of an elliptical notch. In the case where the relative size of the minor axis to the major axis is very small, the ellipse would appear as a straight crack and a small increase in the force applied to the tip would be sufficient to start a tear in the material. Furthermore, he noted that the increase in the length "exaggerates the stress yet further and the crack continues to spread in the manner characteristic of cracks" [1913-Inglis].

So, Griffith used for his purpose an energy balance and developed his theory based on the concept that when a flaw grows in a body under given loading conditions, there is a decrease in its potential energy, and this amount of energy is released in the body by forming new surfaces of the growing flaw.

Consider a through-thickness crack of length  $2a$  located in a large brittle plate of uniform thickness  $B$ , subjected to a constant tensile stress  $\sigma$ . Griffith deduced the net change in potential energy of the large plate (Fig.II-1) to be:

$$W_p = -\frac{\pi a^2 \sigma^2 B}{E'} \quad \text{Eq.II-1}$$

where, for plane strain and plane stress, respectively,

$$E' = \frac{E}{1-\nu^2} \quad \text{and} \quad E' = E \quad \text{Eq.II-2}$$

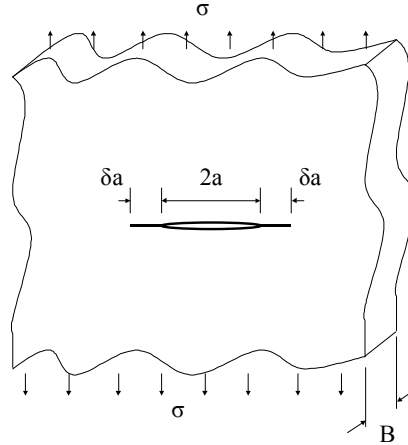


**Fig.II-1: A large plate of an elastic material containing a crack of length 2a**

Here, E is the Young's modulus and  $\nu$  is the Poisson's ratio. The surface energy of the crack system in Fig.II-1 is:

$$W_s = 4aB\gamma_s \quad \text{Eq.II-3}$$

where  $\gamma_s$  is the free surface energy per unit surface area. The total system energy is then given by

$$U = W_p + W_s = -\frac{\pi a^2 \sigma^2 B}{E'} + 4aB\gamma_s \quad \text{Eq.II-4}$$

Griffith noted that the critical condition for the onset of crack growth is

$$\frac{dU}{dA} = \frac{dW_p}{dA} + \frac{dW_s}{dA} = -\frac{\pi a \sigma^2}{E'} + 2\gamma_s = 0 \quad \text{Eq.II-5}$$

where  $A=2aB$  is the crack area and  $dA$  denotes an incremental increase in the crack area. Note that the total surface area of two crack faces is  $2A$ . The resulting critical stress for fracture initiation is

$$\sigma_f = \sqrt{\frac{2E'\gamma_s}{\pi a}} \quad \text{Eq.II-6}$$

As the second derivative  $d^2U/da^2$  is negative, the above equilibrium condition, Eq.II-65, gives rise to unstable crack propagation. In addition, the materials considered by Griffith in this theory are inorganic glasses, which gave almost perfectly brittle cracks in that the energy necessary to create new surfaces equals the surface energy.

For most materials this is not true since the stresses induced at the tip of the flaw cause large deformations and flow, which result in much more energy being dissipated. Considering the failure of steel, independently Orowan [1955-Orowan] and Irwin [1957-Irwin] provided the result that the dissipation was confined to a small zone at the flaw tip. This means that Eq.II-1 could still be used, but a plastic energy dissipation needs to be considered. The resultant expression for fracture initiation is

$$\sigma_f = \sqrt{\frac{2E'(\gamma_s + \gamma_p)}{\pi a}} \quad \text{Eq.II-7}$$

where  $\gamma_p$  is the plastic work per unit area of surface created. Note that  $\gamma_p$  is much larger than  $\gamma_s$ . The criterion for crack growth can be expressed as: the strain energy release rate  $G$  must be larger than the critical work  $G_c$  which is required to create a new unit crack area. The notation  $G$  comes after Griffith.

Irwin extended the Griffith theory using Westergaard's method developed in 1939 [1939-Westergaard] and pointed that in the Eq.II-7, the numerator is a material property. This equation can be rewritten into the form:

$$\sigma = \frac{K}{\sqrt{\pi a}} \quad \text{Eq.II-8}$$

where  $K$  is called the Stress Intensity Factor (SIF). It is said that the notation  $K$  may come from Kies, a colleague of Irwin at the US Naval Research Laboratory [1954-Irwin].

## II.B.2/Energy release rate

### II.B.2.a/Definition of $G$ and $R$

Let us suppose that the body in Fig.II-1 is submitted to a force that leads to crack growth. A change in the energy balance occurs in an irreversible manner during crack growth. A specific energy is needed to propagate the crack over an incremental area  $dA$ . One may define  $R$  as the fracture resistance of the body:

$$R = \frac{dW_s}{dA} \quad \text{Eq.II-9}$$

It is necessary to consider the energy change in the system due to the crack increment  $da$  arising from the changes in external work and internal energy. This is defined as  $G$ , the energy release rate. Consider an elastic body of uniform thickness  $B$  containing a crack of length  $a$  submitted to an external force  $P$  related to a displacement  $u$ . The total mechanical energy of the cracked body  $W_p$  is defined as

$$W_p = \Phi - W_F \quad \text{Eq.II-10}$$

where  $\Phi$  denotes the stored elastic deformation energy and  $W_F$  is the external work done by the external forces. Irwin in 1956 [1998-Suresh] proposed to approach the characterisation of the driving force for fracture in cracked elastic bodies. He introduced the energy release rate  $G$  (ERR) defined as

$$G = -\frac{dW_p}{dA} \quad \text{Eq.II-11}$$

where  $A$  denotes the crack area ( $A=2aB$ ) and  $dA$  denotes an incremental increase of the crack area.

### II.B.2.b/Evaluation of $G$

The cracked body is subjected to a fixed force  $P$ , and the mechanical energy (for a given crack length  $a$ ) can be written as

$$\Phi = \int_0^u P du = \frac{Pu}{2} \quad \text{and} \quad W_F = Pu \quad \text{Eq.II-12}$$

From Eq.II-10 and Eq.II-12 it can be concluded that

$$W_p = -\Phi = -\frac{Pu}{2} \quad \text{Eq.II-13}$$

Consider a crack increment from  $a$  to  $a+\delta a$ , this causes an incremental displacement of  $\delta u$  under the load  $P$ . The energy release rate (ERR) for the body is written as

$$G = -\frac{1}{B} \left( \frac{dW_p}{da} \right)_P = \frac{P}{2B} \left( \frac{du}{da} \right)_P \quad \text{Eq.II-14}$$

The crack advance by an increment  $\delta a$  for fixed  $P$  leads to an increase in the stored strain energy by the amount:

$$\delta\Phi|_P = -\frac{P\delta u}{2} + P\delta u = \frac{P\delta u}{2} \quad \text{Eq.II-15}$$

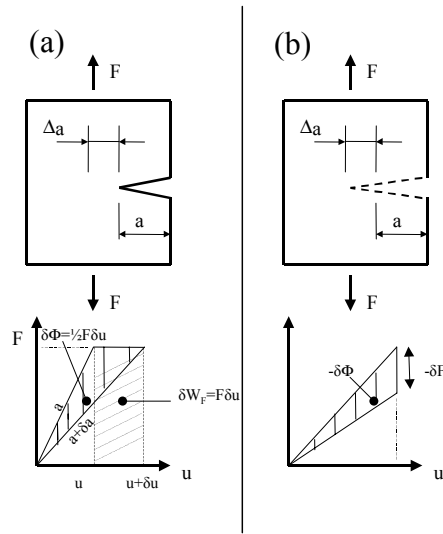


**Fig.II-2: Elastic cracked body under (a) fixed load and (b) fixed displacement**

If the displacement is controlled, the force varies as shown in the Fig.II-2. When the crack advances by  $\delta a$  under a fixed displacement  $u$ , the change in  $W_F$  is zero and  $\delta W_P = \delta \Phi$ . From Eq.II-10 follows

$$\delta \Phi|_u = -G \delta A \quad \text{or} \quad G = -\frac{1}{B} \left( \frac{\partial \Phi}{\partial a} \right)_u = -\frac{u}{2B} \left( \frac{\partial P}{\partial a} \right)_u \quad \text{Eq.II-16}$$

The advance of crack length leads to a net decrease in the stored strain energy by the amount

$$\delta \Phi|_u = -\frac{u \delta P}{2} \quad \text{Eq.II-17}$$

Defining the compliance  $C$  as the inverse of the stiffness ( $C=u/P$ ), the energy release rate is given by

$$G = \frac{P^2}{2B} \frac{dC}{da} \quad \text{Eq.II-18}$$

The above result is valid for both load control or displacement control, i.e. the ERR  $G$  is independent of the type of loading. One may therefore note that:

$$\delta \Phi|_P = -\delta \Phi|_u \quad \text{Eq.II-19}$$

Besides, the definition of  $G$  stays valid for both linear and non-linear elastic deformation of the body.  $G$  is a function of the load (or displacement) and crack length for the cracked body. The Griffith criterion for fracture initiation in a brittle solid (Eq.II-6) can be rephrased in terms of  $G$  such that

$$G = \frac{\pi\sigma a^2}{E'} = 2\gamma_s \quad \text{Eq.II-20}$$

### II.B.3/Linear elastic fracture mechanics

While the Griffith theory is based on the consideration of fracture from an energy point of view, one can derive more precise conditions for the growth of flaws when considering an linear elastic stress analysis. From a macroscopic point of view, one considers the three different modes of fracture by applying stress conditions to the crack front such that each mode is characterised by a stress state in each plane. Mode I is the tensile opening mode in which the crack faces separate in a direction normal to the plane of the crack (Fig.II-3a). By the same way, mode II is the in-plane sliding mode in which the crack faces slide in a direction normal to the crack front (Fig.II-3b), and mode III is the tearing mode (or anti-plane shear mode) in which the crack faces are sheared in a direction parallel to the crack front (Fig.II-3c).

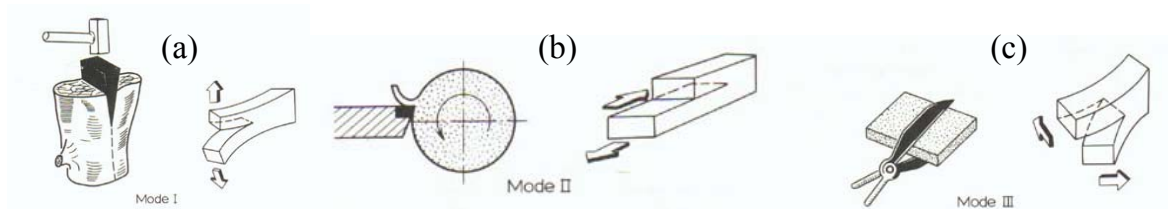


Fig.II-3: The three different modes of fracture

#### II.B.3.a/Stress intensity factors

It is now well established that for cracks in linear elastic media, the stress field near the tip (which is the only area we expect to influence crack growth) contains a singularity and obeys to a power law at the distance  $r$  from the crack tip. Considering only the dominant term, the stress intensity factors will then be defined in three dimension by giving the angular dependence of the stress field (see Fig.II-4) [1993-lawn]

$$\sigma_{ij}(r, \theta) = \frac{K_i}{\sqrt{2\pi r}} f_{ij}^i(\theta) \quad \text{Eq.II-21}$$

The Eq.II-21 shows that the relevant information from the elastic field is reduced to three parameters, the three  $K_i$ . In detail only for the mode I, this gives:

$$\begin{aligned}
 \begin{Bmatrix} \sigma_{xx} \\ \sigma_{yy} \\ \sigma_{xy} \end{Bmatrix} &= \frac{K_I}{\sqrt{2\pi r}} \begin{Bmatrix} \cos(\theta/2)[1 - \sin(\theta/2)\sin(3\theta/2)] \\ \cos(\theta/2)[1 + \sin(\theta/2)\sin(3\theta/2)] \\ \cos(\theta/2)\cos(\theta/2)\cos(3\theta/2) \end{Bmatrix} \\
 \begin{Bmatrix} \sigma_{rr} \\ \sigma_{\theta\theta} \\ \sigma_{r\theta} \end{Bmatrix} &= \frac{K_I}{\sqrt{2\pi r}} \begin{Bmatrix} \cos(\theta/2)[1 + \sin^2(\theta/2)] \\ \cos^2(\theta/2) \\ \sin(\theta/2)\cos^2(\theta/2) \end{Bmatrix} \\
 \sigma_{zz} &= \nu'(\sigma_{xx} + \sigma_{yy}) = \nu'(\sigma_{rr} + \sigma_{\theta\theta}) \\
 \sigma_{xy} = \sigma_{yz} = \sigma_{rz} = \sigma_{\theta z} &= 0
 \end{aligned}
 \tag{Eq.II-22}$$

The corresponding displacements are:

$$\begin{aligned}
 \begin{Bmatrix} u_x \\ u_y \end{Bmatrix} &= \frac{K_I}{2E} \sqrt{\frac{r}{2\pi}} \begin{Bmatrix} (1+\nu)[(2\kappa-1)\cos(\theta/2) - \cos(3\theta/2)] \\ (1+\nu)[(2\kappa+1)\sin(\theta/2) - \sin(3\theta/2)] \end{Bmatrix} \\
 \begin{Bmatrix} u_r \\ u_\theta \end{Bmatrix} &= \frac{K_I}{2E} \sqrt{\frac{r}{2\pi}} \begin{Bmatrix} (1+\nu)[(2\kappa-1)\cos(\theta/2) - \cos(3\theta/2)] \\ (1+\nu)[-(2\kappa+1)\sin(\theta/2) + \sin(3\theta/2)] \end{Bmatrix} \\
 u_z &= -(\nu''z/E)(\sigma_{xx} + \sigma_{yy}) = -(\nu''z/E)(\sigma_{rr} + \sigma_{\theta\theta})
 \end{aligned}
 \tag{Eq.II-23}$$

where

$$\begin{aligned}
 \kappa &= (3-\nu)/(1+\nu), \quad \nu' = 0, \quad \nu'' = \nu, & \text{Plane stress} \\
 \kappa &= (3-4\nu), \quad \nu' = \nu, \quad \nu'' = 0, & \text{Plane strain}
 \end{aligned}$$

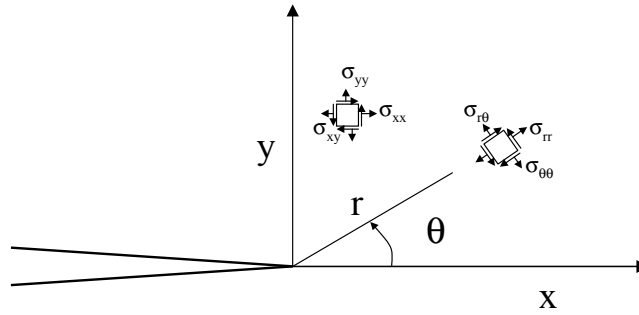


**Fig.II-4: Coordinate system and stresses in the near-tip region of a crack**

A more general form of the stress state can be written considering now the terms of higher orders, introducing a second parameter

$$\sigma_{ij}(r, \theta) = \frac{K_i}{\sqrt{2\pi r}} f_{ij}^i(\theta) + T \delta_{ix} \delta_{jx} + O(r^2) + O(r^{5/2})
 \tag{Eq.II-24}$$

where  $\delta_{ij}$  is the Kronecker symbol and  $O(r^2)$  and  $O(r^{5/2})$  are vanishing terms as  $r \rightarrow 0$ . The second term is generally referred to as the "T stress", containing the singular stress  $\sigma_{xx} = T$ . For example, if the body in Fig.II-1 is submitted to a uniform traction  $\sigma_{xx}^\infty$  and a uniform shear stress  $\sigma_{yy}^\infty$ , then

$$K_I = \sigma_{xx}^{\infty} \sqrt{\pi a} \quad \text{and} \quad T = \sigma_{xx}^{\infty} - \sigma_{yy}^{\infty} \quad \text{Eq.II-25}$$

However, it should be noted that each  $K_i$  gives information on load conditions for the respective mode, but the total loading condition is not represented by a "general  $K$ ", that is to say that  $K_g \neq K_I + K_{II} + K_{III}$ .

### II.B.3.b/Plane stress versus Plane strain

Most of the classical solutions in fracture mechanics reduce the problem to two dimensions [1995-Anderson].

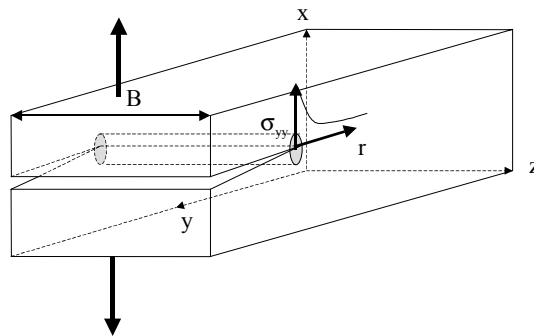


**Fig.II-5: 3D deformation at the crack front**

That is, at least one of the principal stresses (respectively principal strains) is assumed to be blocked, which leads to plane stress (respectively plane strain) conditions. In general, the conditions ahead of a crack are three-dimensional as in Fig.II-5; however limiting cases where a two-dimensional analysis is considered provide a good approximation, depending on the through-thickness variation of stress.

Thus, if we consider a plate of thickness  $B$ , uncracked, subjected to in-plane loading, the plate would be in a plane stress state. When a crack is introduced, material near the crack tip is loaded to higher stresses than the surrounding material. Because of this, the crack tip material tries to contract near the surface (Fig.II-6) while material in the interior is constrained, resulting in a triaxial stress state.

Let  $r$  be the distance from a point in the plane to the crack front (see Fig.II-5). For  $r \ll B$  plane strain conditions exist in the interior of the plate whereas material on the surface of the plate is in a state of plane stress, because there are no stresses normal to the free surface. This may introduce an uncertainty in the determination of the critical stress intensity factor since it is related to the principal stresses, and also in the evaluation of the energy release rate.

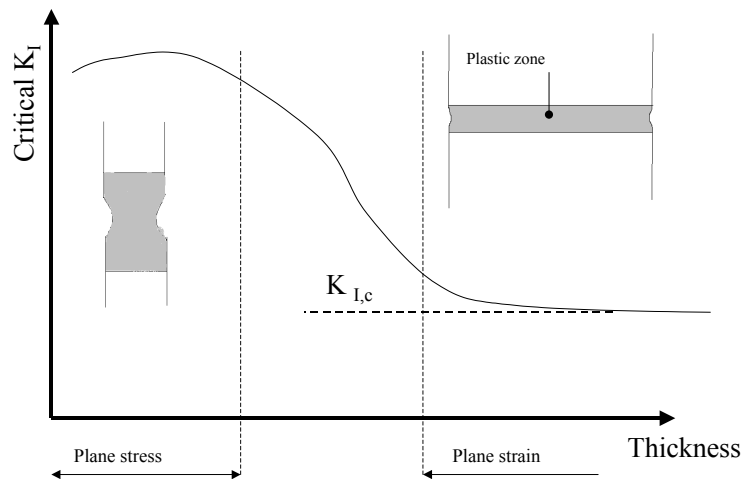


**Fig.II-6: Effect of specimen thickness on  $K_{Ic}$**

Although the stress state at the elastic-plastic boundary is predominately plane stress when the plastic zone size is of the order of half the plate thickness (or larger), a triaxial stress state may exist deep inside the plastic zone.

**II.B.3.c/Evaluation of K**

A possibility to investigate the fracture toughness ( $K_{Ic}$ ) is proposed by the American Society for Testing and Materials (ASTM) under the norm E399 for plane-strain fracture toughness of metallic materials and under the norm D5045-99 for plastics materials [1999-Astm].

This test method covers the determination of the fracture toughness by tests using a variety of fatigue-cracked specimens. The standard offers to use Compact Tension (CT) (Fig.II-7(a)) or Three Points Bending (3PB) (Fig.II-7(b)) specimens.

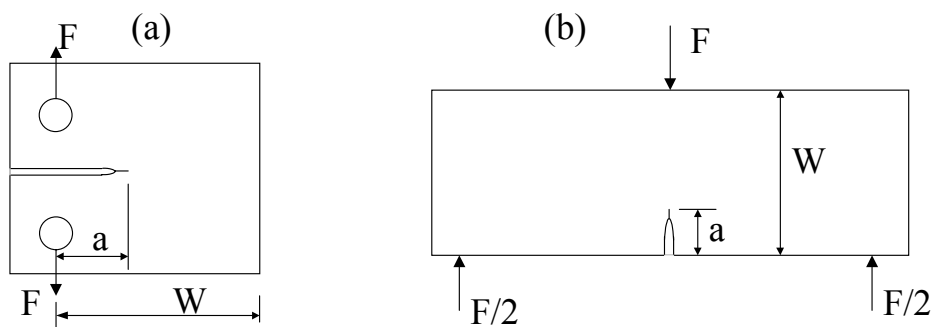


**Fig.II-7: (a) Compact Tension (CT); (b) three point bending (3PB) samples**

As recommended in the ASTM D5045-99, the  $K_{Ic}$  is calculated thanks to:

$$K = \frac{P}{B\sqrt{W}} f\left(\frac{a}{W}\right) \quad \text{Eq.II-26}$$

For the CT sample:

$$f\left(\frac{a}{W}\right) = \frac{\left(2 + \frac{a}{W}\right) \left(0,886 + 4,64 \frac{a}{W} - 13,32 \left(\frac{a}{W}\right)^2 + 14,72 \left(\frac{a}{W}\right)^3 - 5,6 \left(\frac{a}{W}\right)^4\right)}{\left(1 - \frac{a}{W}\right)^{\frac{3}{2}}} \quad \text{Eq.II-27}$$

where B is the thickness, W the width, a is the crack length in cm, P the force in KN. Tab.II-1 shows as example the value of  $K_{Ic}$  and yield stress for different families of materials.

Material	$K_{Ic}$ [MPa.mm <sup>0,5</sup> ]	Rp0,2 [MPa]
High strength steel	800 ... 3000	1600 ... 2000
30CrNiMo8 (-20°)	2000	
30CrNiMo8 (20°)	3650	1100
Ti alloy	1200 ... 3000	800 ... 1200
Al alloy	600 ... 2000	200 ... 600
Al2O3 Ceramic	120 ... 300	
Concrete	5 ... 30	
Polypropylen	0,1 ... 0,2	
Polystyren	0,021 ... 0,083	
PMMA	0,036 ... 0,11	

**Table II-1: Some fracture toughness data from [1996-Gross] and [1987-Kausch]**

However, like other properties as Young's modulus and yield stress, this value also depends strongly on the temperature [1996-Gross] and, in case of polymers which show visco-elastic behaviour, can be time-dependent [2004-Wittler].

## II.B.4/Elastic plastic fracture mechanics

### II.B.4.a/Conditions of K-dominance

In order to respect the presumptions of linear elastic fracture mechanics, the material and geometrical non-linearity are confined to a very small length scale around the crack tip. If one pays attention to the spatial domain where yielding processes appear (see Fig.II-8), one has to consider:

- Fig.II-8(a): the small scale yielding (SSY),
- Fig.II-8(b): the contained yielding,
- Fig.II-8(c): the large scale yielding (LSY)
- and Fig.II-8(d): the fully yielded geometry.

As shown in the equations Eq.II-22 to Eq.II-24, the stresses and displacements ahead of the crack tip are governed by the K factors. However, for ductile materials, even in presence of a crack, the material yields when stresses exceed the flow stress, and the linear elastic solutions are no longer valid. The usefulness of the K-field to describe the onset or the growth of cracks force the stress state to fulfil the so-called "small-scale yielding" conditions.

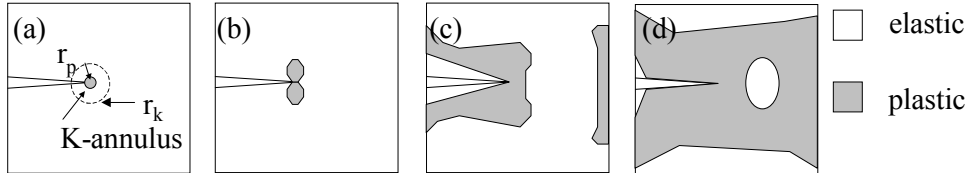


**Fig.II-8: Crack geometry and plastic flow**

These conditions require that the domain where inelastic deformations occur, no matter if they are caused by plasticity, creep, phase changes, has to be confined inside a region in which the asymptotic results still provide a good approximation to the full solution.

Two common approaches to calculate the plastic deformation domain have been proposed: the von Mises yield criterion and the Dugdale model [1987-Kausch].

From the von Mises criterion,

$$\left( (\sigma_I - \sigma_{II})^2 + (\sigma_{II} - \sigma_{III})^2 + (\sigma_{III} - \sigma_I)^2 \right) < 2(\sigma_y)^2 \quad \text{Eq.II-28}$$

where  $\sigma_I$ ,  $\sigma_{II}$  and  $\sigma_{III}$  are the principal stresses, one derives the form of the plastic zone ( $r < r_p$ ) for a plane stress state as

$$r_p = \frac{K_I^2}{\pi\sigma_y^2} \cos^2 \frac{\theta}{2} \left( 1 + 3 \sin^2 \frac{\theta}{2} \right) \quad \text{Eq.II-29}$$

and for plane strain as

$$r_p = \frac{K_I^2}{\pi\sigma_y^2} \cos^2 \frac{\theta}{2} \left[ \left( 1 + 3 \sin^2 \frac{\theta}{2} \right) - 4\nu(1-\nu) \right] \quad \text{Eq.II-30}$$

Barenblatt [1959-Barenblatt] and Dugdale [1960-Dugdale] were the first attempting to include cohesive forces in the crack tip region. Barenblatt assumed that cohesive forces act in a small zone (called "cohesive zone") near the crack tip such that the crack faces are closed smoothly. For Dugdale, the distribution of these closing forces obeys to the laws of an elastic, perfectly plastic material.

He considered a virtual crack which included the plastic zone (Fig.II-9) and added an acting stress corresponding to the yield

stress so that it tends to bend the surface of the virtual crack. Thus

$$r_p = \frac{\pi a \sigma_{yy}^2}{8 \sigma_y^2} \quad K_I = \sigma_{yy} \sqrt{\pi(a + r_p)} \quad \text{Eq.II-31}$$

It can be shown that the crack tip opening displacement takes the form

$$\delta(a) = \frac{8 \sigma_y a}{\pi E'} \ln \left[ \sec \left( \frac{\pi \sigma}{2 \sigma_y} \right) \right] \quad \text{Eq.II-32}$$

And asymptotically, when  $\sigma \ll \sigma_y$

$$\delta(a) = \frac{K_I^2}{\sigma_y E'} \quad \text{Eq.II-33}$$

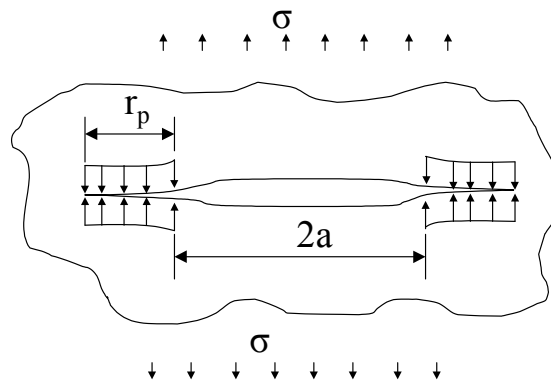


**Fig.II-9: The Dugdale plastic zone model**

### II.B.4.b/The J-Integral

Let us consider a crack in an homogeneous body of a linear or non-linear elastic material free of body forces and subjected to a two-dimensional deformation field. Assume that the body possesses a notch as in Fig.II-10. A straight crack is a limiting case. Define the strain-energy density  $w$  by:

$$w = w(x, y) = w(\boldsymbol{\varepsilon}) = \int_0^{\boldsymbol{\varepsilon}} \boldsymbol{\sigma}_{ij} d\boldsymbol{\varepsilon}_{ij} \quad \text{Eq.II-34}$$

where  $\boldsymbol{\varepsilon} = [\varepsilon_{ij}]$  is the infinitesimal strain tensor. Now consider the integral  $J$  defined by:

$$J = \int_{\Gamma} \left( w dy - t \frac{\partial u}{\partial x} ds \right) \quad \text{Eq.II-35}$$

Here  $\Gamma$  is a curve surrounding the notch tip, the integral being evaluated from the lower notch surface and continuing along the path  $\Gamma$  to the upper surface,  $t$  is the traction vector defined according to the outward normal along  $\Gamma$ ,  $u$  is the displacement vector and  $ds$  is an element of arc length along  $\Gamma$ .

Rice [1968-Rice] proved that the integral  $J$  according to Eq.II-35 is path independent. He noticed that  $J$  is the rate of change of potential energy, and that for an elastic body  $J$  is reduced to the ERR.

$$J = G = -\frac{dW_P}{dA} \quad \text{Eq.II-36}$$

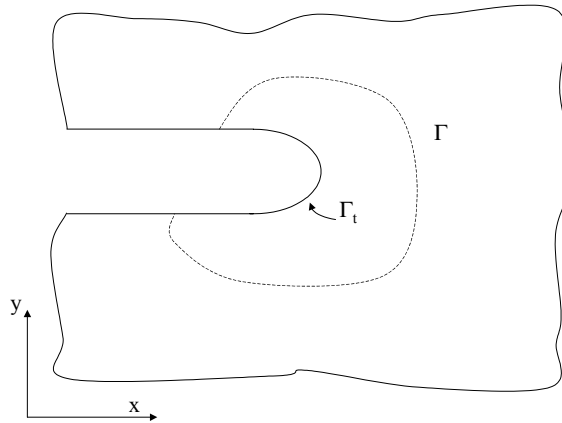


**Fig.II-10: 2D Body containing a notch**

If one applies  $J$  on a neighbored contour around the crack tip with the Westergaard displacement and stress fields in mixed mode, the superposition of the two particular fields yields:

$$J = \frac{1-\nu^2}{E} (K_I^2 + K_{II}^2) + \frac{1+\nu}{E} K_{III}^2 \text{ for plane strain} \quad \text{Eq.II-37}$$

$$\text{and } J = \frac{(K_I^2 + K_{II}^2)}{E} \text{ for plane stress}$$

In the case of the SSY (Fig.II-8(a)), plastic zones are so small that they do not interfere with the results of the LEFM approach. In the case of contained yielding, Rice's J-Integral sets the amplitude of the stress singularity and the size scale of large geometry changes (LGC). Assume that the region of J-dominance is larger than the region where microfracturing mechanisms and LGC take place, the J-Integral remains to be a reliable fracture parameter. This situation is the so-called "fracture under constrained conditions".

On the contrary, if the J-domain is smaller than the microfracturing zone, the J-Integral may depend on factors like thickness, the a/W ratio (crack length / specimen width) and loading conditions.

Under such assumptions, various additional fracture parameters have been introduced, among these we find: the quantity Q (hydrostatic stress,  $Q=(\sigma_{rr}+\sigma_{\theta\theta})/2$ ), the T-stress (corresponds to  $K_{II}=0$ ) and the higher order amplitude. Like the "K-dominance", one denotes by the J-Q annulus the domain of influence where both parameters J and Q characterise the stress state [2002-Dollhofer].

## II.B.5/Crack propagation

To study crack propagation, it is convenient to rewrite the energy balance of Eq.II-4 by considering the kinetic energy  $U_k$ , which was until now neglected.

$$G = -\frac{d(\Phi - W_F)}{dA} = R + \frac{dU_k}{dA} \quad \text{Eq.II-38}$$

For fracture initiation, the body is stationary so  $U_k=0$  and  $dU_k/dA > 0$ . When fracture occurs if

$$G - R \geq 0 \quad \text{Eq.II-39}$$

If  $G > R$ , then the system is unstable since  $dU_k/dA$  is positive, leading to an increase in fracture velocity. If we consider a case in which G monotonically increases, then at fracture:

$$G = R \quad \text{Eq.II-40}$$

And the stability of the subsequent behaviour depends on G and R at  $A+\delta A$ , i.e. the fracture is unstable if:

$$G + \frac{dG}{dA} \delta A > R + \frac{dR}{dA} \delta A \quad \text{Eq.II-41}$$

And since  $G=R$ , we have the following condition for instability:

$$\frac{dG}{dA} > \frac{dR}{dA} \quad \text{Eq.II-42}$$

Note that for moving cracks where  $U_k > 0$ ,  $\delta U_k$  can be negative and hence helps drive the crack by decelerating so that the criterium becomes:

$$G > R + \frac{dU_k}{dA} \quad \text{Eq.II-43}$$

with

$$\frac{dG}{dA} > \frac{dR}{dA} + \frac{d^2U_k}{dA^2} \quad \text{Eq.II-44}$$

It should be noted that equations Eq.II-39 and Eq.II-40 are the Lagrangian conditions for stable equilibrium of a minimum in potential energy.

### II.B.6/The R-curve

The criteria are often represented on a diagram, as shown below in Fig.II-11. Let us consider a crack of initial area  $A_0$ , the energy required for propagation may be represented by  $R$  as a function of  $A$ . The curves for  $G$  are represented by lines, ordered in the sense of increasing load  $P$ .

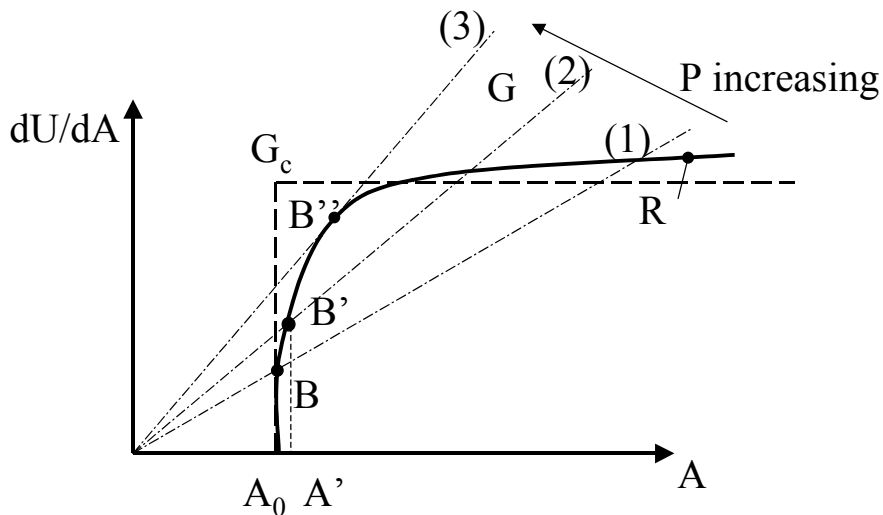


Fig.II-11: G and R curves as functions of fracture area A

On line (1), for the initial part of the R-curve,  $G=R$  so that  $\delta A$  is zero. On line (2)  $G=R$  at point  $B'$  which corresponds to a crack extension from  $A_0$  to  $A'$ . For  $A > A'$  we can see that  $G < R$  i.e.  $dG/dA < dR/dA$  so that the crack grows a stable manner. This is true until the tangency point  $B''$ , after which  $dG/dA > dR/dA$  and the fracture is unstable. Thus, for the system represented by the R-curve of the Fig.II-11 only the part up to  $B''$  is accessible for measurement.

A limiting case for  $R$  is shown by the dashed lines. Here there is no stable crack growth: whether  $G < G_c$  or  $G = G_c$ . This case is the general form described by the Griffith criterion for perfectly brittle crack where  $G_c = 2\gamma$ .

The concept of the R-curve defines the behaviour of cracks when this is determined by the single parameter  $G_c$ . This implies that the energy dissipation processes are localised around the crack tip and

that the rest of the body is not involved. This assumption is reasonable in a physical way for brittle cracks in elastic systems which we are concerned with.

## II.B.7/Fatigue crack growth

### II.B.7.a/Subcritical crack growth or static fatigue

Loading the sample above a critical value of  $K_{Ic}$  (or  $G_c$  or  $J_c$ ) leads in general to elastic loading of the crack tip region, viscoelastic and time-dependent response of the material and sometimes to plastic deformations within the fracture process zone. But when the loading conditions are below the critical value, which is a material parameter, subcritical crack growth can occur.

This phenomenon characterises the weakening process of the material at the crack tip and when the process zone displaces itself. The fact is that during all the process of propagation, virgin material is resisting to crack advance. This explains the relative stability of the phase of subcritical crack growth.

Since subcritical crack growth precedes catastrophic fracture, a delay to failure is often observed in components subjected to a static load. Subcritical crack growth also leads to a time dependence of the strength, the slower the loading rate, the weaker the material. The science of fracture mechanics provides a logical framework for understanding the effect of subcritical crack growth on structures and for predicting lifetime.

As a matter of fact, the rate of crack growth  $da/dt$  is governed by the laws of material deformation and breakdown. Several relations between  $K_I$  and  $da/dt$  have been established but the most popular form has been found to be [1975-Beaumont]:

$$\frac{da}{dt} = A_I K_I^{n_I} \quad \text{Eq.II-45}$$

where  $A_I$  and  $n_I$  are material parameters. One should mention the effect of environment on crack propagation. Even at sustained load below the critical level, rate-dependent growth appears when the cracked body is in contact with an interactive fluid environment [1993-Lawn]. Lawn used the term "kinetics" rather than "dynamics" to qualify these phenomena to distinguish the velocity range (typically in the magnitude of the  $m.s^{-1}$  down to and below  $nm.s^{-1}$  for kinetics to compare with the  $m.s^{-1}$  to  $km.s^{-1}$ ).

From Eq.II-8 and Eq.II-45, one can determine the time  $\Delta t$  necessary for the growth of a crack of length  $a_1$  to a length  $a_2$ . For a constant stress  $\sigma_0$ :

$$\Delta t = \int_{a_1}^{a_2} \frac{da}{da/dt} = \frac{2}{\sigma_0^2} \int_{K_{I1}}^{K_{I2}} \frac{K_I}{A_I K_I^{n_I}} dK_I = \frac{2[(K_{I1}^{2-n_I} - K_{I2}^{2-n_I})]}{[(n_I - 2)A_I \sigma_0^2]} \quad \text{Eq.II-46}$$

If one assumes that instantaneous fracture occurs when  $K_I$  reaches the critical  $K_{Ic}$ , and if one considers a geometrical scaling factor  $Y$ , then the time-to-failure  $t_f$  is given by:

$$t_f = \frac{2[(K_{I1}^{2-n_I} - K_{Ic}^{2-n_I})]}{[(n_I - 2)A_I Y^2 \sigma_0^2]} \quad \text{Eq.II-47}$$

### II.B.7.b/Cyclic fatigue

Fatigue loading, repeated application of varying stress or strain amplitudes, has been widely studied for metals since the work of Albert in 1837 who presented the first results known on fatigue tests of driving ropes [2001-Toth]. Numerous authors were involved afterwards in the study of unexpected railway failures during services. York and separately Rankin in 1843 published papers on the design of railway axles and the term of "Fatigue" for materials appeared in 1854. Then, from 1858 Wöhler carried out experiments on smooth and notched railway axles using axial, bending and torsion loading conditions. But it is only after 1920 that Basquin represented the finite life of the Wöhler curve with the equation:

$$\sigma_f = A_f \left( \frac{\sigma_{\min}}{\sigma_{\max}} \right)^{n_f} \quad \text{Eq.II-48}$$

The main problem was always related to fatigue crack growth ( $da/dN$  i.e. the crack growth rate) as a function of the loading condition. From Wöhler until the late 1950's, the loading condition was characterised only by the stress amplitude, with the disadvantage that the crack length has to be explicitly added to test reports. But in 1961, Paris [1961-Paris] proposed the range of stress intensity factors ( $\Delta K$ ) as a characteristic parameter for fatigue tests. This approach on the contrary requires direct evaluation of the crack advance. The "Paris law" can be written as

$$\frac{da}{dN} = A_n (\Delta K)^{n_n} \quad \text{Eq.II-49}$$

where  $A_n$  and  $n_n$  are material parameters and  $\Delta K$  the applied stress intensity factor range. This is completely analogous to the expression of the subcritical crack growth law in Eq.II-45. The acceptance of the Paris law was limited because the  $\Delta K$  value is based on a totally elastic material response even in the crack vicinity, while the fatigue crack growth is the result of plastic deformation and degradation in the crack vicinity. Other drawbacks of this "law" is that one neither takes into account the influence of a static mean stress nor the influence of a lower threshold value of  $K$  (i.e. a value below which no fatigue crack propagation occurs).

### **I.A.1 Creep and visco-elastic fracture**

Since the fracture mechanics was developed for steel and other metals, it cannot directly be applied to polymers. Visco-elastic fracture mechanics requires the incorporation of visco-elastic material response. The physical phenomena which take place at a crack tip in a stressed polymer point out that the breaking of macro-molecule chain bonds plays a fundamental role in the fracture of polymers. Fundamental to the development of visco-elastic fracture mechanics is the work by Scharpery [1975-Scharpery] who assumed a nonlinear visco-elastic constitutive equation in the form of a hereditary integral and, by means of the well known correspondence principle, developed a generalised J-integral [1984-Shapery]. Major contributions to the field of visco-elastic fracture mechanics may be found in the book by J.G. Williams [1984-Williams].

When submitted to high temperatures, even metals are subjected to uniform slow and stable deformation, termed creep. Whereas in fracture mechanics, creep is localised in the vicinity of a crack tip, under such conditions the classical hypotheses are no longer valid. The crack tip zone has to be replaced by a process zone embedded in a zone under creep conditions, itself surrounded by elastic material. For this purpose, the J-Integral was adapted to characterise steady state creep behaviour and became the  $C^*$ -Integral. However, if crack growth becomes larger and eventually overtakes creep growth then the  $C^*$  characterisation becomes invalid and the K approach is adapted.

## **II.C/Conclusion**

*Of course, this chapter has not the pretention to describe the whole historical development of Fracture Mechanics. Many fields, many subjects were touched and developed since Galilei measured the strength of iron wire. One may note the contribution of Hutchinson, Rice and Rosengren in the development of the Elastic Plastic Fracture Mechanics, the numerous contributions in the field of fatigue since the middle of the eighteenth century and the study of dynamic fracture or effect of crack arrest. In the scope of developing a science for engineering reliability, one would have to consider the application of the Continuum Damage Mechanics too.*

*The basic concepts of fracture mechanics were introduced which will be useful in the following work. We will limit ourselves to the framework of linear elastic fracture mechanics. In this scope, we will consider the characteristic material parameter which is the Stress Intensity Factor  $K$ . It will be determined thanks to the procedure described in the ASTM-Standard. By the same time, we will attempt to determine the Paris law for subcritical crack growth and implement it in a finite element software.*

---

---

## **Chapter III**

### CRACKS BETWEEN TWO DISSIMILAR MATERIALS

## **III/ Cracks between two dissimilar materials**

### **III.A/Introduction**

*A bimaterial interface is the conjoining surface between two dissimilar materials that are typically fused or bonded together. Such interfaces are common in electronic packages, and are often sources of severe discontinuities in thermal and mechanical properties. The predominant failure mode in multi-layered structures wherein cracks are constrained to grow along the interfaces is termed "interfacial fracture".*

*Nevertheless, materials where such failure modes are observed are more and more employed in civil engineering and in avionics or vehicle engineering. Aggregated-bitumen composites are used in highways bridges, mortar-aggregate composites are used in buildings and construction, multi-layered composites materials are used in plane structures and the use of microcircuits encapsulated by plastic becomes increasingly popular.*

*We will present in this part many concepts which were suggested to understand the phenomena occurring when we are in presence of an interfacial crack. Then will comes a theoretical development where fracture mechanics concepts are adapted in order to describe the special stress state at interfacial crack tips and finally we will focus on the experimental determination of convenient parameters.*

### III.B/Overview of interfacial fracture mechanics

Elastic fracture mechanics concepts were re-examined for the case of an elastic interface crack [1988-Rice]. Williams in 1959 determined the characteristic oscillating stress singularity. Cherepanov in 1962 gave the solution to specific problems as well as England, Erdogan and Rice & Shih. The case of crack penetration and/or crack deflection at an interface were also analysed during the 1970s by Cook & Erdogan in 1972, Erdogan and Biricikoglu in 1973 who investigated the behaviour of a crack penetrating the interface at right angles and in 1977 by Goree and Venezia who analysed several problems involving penetration and deflection of a crack. Additional works are reported in 1983 and in 1989, He & Hutchinson studied cases where a crack approaches an interface which leads to the competition between deflection and penetration [1989-He].

#### III.B.1/Presentation of different concepts

In the framework of multi-materials assemblies, it is well known that some geometries (corners, edges, notches, see Fig.III-1) can lead to harmful stress concentrations for structures or components. For instance, in electronic components, debonding at the microchip-encapsulant interface can cause immediate or intermittent electrical failure and can have negative effect on the long-term performance of the microchip by providing a site for the collection of moisture and ionic contaminants.

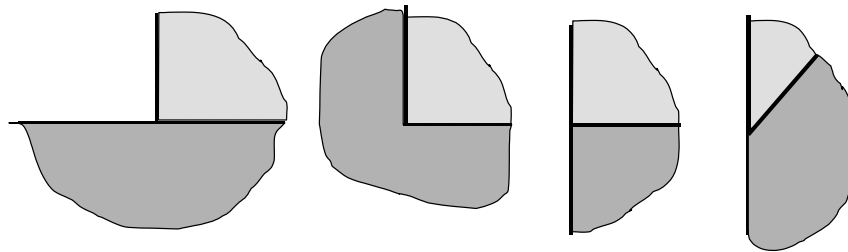


**Fig.III-1: Configurations promoting stress concentration**

The analysis of stress singularities at a wedge tip and at an interface corner (i.e. the intersection of an interface with a traction-free surface) of bimaterial joints and at a corner of a fully embedded inclusion has been examined by various authors.

Qian [2002-Qian] analysed the stress distribution at the interface junction of an elastic inclusion embedded in a brittle matrix. He derived the solutions for the stress and displacement fields and determined that the fields consist of symmetric and skew-symmetric (anti-symmetric) components identified as mode I and mode II. Reedy and Guess [2001-Reedy] have analysed the stress field near the

interface junction of a square rigid inclusion embedded in an epoxy resin and subjected to a uniform cooling or to an external applied pressure. Both fully bonded and unbonded conditions were considered. They found that in the case of the bonded inclusion, the singular stress state differed from the case where the inclusion was unbounded. It appeared that the unbonded inclusion was more likely to crack when cooled. Pahn and Earmme [2000-Pahn] determined the crack tip stress intensity factors as a function of the intensity of the singularity at the junction.

The interface behaviour plays a non-negligible role in the integrity of structures realised by composite materials where the adhesion between the different components influences strongly the quality of the global structure. To investigate and to characterise the fibre/matrix interface, micromechanical testing techniques such as the pull-out test (Fig.III-2) are used to measure the debond force [1999-Zahndarov]. Another way to characterise the fibre/matrix interface is to consider the adhesion in terms of an interphase with infinitesimal thickness [1997-Chaboche]. This interphase, called a cohesive surface was initially proposed by Needleman in 1987 and taken up by Tveergard in 1990. This model relates directly the interface traction to the corresponding displacement discontinuities.

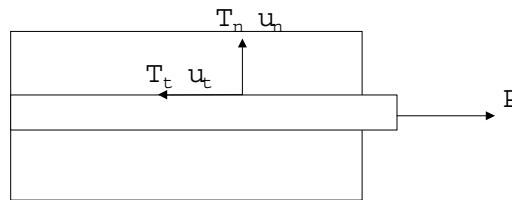


**Fig.III-2: Force applied to the fibre and acting at the fibre/matrix interface**

The forces  $T_n$  normal and  $T_t$  tangential are modelled as

$$T_n = \begin{cases} P(D_{\max}) \frac{u_n}{u_{nc}} & \text{if } u_n > 0 \\ E_k \frac{u_n}{u_{nc}} & \text{if } u_n < 0 \end{cases} \quad \text{Eq.III-1}$$

$$T_t = \frac{E_t}{E_n} P(D_{\max}) \frac{u_t}{u_{tc}}$$

where  $u_{nc}$  and  $u_{tc}$  represent maximum values of  $u_n$  and  $u_t$  for which total separation occurs.  $E_k$  is a high stiffness value in compression,  $E_t$  and  $E_i$  are the tangential and normal initial stiffness.  $D$  is a damage variable defined by

$$D = \sqrt{\left(\frac{|u_n|}{u_{nc}}\right)^2 + \left(\frac{u_t}{u_{tc}}\right)^2} \quad \text{Eq.III-2}$$

The function  $P(D)$  can be chosen by any function with  $P(0) \rightarrow \sigma_{\max}$  and  $P(1)=0$  but Tveergard used

$$P(D) = \frac{4}{27} \sigma_{\max} (1 - D^2) \quad \text{Eq.III-3}$$

The model of a cohesive surface can be implemented in numerical simulation codes. But this description does not account for strain rate dependence. However, crack initiation, crack growth and crack arrest emerge naturally as a result of the load. Quasi-static crack growth was modelled by Needleman in 1990 and in 1994. In 1997, dynamic studies were made by Siegmund et al [1997-Siegmund]. They carried out analyses of a crack growing first in an elastic solid and then across an interface and into an elastic-viscoplastic solid. They also highlighted the role of the crack speed. Friction and sliding contact have a role to play in such simulations. Monerie and Raous [2001-Monerie] take friction into account by adding an adhesion condition under the form of a Coulomb friction and showed numerically that a convenient choice of interfacial properties allows to increase the ductility or toughness of the component. Mechanisms involved in these improvements are the bridging and the trapping of matrix cracks by fibers.

Interface models where the bond between the two materials is described by a zero-thickness medium (Fig.III-3) are very common and straightforward to implement in numerical codes by means of double nodes. The constitutive laws for the interface relate the traction vector  $[t]$  on the interface to the vector of displacement discontinuities  $[u] = u_3^{mat1} - u_3^{mat2}$  between the material 1 and material 2.

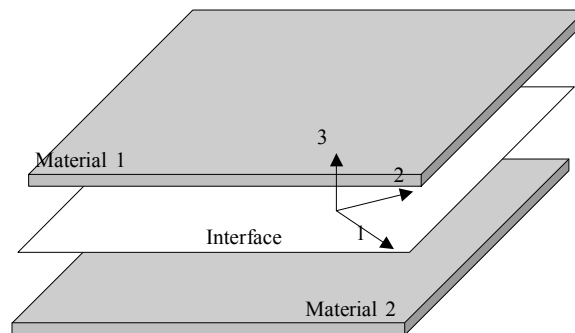


**Fig.III-3: Schematic representation of an interface**

The Tveergard model can be considered as a constitutive law for interfaces. It has the convenience to introduce a parameter which can be interpreted as a damage parameter. Depending on the cohesive law used in the description of the interface, different types of phenomena can be modelled: elastic damage, elastic-plastic softening, elastic-plastic damage [1999-Walrick and 2000-Coutellier], or more sophisticated models which describe the strain rate dependence by a viscous stress [2003-Rozycki]. In order to introduce a damage parameter, one has to consider the strain energy per unit surface transmitted by the interface. A possible expression is as follows [2000-Corigliano]:

$$W_s = \frac{1}{2}(1-D_1)E_1[u_1]^2 + \frac{1}{2}(1-D_2)E_2[u_2]^2 + \frac{1}{2}(1-D_3)E_3^+ \langle [u_3] \rangle_+^2 + \frac{1}{2}(1-D_3)E_3^- \langle [u_3] \rangle_-^2 \quad \text{Eq.III-4}$$

where the subscripts 1,2 refer to in-plane directions, 3 to normal direction relative to the interface, and  $D_i$  are three non-dimensional scalar damage variables which may vary between 0 (no damage) and 1 (total damage).  $E_i$  and  $E_3^{+/-}$  denote the interface stiffness, and the symbols  $\langle \cdot \rangle_+$  and  $\langle \cdot \rangle_-$  denote the positive and negative parts of  $u_3$ . the traction forces are obtained by computing the derivate of the strain energy with respect to the displacement discontinuities

$$t_i = \left. \frac{\partial W_s}{\partial [u_i]} \right|_{D_i}, i=1,2,3 \quad \text{Eq.III-5}$$

By the same way, thermodynamic forces  $Y_i$ , called the damage energy release rates, are obtained from the derivatives with respect to the damage variables

$$Y_i = - \left. \frac{\partial W_s}{\partial D_i} \right|_{[u_i]} \geq 0, i=1,2,3 \quad \text{Eq.III-6}$$

Such approaches of cohesive zones can eventually be applied to multiscale analyses (Fig.III-4). One may consider interfacial cohesive laws to be part of micromechanics which have to be distinguished from macroscopic constitutive models.

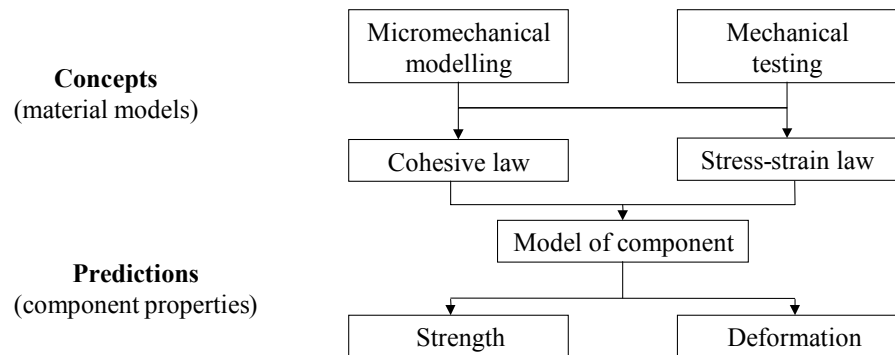


**Fig.III-4: The stress-strain and cohesive laws are key issues in the analysis of engineering structures**

Examples are given by Sørensen [2004-Sørensen] who described the determination of cohesive laws by measurement of the J Integral and end-opening of the cohesive zone of double cantilever beam specimen. On the contrary, other approaches can be found considering that the knowledge of constituent characteristic laws at the microscale is enough to reproduce the response at a macroscopic scale. Chaboche and Feyel [2000-Chaboche] used a finite element method called FE<sup>2</sup> technique (Fig.III-5) where the micromechanical local behaviour and criteria are incorporated directly into the finite element structural analysis.

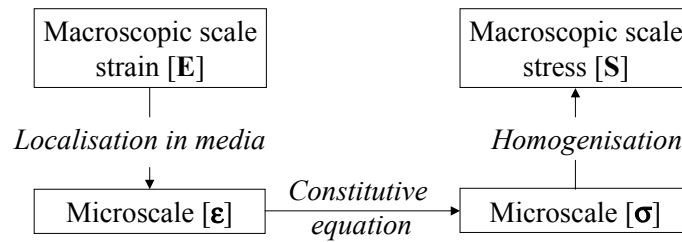


**Fig.III-5: Principle of FE<sup>2</sup> models**

### III.B.2/Dundurs parameters

In the following, a crack between two dissimilar materials is considered. The co-ordinate system is centred at the crack tip and the x axis lies parallel to a crack face (Fig.III-6).

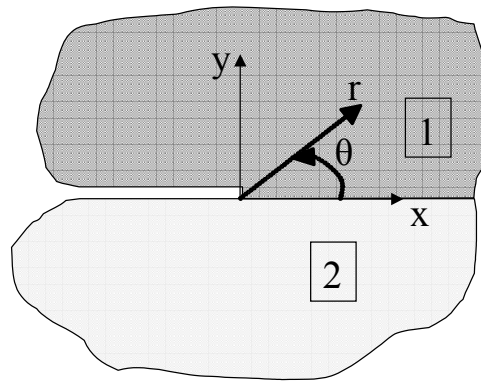


**Fig.III-6: Interface crack tip region**

When both materials are considered as elastic, homogeneous and isotropic with shear moduli  $\mu_1$  and  $\mu_2$ , Poisson's ratios  $\nu_1$  and  $\nu_2$ , respectively, the stress field depends on the two Dundurs elastic mismatch parameters [1969-Dundurs]. Dundurs has observed that the solutions to plane problems of elasticity for bimetals depend on these two non-dimensional combinations of the elastic moduli  $\alpha$ ,  $\beta$  and on the parameter  $\varepsilon$ .

$$\alpha = \frac{\frac{1-\nu_2}{\mu_2} - \frac{1-\nu_1}{\mu_1}}{\frac{1-\nu_2}{\mu_2} + \frac{1-\nu_1}{\mu_1}}; \beta = \frac{1-2\nu_2}{\mu_2} - \frac{1-2\nu_1}{\mu_1}; \varepsilon = \frac{1}{2\pi} \ln\left(\frac{1-\beta}{1+\beta}\right) \quad \text{Eq.III-7}$$

The bimaterial constant  $\varepsilon$  is responsible for the main differences of the linear elasticity solution for interfacial cracks in comparison to cracks in homogeneous media.

### III.B.3/Stress singularity

The stress field for an interfacial crack is described by a power-law stress (see Eq.III-8). Such a field can exist at the tip of a crack between two dissimilar materials or at the corner of an inclusion. The order of the stress singularity  $\lambda$  (complex or real) depends on boundary conditions and elastic properties.

$$\sigma(r,\theta) \cong kr^{\lambda-1}\tilde{\sigma}(\theta) \quad \text{Eq.III-8}$$

The coefficient  $k$  characterises the magnitude of the stress state in the region of the inclusion tip and is called the generalised stress intensity factor (GSIF) and is expressed in  $\text{Mpa}\cdot\text{mm}^{1-\lambda}$ . It is reasonable to make the hypothesis that failure occurs at a critical  $k$  value,  $k_c$ , like in a classical linear elastic fracture mechanics formulation, except that the critical value is associated with a discontinuity different from a crack in a homogeneous material.

The elastic solution can be expanded in the vicinity of the corner [2003-Leguillon] as

$$U(x,y) = U(0,0) + k_I r^{\lambda_I} u(\theta) + k_{II} r^{\lambda_{II}} u(\theta) + \dots \quad \text{Eq.III-9}$$

where  $(x,y)$  and  $(r,\theta)$  are respectively the cartesian and the polar coordinate system with the origin at the corner (see Fig.III-7) and  $U$  is the displacement of a point.

The first term of the development in the Eq.III-9 is a constant and corresponds to the rigid translation of the origin. The real exponents  $\lambda_I$  and  $\lambda_{II}$  lie between 0 and 1 and equal 1 only if the two materials are identical. They are called the singularity exponents and depend on the Young's moduli and Poisson's ratio of both materials. The associated modes are  $u_1(\theta)$  and  $u_2(\theta)$ . The coefficients  $k_I$  and  $k_{II}$  are assimilated to the generalised stress intensity factors.

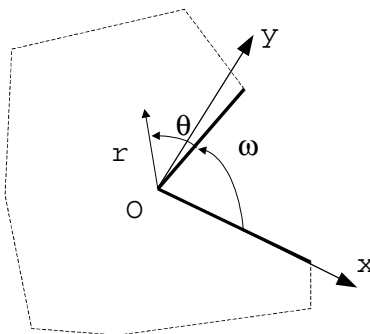


Fig.III-7: Coordinate systems

In the case of a notch where  $\omega=90^\circ$  in a homogeneous isotropic material,  $\lambda_I = 0,545$  and  $\lambda_{II} = 0,908$ . For a crack in a homogeneous isotropic material ( $\omega=0^\circ$ ),  $\lambda_I=\lambda_{II}=1/2$  like in linear elastic fracture

mechanics. Noda in [2004-Noda] proposed formulas to express the generalised stress intensity factors as a function of the Dundurs parameters for a crack in a homogeneous material under mixed mode loading as well as the case of a crack perpendicular to and terminating at a bimaterial interface with any aspect ratio under any combination of the materials.

It is interesting to remark that the main property of the J-Integral is to be path-independent. This remains valid as long as we consider only mechanical loads (mainly because in the considered contours to compute J, all sources of energy are outside). But under thermal loading conditions, sources of energy are located everywhere in the structures, including the considered contour, what leads to a path-dependence of a J Integral [2003-Leguillon]. To avoid this difficulty, Leguillon proposes a way to compute the GSIF by another contour integral (always path dependent under thermal loads), but shifts the stress state solution by a quantity of  $\alpha_i \Delta T$  where  $\alpha_i$  denotes the expansion coefficient of material i and  $\Delta T$  is the thermal load.

In the case of interfacial cracks, the singularity exponents  $\lambda_I$  and  $\lambda_{II}$  are equal to  $\lambda=1/2+i\varepsilon$  [1990-Hutchinson]. The near tip stress field is then described by the GSIF. It can be decomposed in a linear combination of two types of singularities, namely a coupled oscillatory field scaled by a complex k and a non-oscillatory field scaled by a real  $k_{III}$  [1991-Shih].

$$\sigma_{ij} = \frac{1}{\sqrt{2\pi}} \left( \operatorname{Re} \left( k r^{\frac{1}{2}+i\varepsilon} \right) f_I(\theta, \varepsilon) + \operatorname{Im} \left( k r^{\frac{1}{2}+i\varepsilon} \right) f_{II}(\theta, \varepsilon) + k_{III} r^{\frac{1}{2}} f_{III}(\theta) \right) \quad \text{Eq.III-10}$$

If we restrict the case to two dimensions and consider the stress state along the interface ( $\theta=0^\circ$ ) [2002-Dollhofer], the GSIF which measures the amplitude and phase of the external loading, allow to write

$$\sigma_{yy}(r) + i\sigma_{xy}(r) = \frac{1}{\sqrt{2\pi}} k r^{\frac{1}{2}+i\varepsilon} \quad \text{Eq.III-11}$$

Depending on the authors [2001-Molski], some think that it would be convenient to introduce a logarithm in the definition of this k:

$$k = k_I - ik_{II} = \frac{(1-2i\varepsilon)\sqrt{\pi r}(\sigma_{yy} - i\sigma_{xy})e^{i\varepsilon \ln(2a)}}{\cosh(\pi\varepsilon)} \quad \text{Eq.III-12}$$

where  $\varepsilon$  is the imaginary part of the stress field exponent  $\lambda$  at the crack tip, related to the Dundurs parameter  $\beta$ . The introduction of the logarithm leads to a loss of physical meaning of the k factors which no longer represent the material properties of structures. Thus, mixed mode conditions are always present at the crack tip and, as is the case for the decomposition into mode I and mode II, the k is then divided into symmetrical and anti-symmetrical components.

The stress intensity factors have the following units:

$$k = [\text{stress}][\text{length}]^{\frac{1}{2}-i\varepsilon} \quad \text{Eq.III-13}$$

$$k_{III} = [\text{stress}][\text{length}]^{\frac{1}{2}}$$

One may note that the displacement fields  $\delta_i$ ,  $i=x,y$ , or  $z$ , at a distance  $r$  behind the crack tip are given by

$$\delta_y + i\delta_x = \frac{2}{(1+2i\varepsilon)\cosh(\pi\varepsilon)} \left( \frac{1}{E_1'} + \frac{1}{E_2'} \right) k r^{i\varepsilon} \sqrt{\frac{2r}{\pi}} \quad \text{Eq.III-14}$$

$$\delta_z = \left( \frac{1}{\mu_1'} + \frac{1}{\mu_2'} \right) k_{III} \sqrt{\frac{2r}{\pi}}$$

with  $E' = E/(1-\nu^2)$  for plane strain and  $E' = E$  for plane stress.  $\mu$  is the shear modulus of each material. The relation  $1/\cosh^2(\pi\varepsilon) = 1-\beta^2$  should be noted.

### III.B.4/Mixed mode

According to [1990-Hutchinson], the relative proportion between normal and shear stresses varies in the sense of

$$r^{i\varepsilon} = \cos(\varepsilon \ln r) + i \sin(\varepsilon \ln r), \quad \text{Eq.III-15}$$

and this feature complicates the implementation of interfacial mechanics in several aspects. When  $\varepsilon \neq 0$ , the traction free line crack hypothesis is not fully respected. This implies that the crack faces interpenetrate behind the tip (with respect to Eq.III-14). Moreover, the factors  $k_I$  and  $k_{II}$  can not be straightforwardly interpreted as the mode I or mode II stress intensity factors. So, in order to introduce a characteristic quantity which represents mode I and mode II, one may define the mixed mode ratio  $\psi$  as the angle represented by

$$\psi = \text{Arc tan} \left( \frac{k_{II}}{k_I} \right) \quad \text{Eq.III-16}$$

In the case of an interfacial crack, these factors  $k_i$  are not well defined as we approach the crack tip. Since  $r$  tends to zero, the stress field shows an oscillatory part. Besides, one may choose between two different ways to define this mode mixity angle. One definition is based on the ligament stresses (stresses for  $\theta=0$ ) or on the stress intensities. For that, one may fix the distance  $L_0$  ahead of the crack tip where the stresses are taken, and then define  $\psi$  as a function of the length  $L_0$ .

$$\psi_{L_0} = \text{Arc tan} \frac{\sigma_{xy}(L_0, 0)}{\sigma_{yy}(L_0, 0)} = \text{Arc tan} \frac{\text{Re}(kL_0^{i\varepsilon})}{\text{Im}(kL_0^{i\varepsilon})} \quad \text{Eq.III-17}$$

The problem of the choice of  $L_0$  remains. Molski proposed to take the length equal to the crack length [2001-Molski]. Some authors [1998-Ikeda] choose twice the crack length, depending on the crack configuration (is the crack propagating along the free surface or within the material). One may have to take account of the different orientation in the coordinate system if a crack presents two tips (e.g. in Fig.III-8).

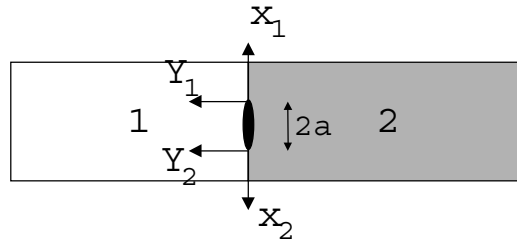


**Fig.III-8: Embedded crack between two dissimilar materials**

A length between the inelastic zone size and the specimen size is another sensible choice of  $L_0$ . Since the length  $L_0$  is arbitrarily chosen, it must be constant for a material pair, i.e.  $L_0$  must be independent of specimen size and specimen types. Let us note that when the distance  $L_0$  is changed to the distance  $L_1$ , the mode mixity angle is changed according to

$$\psi_{L_1} = \psi_{L_0} + \varepsilon \ln \left( \frac{L_0}{L_1} \right) \quad \text{Eq.III-18}$$

It may be necessary to underline that a mixed mode angle  $\psi_{L_0}=0$  is not generally associated with a pure mode I but represents a mode I at  $r=L_0$ , whereas at any  $r \neq L_0$  both mode I and II appear in combination.

A convenient measure of material mismatch producing phase variation with distance is the quantity  $\varepsilon^* = (180/\pi)\varepsilon \ln(10)$ . It can be interpreted as the change of the mixed mode angle in degrees for a distance increasing by a decade. One may introduce a second angle to complete the definition of the stress state: when  $\varepsilon=0$ , for cracks in a bulk material, the mode mixity can be defined in the usual way. In the space of the interface traction vector  $\mathbf{t} = \{\sigma_{yx}, \sigma_{yy}, \sigma_{yz}\}$ , one uses two angles  $\psi$  and  $\phi$  (Fig.III-9), where:

$$\tan \psi_{L_0} = \frac{\text{Re}(kL_0^{i\varepsilon})}{\text{Im}(kL_0^{i\varepsilon})} \quad \text{and} \quad \cos \phi = \frac{k_{III}}{\sqrt{|k|^2 + k_{III}^2}} \quad \text{Eq.III-19}$$

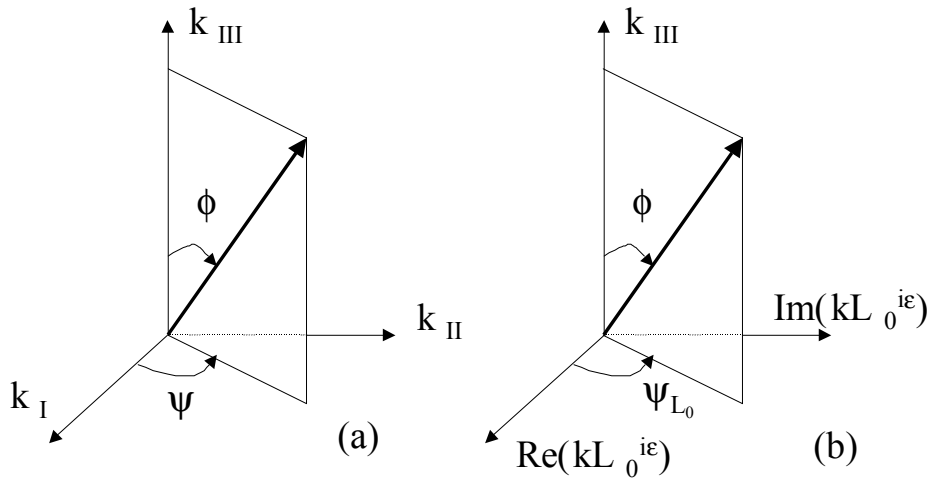


Fig.III-9: Mixed mode angle in the  $k_i$  space

### III.B.5/Energy release rate

The reason why the energy release rate  $G$  (or the  $J$  Integral in elastic solutions) is usually used for modelling the fracture process is that they are proportional to the sum of the square values of the Generalised Stress Intensity Factor [1988-Rice]

$$G = \left( \frac{\kappa_1 + 1}{\mu_1} + \frac{\kappa_2 + 1}{\mu_2} \right) \frac{k_I^2 + k_{II}^2}{16 \cosh^2(\pi \epsilon)} + \left( \frac{1}{\mu_1} + \frac{1}{\mu_2} \right) k_{III}^2 \quad \text{Eq.III-20}$$

where  $\kappa_i = (3 - 4\nu_i)$  for plane strain and  $\kappa_i = (3 - \nu_i)/(1 + \nu_i)$  for plane stress,  $\mu_i$  is the shear modulus for material  $i$ . Thus, for given loading conditions, that is to say in a given mixed mode angle  $\psi_{L_0}$ , one may measure the loading amplitude  $G$  necessary to break the interface and one can get the so-called toughness curve of the interface for the phase  $\psi_{L_0}$ , noted as  $G_c(\psi_{L_0})$ .

### III.B.6/Interface toughness curves

It has been generally observed that cracks in homogeneous isotropic brittle solids try to propagate on planes where local mode I conditions exist. As a consequence, one single critical parameter,  $K_{Ic}$ , is enough to control and predict fracture. By contrast, whenever planes of low crack resistance exist (e.g. composite materials with different fibre orientation in each ply) cracks may be led into these planes, independently of local mode mixity. Orthotropic materials are a good example where defined weak planes exist. By the same way, interfaces offer weak planes for crack propagation compared to bulk materials and depend strongly on mode mixity. In such cases, fracture resistance of weak planes is fully characterised by toughness values at various mixed mode angle (MMA).

For a given mixed mode angle (MMA)  $\psi_{L_0}$  (and  $\phi$  is given in three dimensions), the interface fracture energy (or interface crack

resistance)  $\Gamma$  is defined as the energy release rate at the onset of crack growth. The fracture energy  $\Gamma(\psi_{L_0}, \phi)$  is a property of the bimaterial interface. For a given material pair, it is a surface in  $k_i$  space, which, in principle, can be fully determined by experiments. A crack will not propagate unless the driving force reaches the toughness surface, i.e. the mixed mode fracture condition is

$$G(\psi_{L_0}, \phi) = \Gamma(\psi_{L_0}, \phi) \tag{Eq.III-21}$$

This prevails for a given length  $L_0$  in the definition of  $\psi_{L_0}$ . Especially,  $\Gamma(\psi_{L_0}, \phi)$  is the critical value of the energy release rate required to advance the crack along the interface under the MMA  $\psi_{L_0}$  and  $\phi$ , the latter being defined by the relative magnitudes of the in-plane shear to normal traction at  $r=L_0$ .

Liechti & Chai [1991-Liechti] describe a method to establish the range of in-plane fracture mode mixity and contact zone that can be obtained from a bimaterial sample. They measure the crack opening displacement and match the obtained values with finite element solutions to extract the mixed mode fracture parameters. They obtained an interfacial fracture energy as a function of mode mixture [1992-Liechti]. The Fig.III-10 shows an interfacial fracture energy curve obtained for Epoxy/Glass specimens for two different lengths  $L_0$  and for two different roughness  $\lambda$  of the glass surface.

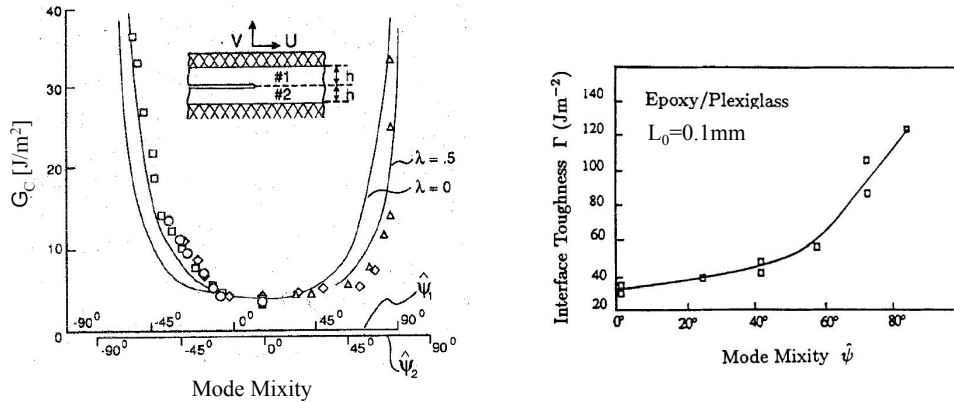


**Fig.III-10: Interfacial fracture energy curves for Epoxy/Glass from Liechti&Chai [1991-Liechti] and Wang&Suo [1990-Wang]**

### **III.C/Interfacial fracture toughness tests**

#### **III.C.1/Most common tests**

Many studies [1999-Sundararaman], [1988-Williams], [2001-Auersperg] deal with a large number of sample geometries for the experimental determination of interfacial toughness (Fig.III-11). Among them, the most common design are the Asymmetric Double Cantilever Beam ADCB and the Asymmetric End Notched Flexure ENF. While each beam can have the same thickness, it is called "asymmetric" since it consists of dissimilar materials. This double beam geometry is very convenient since it allows a variation in the loading with just one geometry. Generally, the validity of such tests is ensured through the control of the flaw inserted as pre-crack, the analyses of results and independence of geometry [2000-Davies].

Others tests for mixed mode conditions include: the Single Leg Bending (SLB), Mixed Mode Flexure (MMF) and the Cracked Lap Shear (CLS). In the Single Leg Bending test (SLB), a part of the bottom leg is missing so that the entire reaction force at this end is transmitted to the top leg. One may note that two configurations exist for this test: the stiffer material at the top or at the bottom to induce two distinct mixed mode fracture conditions in the interfacial crack tip neighbourhood. The MMF is convenient because a single load is applied and produces simultaneously mode I and mode II. The CLS is more used in composite materials characterisation.

Otherwise, a lot of tests are discussed in the literature. Some are designed to avoid the unstability of tests like the Stabilised End-Notched Flexure (SENF), the Four points End-Notched Flexure (4ENF), the Symmetric beam under three point-bending (S3PB) or the Asymmetric beam under three point-bending (A3PB).

The Symmetric Centre Cracked Beam (SCCB) specimen deserves special attention. Charalambides et al [1989-Charalambides] developed this specimen and provided analytical and finite element solutions. However, it was noted that this geometry allows the determination of the fracture resistance of bimaterial interfaces where the fracture toughness of the debonding layer material is relatively high. In this case, one has to take care to avoid a deviation of the crack path from the interface into the bulk. [1998-Hofinger].

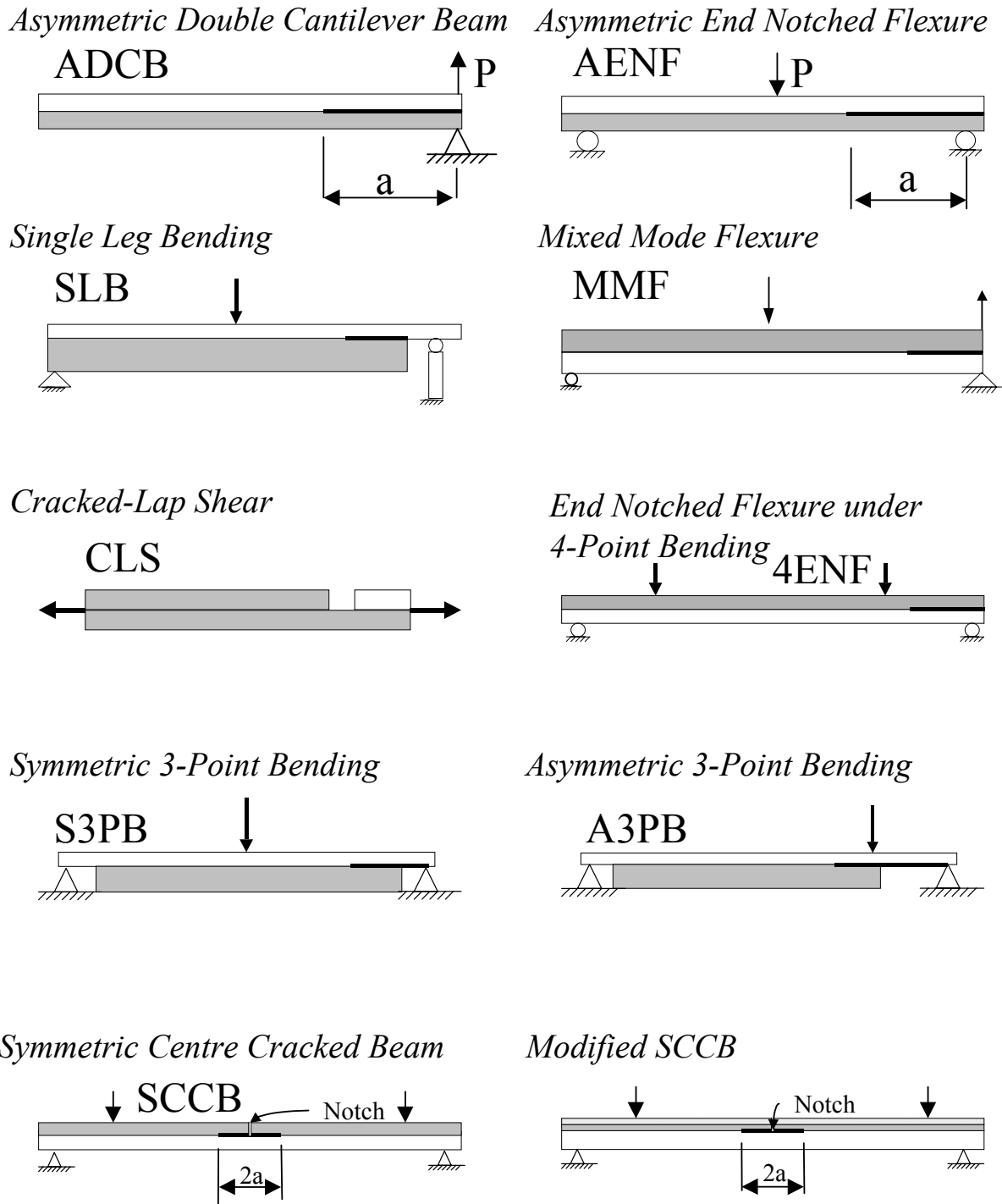


Fig.III-11: Interfacial fracture tests specimens

### III.C.2/Sandwich specimen

Another possibility to investigate interface toughness was developed for the study of metal-ceramic interfaces [1998-Diemer]. Diemer made use of a small DCB specimen which is embedded in a CT specimen.

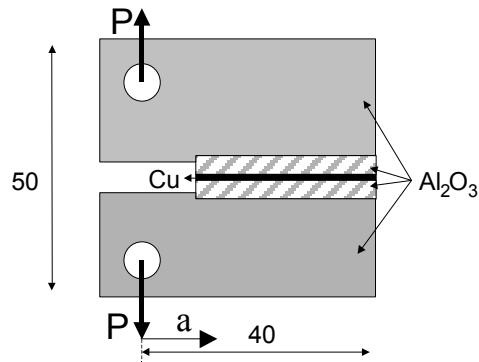


Fig.III-12: Sandwich specimen in CT-Clamps

In Fig.III-12,  $a$  is the crack length and  $F$  the force. The width of the copper layer is really small, in the order of  $100\mu\text{m}$ .

The idea of a sandwiched sample is also common to the Double Cleavage Drilled Compression test (DCDC) presented in Fig.III-13. This configuration was used By Turner and Evans [1996-Turner], Mao and Evans [1997-Mao] and Gaudette *et al* [1999-Gaudette] to study the mechanisms of crack growth along interfaces in glass specimen.

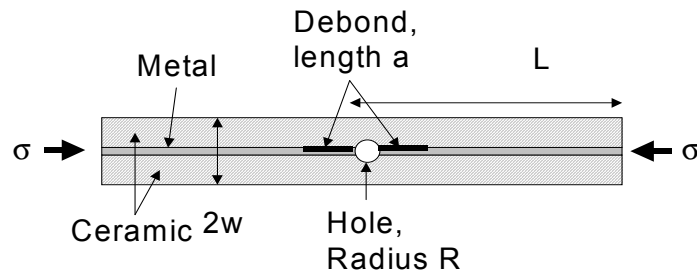


Fig.III-13: Double Cleavage Drilled Compression specimen

### III.C.3/Experimental determination of the Energy Release Rate

#### III.C.3.a/The compliance method

An analytical method to interpret the experimental results comes from the Linear Elastic Fracture Mechanics. It allows to compute the critical energy release rate (ERR) by derivation of the specimen compliance. This may be reached by the classical beam theory [1988-Williams]. Using the hypothesis that the global behaviour of the specimen is linear for each fixed crack length  $a$ , the ERR for a DCB test can be expressed as

$$G = \frac{P^2}{2B} \frac{dC}{da} \quad C = \frac{\delta}{P} \quad \text{Eq.III-22}$$

where  $P$  is the applied loading force,  $B$  is the width,  $a$  is the crack length and  $\delta$  is the crack opening in the case of the Asymmetric Double Cantilever Beam.  $\delta$  is also defined as the vertical displacement in the case of a bending test (like End Notched Flexure or Symmetric 3-Point Bending).

From the load-unload curves for different crack lengths, it is possible to determine the compliance corresponding to each crack length. The compliance  $\delta/P$  corresponds to the slope of the curve  $P=f(\delta)$ . From the measured data for  $C=f(a)$ , a linear regression allows to estimate an analytical function for  $C$ . Kanninen [1973-Kanninen] or Bathias [2003-Surcin] proposed a 3<sup>rd</sup> order polynome for  $C(a)$ . With this function it becomes easy to derive the compliance and to make use of the Eq.III-22.

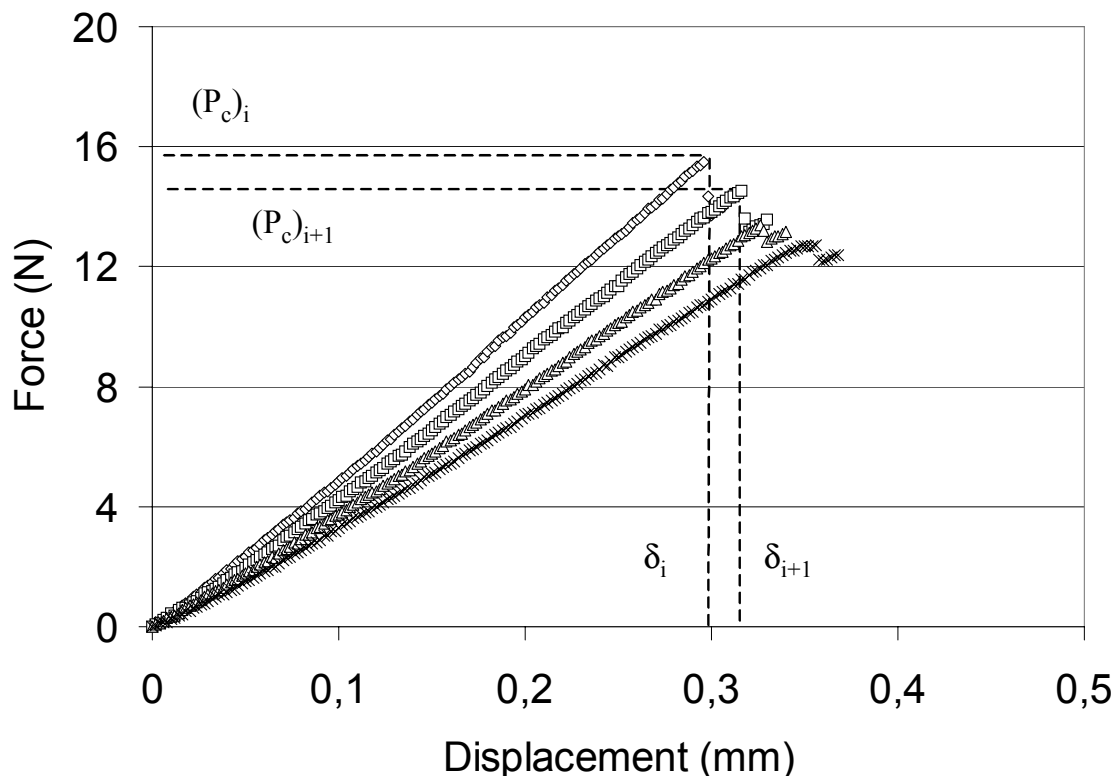


**Fig.III-14: Typical load-displacement responses of interfacial fracture test**

This method is widely used for specimens with a linear response which is the case for most configurations. Besides the Compliance Method, some studies deliver other forms of data processing to achieve the determination of the energy release rate.

### III.C.3.b/Area method of data reduction

An area method of direct data reduction can be used to determine the critical energy release rate from the test results. Using this method the interfacial fracture toughness can be determined without knowing any material properties but it is viable only if the interfacial crack is stable. The experimental procedure involves the loading of the Asymmetric Double Cantilever Beam with an initial crack length until a crack advance is noticed. The specimen is then unloaded (the crack growth stops) and reloaded further crack advance occurs. The data required for the area method is obtained by the load-deflection response for many load-unload cycles.  $G_c$  is calculated for each cycle as the difference in areas under the load-displacement curves divided by the incremental area of crack growth for that particular cycle. According to Sundararaman [2001-Sundararaman], the fracture toughness can be given by

$$(G_c)_i = -\frac{\Delta U}{b\Delta a} = \frac{(P_c)_i(P_c)_{i+1}}{2b(a_{i+1} - a_i)}(C_{i+1} - C_i) \quad \text{Eq.III-23}$$

The area is calculated using the compliance  $C_i$  and  $C_{i+1}$  with the critical load  $(P_c)_i$  and  $(P_c)_{i+1}$  corresponding to the crack length  $a_i$  and  $a_{i+1}$  and  $b$  is the width of specimen. The index  $i$  denotes the number of the crack increment.

### III.C.3.c/Closed-form analysis of the ADCB specimen

For the Asymmetric Double Cantilever Beam, Sundararaman gives the analytical solution from the classical plate theory.

$$G = \frac{P^2 a^2}{2B^2} \left( \frac{D_1 + D_2}{D_1 D_2} \right) \quad C = \frac{\delta}{P} = \frac{a^3}{3B} \left( \frac{D_1 + D_2}{D_1 D_2} \right) \quad D_i = \frac{E_i' h_i^3}{12} \quad \text{Eq.III-24}$$

where  $E_i' = E_i$  for plane stress and  $E_i' = E_i / (1 - \nu_i^2)$  for plane strain constraints, and  $D_i$  is the bending rigidity. Williams gives a general formula to compute the ERR also when the loads applied on the beams are not symmetric. It enables  $G$  to be found exactly at the crack tip

$$G = \frac{1}{16BEI} \left( \frac{M_1^2}{\xi^3} + \frac{M_2^2}{(1-\xi)^3} - (M_1 + M_2)^2 \right) \quad \text{Eq.III-25}$$

where  $M_i$  is the moment applied on the beam  $i$ ,  $\xi = [h_1 / (h_1 + h_2)]$ . To determine the mode mixity, the ADCB can be used and the ERR for each mode is given by

$$G_I = \left( \frac{P^2 l^2}{B^2 E h^3} \right) \frac{3}{4} \left[ 1 - \left( \frac{l}{a} \right)^2 \right]^2 \quad \text{and} \quad G_{II} = \left( \frac{P^2 l^2}{B^2 E h^3} \right) \frac{9}{4} \left[ 1 - \left( \frac{a}{L} \right)^2 \right]^2 \quad \text{Eq.III-26}$$

This is true for a crack in a homogeneous material in case of delamination. At  $a=l$  (Fig.III-15), we have pure mode II and at  $a=L$  pure mode I. Thus, a complete variation of the ratio is obtained from one specimen.

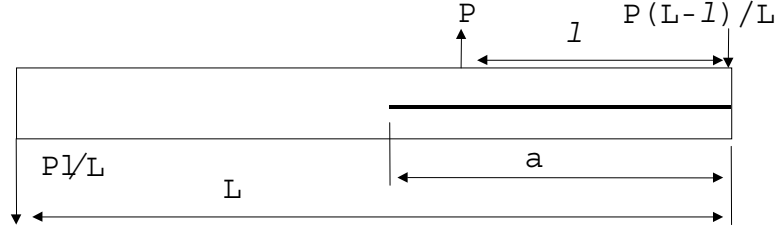


Fig.III-15: Variable ratio for mixed mode test

### III.C.3.d/Closed-form analysis of the SLB specimen

In the case of the Single Leg Bending (Fig.III-11) the compliance is defined as the displacement applied at the center-point  $\delta$  (the deflection) divided by the force  $P$

$$C = \frac{\delta}{P} = \frac{2L^3 + a^3(\rho - 1)}{12BD} \quad \text{Eq.III-27}$$

And the total ERR can be shown to be [1999-Sundararaman]

$$G = \frac{P^2 a^2 (\rho - 1)}{8B^2 D} \quad \text{Eq.III-28}$$

where  $B$  is the uniform width and the ratio  $\rho = D/D_T$ .  $D$  is defined as the effective bending rigidity of the uncracked regions and  $D_T$  as the effective bending rigidity of the top cracked regions

$$D_T = \frac{E'_T t_T^3}{12} \quad \text{and} \quad D = D_u - \frac{B_u^2}{A_u} \quad \text{Eq.III-29}$$

where  $t_T$  is the thickness of the top beam and  $E'$  the Young modulus, depending on the plane stress or plane stress constraints. In the above equations,  $A_u$ ,  $B_u$  and  $D_u$  are the axial, coupling and bending stiffnesses of the uncracked portion of the specimens, respectively and are given by

$$\begin{aligned} A_u &= E'_1 t_1 + E'_2 t_2 \\ B_u &= \frac{(E'_2 - E'_1) t_1 t_2}{2} \\ D_u &= \frac{E'_1 t_1 (t_1^2 + 3t_2^2) + E'_2 t_2 (t_2^2 + 3t_1^2)}{12} \end{aligned} \quad \text{Eq.III-30}$$

where the subscript 1 or 2 refers to material 1 or 2 and  $t_i$  is the thickness of beam  $i$ .

### III.C.4/About deflection and penetration

Whether an interface crack propagates within the interface or kinks out of the interface into one of the joined materials depends essentially on the mixed mode acting on the crack tip. An efficient criterion to predict the behaviour of the crack in a configuration (see Fig.III-16) has been proposed by He et Hutchinson [1989-He], [1990-Hutchinson]. The analysis is based on the classical competition of the ERR at the tip of a virtual extension either penetrating in the second material or deflecting along the interface.

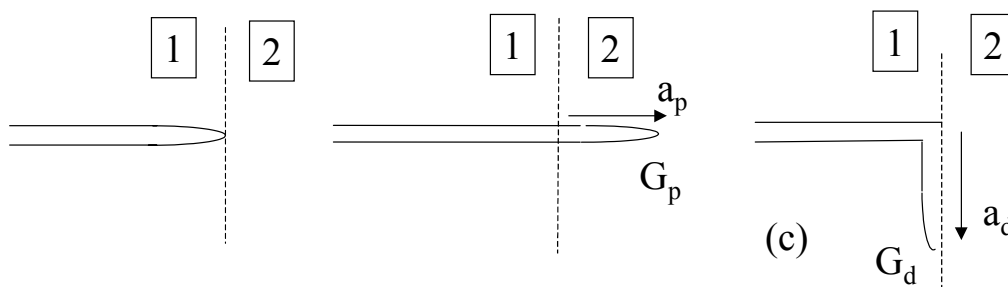


**Fig.III-16: (a) main crack at the interface ; (b) penetration of the interface ; (c) deflection at the interface**

Considering the two trajectories of crack advance: let  $G_p$  denote the Energy Release Rate for penetration and  $G_d$  for deflection. The penetration is possible if

$$G_{lc}^{(2)} \geq G_p \quad \text{Eq.III-31}$$

Eq.III-31 becomes a necessary condition to propagate in material 2. The penetrating crack is under a pure mode I. By the same way, a condition to deflect is

$$G_c(\psi) \geq G_d \quad \text{Eq.III-32}$$

The assumption made by Hutchinson is that the length increment  $a_p$  and  $a_d$  involved in these virtual processes of extension are assumed to be small and equal. The ratio  $G_d/G_p$  which turns out to be independent of the applied loads is compared to the ratio between the interface toughness  $G_c(\psi)$  for the relevant mode mixity and the toughness of material 2 in mode I. The condition for the crack to be deflected along the interface instead of penetrating is [1989-He]:

$$\frac{G_c(\psi)}{G_{lc}^{(2)}} < \frac{G_d}{G_p} \quad \text{Eq.III-33}$$

The assumption of  $a_p=a_d$  is a posteriori not intuitive. Leguillon [2001-Leguillon] proposed to revisit the He and Hutchinson's criterion assuming that  $a_d \neq a_p$ . The criterion is then written under the form:

$$\frac{G_c(\psi)}{G_{Ic}^{(2)}} < \frac{G_d}{G_p} = \frac{k_d}{k_p} \left( \frac{a_d}{a_p} \right)^{2\lambda-1} \quad \text{Eq.III-34}$$

Where  $k_i$  denotes the generalised SIF and  $\lambda$  is the exponent of singularity. It is obtained by assuming  $G_d=G_c(\psi)$  and  $G_p < G_{Ic}^{(2)}$  i.e. deflection can occur while penetration is inhibited.

### **III.D/Conclusion**

We introduced here the notions to apply in the case of an crack lying at the interface between different materials. We found that this topic was studied in different engineering frameworks such as composite materials, structural adhesive joints or electronic packaging. We presented specimens as well as methods designed for the experimental determination of the energy release rate. However, some fields of study are not mentioned. We do not consider either dynamic or fatigue effects although some studies appeared in the past few years ([1998-Abou-Hamda] or [2004-Pirondi]) deal with these topics. The influence of ambient medium may be noted.

In our work, we will study the behaviour of double beam specimens and attempt to determine the interfacial fracture energy curve. The linear response of the specimens tested in this work allows the use of the Compliance Method and the Area Method of Data Reduction will be chosen thanks to their easy implementation. The mixed mode angle will be extracted after the post processing from the numerical simulations.

---

# **Chapter IV**

## NUMERICAL METHODS AVAILABLE FOR FRACTURE MECHANICS ANALYSIS

## **IV/ Numerical methods available for fracture mechanics analyses**

### **IV.A/Introduction**

*Numerical modelling has become an indispensable tool in fracture mechanics, since few practical problems have closed-form analytical solutions. Moreover, geometry encountered in industrial environments and treated by simulations are more and more complicated and asked for more and more computational resources.*

*In this part, the main concepts are described, which were developed in the last decades for the treatment of fracture mechanics. Some numerical methods employed to solve fracture mechanics equations are browsed. We will see that the Finite Element Method is a widespread method, used in virtually all domains of structural mechanics. Since one of the fundament of FEM is the partition of the geometry into small shapes, the modelling of moving discontinuities like cracks becomes troublesome. That is why this method has been improved to model crack growth without remeshing. But there exist other methods the decomposition of the volume in small elements.*

## IV.B/Finite Element Implementation

The following methods for inferring energy release rate in elastic bodies were proposed in the mid 70's [1995-Anderson] and extended later to non-linear behaviour and large deformation at the crack tip. The FEM notations used afterwards are the classical ones.

### IV.B.1/Stiffness Derivative Formulation

Consider a two-dimensional cracked body with unit thickness, subject to Mode I loading. The potential energy of the body  $W_p$  in terms of the finite element solution is given by:

$$W_p = \frac{1}{2} [u]^T [K] [u] - [u]^T [P] \quad \text{Eq.IV-1}$$

where  $[u]$  is the vector of nodal displacements,  $[K]$  is the matrix of rigidity and  $[P]$  is the vector of nodal forces. We can also write  $G$  under this form:

$$G = -\frac{\partial W_p}{\partial a} = -\frac{\partial [u]^T}{\partial a} \{ [K] [u] - [P] \} - \frac{1}{2} [u]^T \frac{\partial [K]}{\partial a} [u] + [u]^T \frac{\partial [P]}{\partial a} \quad \text{Eq.IV-2}$$

where  $a$  denotes the crack length. Since  $[K] [u] = [P]$  and in the absence of traction on the crack face, the first and the third terms also vanish (loads are held constant). The energy release rate is therefore given by :

$$G = -\frac{1}{2} [u]^T \frac{\partial [K]}{\partial a} [u] \quad \text{Eq.IV-3}$$

Suppose that we have generated a finite element mesh for a body with crack length  $a$ , extended thereafter by  $\Delta a$ , there is no need to redraw the whole mesh, but just to accommodate the crack growth by moving elements near the crack tip and leaving the rest of the mesh intact. In such a process, the elements between  $\Gamma_0$  and  $\Gamma_1$  are distorted (see Fig.IV-1), such that their stiffness changes. This allows to determine the energy release rate from:

$$G = -\frac{1}{2} [u]^T \left( \sum_{i=1}^{N_c} \frac{\partial [K_i]}{\partial a} \right) [u] \quad \text{Eq.IV-4}$$

where  $[K_i]$  are the elemental stiffness matrices and  $N_c$  is the number of elements between the contours. It was demonstrated by Parks [1995-Anderson] that this expression of  $G$  is equivalent to  $J$  and is independent of the choice of the inner and outer contours.

One problem with the stiffness derivative approach is that it involves numerical differentiation, especially for thermal strain problems. That is why another approach has been developed to overcome these difficulties.

### IV.B.2/Continuum approach

DeLorenzi improved the virtual crack extension by considering the energy release rate of a continuum. This approach offers two advantages: the methodology is not restricted to FEM and it does not require numerical differentiation. The Fig.IV-1 illustrates this method. Material points inside  $\Gamma_0$  are translated to a distance  $\Delta a$  in the  $x_1$  direction, while points outside of  $\Gamma_1$  remain fixed. For an elastic material, or one that obeys to plastic deformation theory, deLorenzi showed that the energy release rate is given by

$$G = \frac{1}{\Delta A_c} \int_V \left[ \left( \sigma_{ij} \frac{\partial u_j}{\partial x_k} - w \delta_{ik} \right) \frac{\partial \Delta x_k}{\partial x_i} - P_i \frac{\partial u_i}{\partial x_j} \Delta x_j \right] dV - \frac{1}{\Delta A_c} \int_S t_i \frac{\partial u_j}{\partial x_k} \Delta x_j dS \quad \text{Eq.IV-5}$$

where  $w$  is the strain energy density,  $\Delta A_c$  the increase in crack area generated by the virtual crack advance,  $V$  the volume of the body and  $P_i$  the body forces and  $t_i$  are components of the traction vector. This expression, however, only applies to virtual crack advance normal to the crack front, in the plane of the crack.

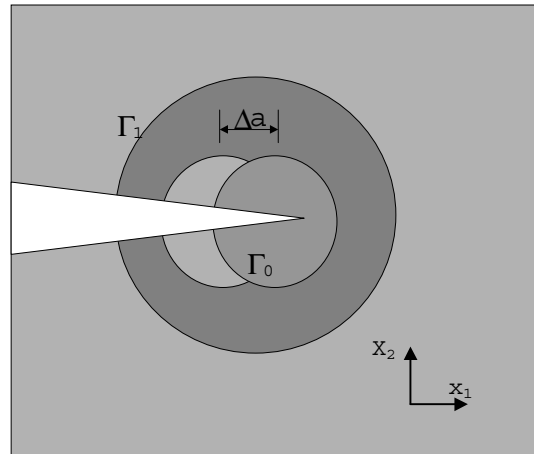


**Fig.IV-1: Continuum approach**

### IV.B.3/The domain integral method

Using the divergence theorem, we have seen that the contour integral can be expanded into an area integral in two dimensions or a volume integral in three dimensions over a finite domain surrounding the crack front. This domain integral is used to evaluate contour integrals in Abaqus [2004-Abaqus]. The method is quite robust in the sense that accurate contour integral estimations are usually obtained even with quite coarse meshes; because the integral is taken over a domain of elements surrounding the crack front, errors

in local solution parameters have less effect on energy-like quantities.

#### IV.B.4/Mesh design

The design of a finite element mesh is as much an art form as it is a science. Although many commercial codes have automatic mesh generation routines, crack problems require a specific sort of meshing. Crack tips cause stress concentrations. Thus, the closer a region is located at the crack tip, the more refined the mesh has to be. The J-integral is an energy measure; accurate J values can be obtained in linear elastic materials with a quite coarse mesh whereas non-linear cases need a reasonable refinement.

Concerning the kind of elements required for meshing of 2D and 3D problems, second order elements are commonly used, and to model the crack tip singularity, one side has to be collapsed (see Fig.IV-2). The square root and the  $1/r$  singularity can be built into a mesh using standard elements, provided that the crack tip is modelled with a ring of collapsed elements.

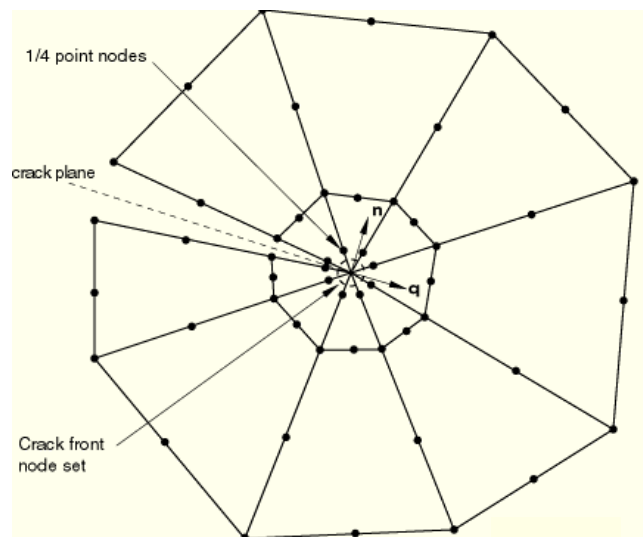


**Fig.IV-2: Adequate mesh for Fracture Mechanics**

If the nodes a, b and c are constrained to move together and if the midside nodes are moved to the fourth of the element length (see Fig.IV-3 and Fig.IV-4), then the stresses and strains obey a square root singularity. This combination is suitable for Linear Elastic Fracture Mechanics (LEFM) (Fig.IV-3(a)).

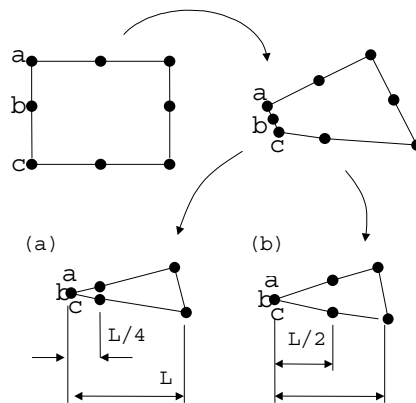


**Fig.IV-3: Degenerated 2<sup>nd</sup> order element, combination suitable for (a) LEFM and (b) EPFM**

If the midside nodes remain at the midside points and nodes a, b, c are allowed to move independently, only the  $1/r$  singularity is created. This combination is suitable for Elastic Plastic Fracture Mechanics (EPFM) (Fig.IV-3 (b)).

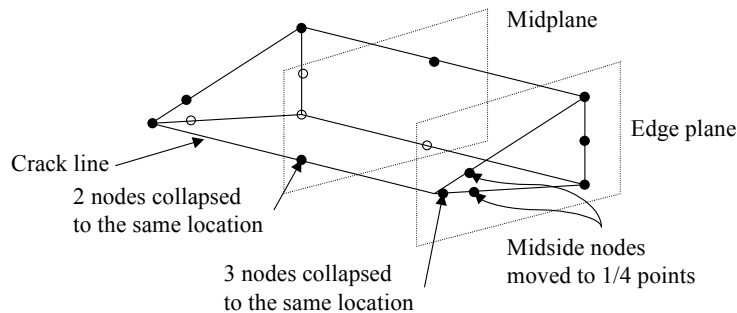


**Fig.IV-4: Collapsed 3D element**

## IV.B.5/Zencrack

The program Zencrack is a commercial software product of Zentech international Ltd. This program is interfaced with Abaqus or MSC.Marc (from MSC Software) or more recently with Ansys (from SAS IP, Inc.). It can be used in three ways [2002-Zentech]:

- To generate 3D finite element meshing containing one or more cracks
- To determine the distribution of maximal energy release rates and stress intensity factors along the crack fronts in bulk materials
- To calculate automatically fatigue crack growth in 3D bodies containing one or more cracks under arbitrary loading conditions.

Cracks are introduced into a valid mesh of the "virgin" structure by a mapping scheme which replaces standard brick elements by a "crack-block" [2000-Timbrell]. These crack-blocks represent either a quarter circular or a straight through crack front on one face using degenerated elements along the front (Fig.IV-5).

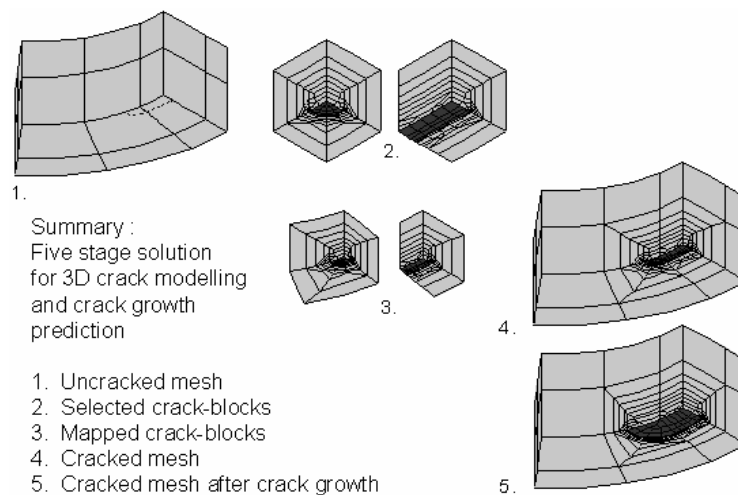


**Fig.IV-5: Example of meshing using crack-blocks**

Zencrack is interfaced with Abaqus or MSC.Marc or Ansys by a script where the user can control the location where the crack will be introduced, the size of the generated crack front section for each crack-block as well as the movement control of through-thickness crack-blocks through the mesh. The user can also define which type of loads is applied (sustained load, cyclic, randomised) and the options for crack propagation (e.g. propagation laws). Zencrack generates automatically the options for the computation of the J Integral, which avoids the difficult tasks for the user of generating an adequate mesh and introducing the contour integral keyword.

The result is a mesh containing the initial crack. This mesh is submitted for analysis to Abaqus [1994-Timbrell]. The results of the J Integral evaluations from Abaqus are post-processed by Zencrack which evaluates if crack propagation occurs or not and calculates if necessary, the propagation increment and the new position of the crack front. The new position is not necessarily in the same plane as the initial crack but can take into account an out of plane angle, estimated from the ERR after different positions. Further developments account for many parameters in crack growth such as multiple loads, thermal stresses and residual stresses [2002-Cook]. Techniques like heat transfer simulations or submodeling are compatible with Zencrack.

## **IV.B.6/Calculation of the Energy Release Rate**

### **IV.B.6.a/Virtual Crack Closure Technique**

An alternative method to calculate the crack driving force is the virtual crack closure technique. This method is based on the premise that the ERR equals the work required to close a unit area of the crack. This is done in a 2D analysis using eight-node finite elements (see Fig.IV-6)

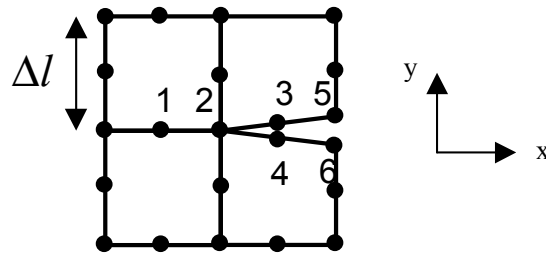


**Fig.IV-6: Scheme of the near tip nodes for VCCT**

In [2001-Harries], the following formulation is proposed for the 2D-case:

$$G = \frac{t_{y1}\Delta y_{34} + t_{y2}\Delta y_{56} + t_{x1}\Delta x_{34} + t_{x2}\Delta x_{56}}{2B\Delta l} \quad \text{Eq.IV-6}$$

In Eq.IV-6,

- B is the uniform crack width,
- $t_{y1}$  and  $t_{y2}$  are the nodal forces in y-direction at node 1 and node 2 respectively
- $t_{x1}$  and  $t_{x2}$  are the nodal forces in x-direction at node 1 and node 2 respectively
- $\Delta y_{34}$  and  $\Delta y_{56}$  are relative displacements in y direction
- $\Delta x_{34}$  and  $\Delta x_{56}$  are relative displacements in x direction
- $\Delta l$  is the characteristic length of elements surrounding the crack tip.

The advantages of this method are that it requires only one simulation step, and that the ERR for mode I and mode II can be distinguished. Since the materials properties do not appear in Eq.IV-6, the VCCT is convenient either for crack analysis in bulk materials or at the interface between two materials. It is, then, possible to compute the mode mixity angle. A third advantage is that it can be used with elastic or viscoelastic materials like resins whereas some limitations were found in [2002-Witller], for instance when the temperature domain involved in the simulation includes the glass transition temperature.

Another formulation for the VCCT can be found in [2000-Xiong]:

$$G_I = \frac{1}{2\Delta l} \{P_{yi} [t_{11}(v_m - v_{m'}) + t_{12}(v_l - v_{l'})] + P_{yj} [t_{21}(v_m - v_{m'}) + t_{22}(v_l - v_{l'})]\} \quad \text{Eq.IV-7}$$

$$G_{II} = \frac{1}{2\Delta l} \{P_{xi} [t_{11}(u_m - u_{m'}) + t_{12}(u_l - u_{l'})] + P_{xj} [t_{21}(u_m - u_{m'}) + t_{22}(u_l - u_{l'})]\}$$

$$t_{11} = 6 - \frac{3}{2}\pi \quad t_{12} = 6\pi - 20 \quad t_{21} = 0,5 \quad t_{22} = 1$$

$\Delta l$  is the crack tip element size,  $P_x$  and  $P_y$  are the x and y components of nodal forces, u and v are the x and y components of nodal displacements at the crack tip node i and surrounding nodes l, l', m, m'.

### IV.B.6.b/Modified crack closure integral

To evaluate the crack load in FE simulations, a virtual crack extension can be used. Furthermore a modified crack closure integral may be applied to analyse viscoelastic effects on interfacial delamination [2002-Wittler]. This was generalised for the 3D case:

$$G_I^* = \lim_{\Delta a \rightarrow 0} \int_0^{\Delta a} \sigma_{11}(\Delta a - r) \Delta u_1(r) dr \quad \text{Eq.IV-8}$$

$$G_{II}^* = \lim_{\Delta a \rightarrow 0} \int_0^{\Delta a} \sigma_{12}(\Delta a - r) \Delta u_2(r) dr$$

$$G_{III}^* = \lim_{\Delta a \rightarrow 0} \int_0^{\Delta a} \sigma_{23}(\Delta a - r) \Delta u_3(r) dr$$

where  $\Delta a$  is the virtual crack extension in x-direction and  $r$  is the distance of a given point in a polar coordinate system from the crack tip. The three modes are computed separately, and the sum of the three terms yields  $G^*$ , which is the ERR. The star in the exponent indicates that the calculation was performed via the crack closure integral. These integrals lead to the numerical form:

$$G_i^* = \frac{1}{2B\Delta l} (k_{12}(F_i^{(1)} \Delta u_i^{(1)} + F_i^{(2)} \Delta u_i^{(2)}) + k_{45}(F_i^{(4)} \Delta u_i^{(4)} + F_i^{(5)} \Delta u_i^{(5)}) + F_i^{(3)} \Delta u_i^{(3)}) \quad \text{Eq.IV-9}$$

where  $i=1$  to  $3$ ,  $k_{12}=0,5$  and  $k_{45}=0,5$ . When the nodes 1 and 2 respectively 4 and 5 are laying on the free edge then  $k_{12}=1$  respectively  $k_{45}=1$  (see Fig.IV-7).

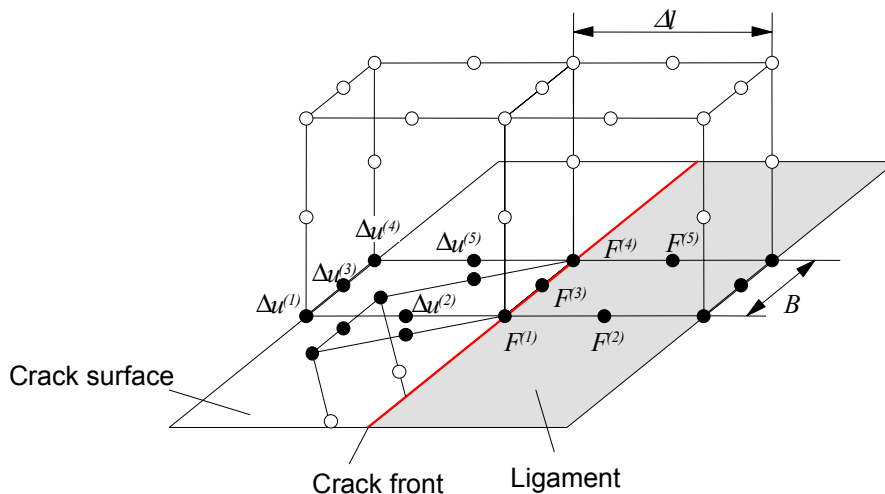


Fig.IV-7: Scheme of the near tip for the MCCI

## IV.B.7/Alternatives Methods

### IV.B.7.a/Meshless methods

The finite element method (FEM) is a powerful tool widely used in computational fracture mechanics. However, as indicated earlier, it induces complications since the crack must be taken into account in the topology of the studied device and that the crack tip singularity must be modelled accurately with degenerated elements to provide reasonable results. To avoid these laborious tasks, other alternative methods were developed in the FE framework where the crack problem is independent of the mesh. Such methods have been found to be efficient while simulating dynamic cases [2002-Chen].

The element-free Galerkin method (EFG) differs from the FE method in that the description is achieved by a model consisting of nodes and a description of the surfaces of the model [1996-Belythschko]. Each node possesses a domain of influence, usually circular in 2D and spherical in 3D, but does not extend across the boundaries. The crack is modelled in the EFG by free surfaces which can pass through the body. It is considered as a border for the domain of influence which can not be crossed.

In the example of Fig.IV-8, the initial crack (solid line) does not affect the shape function of the quadrature point  $q$  since straight lines connecting  $q$  to any surrounding nodes will not intersect the crack. But when the crack advances (shown in dashed lines) the point  $q$  will no longer belong to the domain of influence for node 1 and 2.

The shape functions can also take different forms. If the domain of influence is completely cut by the crack, the approximation will be discontinuous across the crack since the domain of influence will stop at the crack surfaces (see Fig.IV-9). However, near the crack tip, the domain is not completely cut by the crack, and how it is considered in the domain is a crucial parameter for the accuracy of the method [1996-Organ].

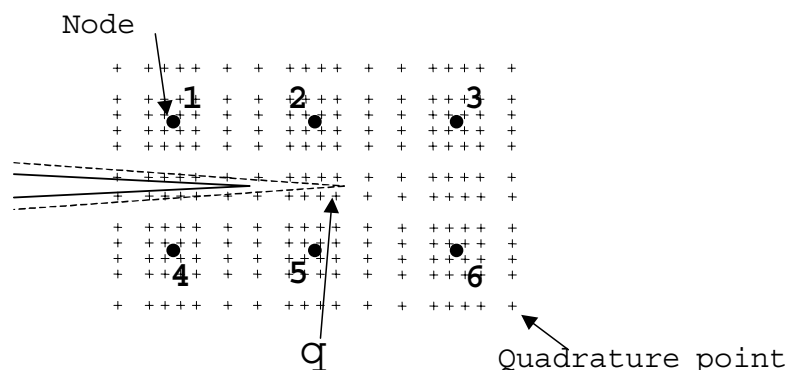


**Fig.IV-8: Crack advancing through two cells with 6x6 Gauss quadrature**

In Fig.IV-9(b), the node I still "sees" the crack tip and the domain behind the tip. The problem comes from the border line AB. The discontinuity within the domain has to be considered with special care. The solution employed in Fig.IV-9(b) is the so-called visibility method [1996-Belytschko-2]. Another method to treat the discontinuity is to employ the diffraction method in the approximation (see Fig.IV-10).

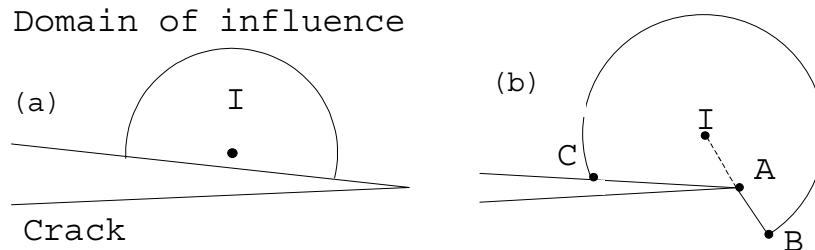


**Fig.IV-9: Domain of influence (a) completely cut ; (b) near the crack tip**

Furthermore, an enriched EFG has been developed to incorporate the singular stress function applied in the LEFM. This incorporation was found to be simpler and causes substantially less trouble than FEM techniques [1997-Fleming].

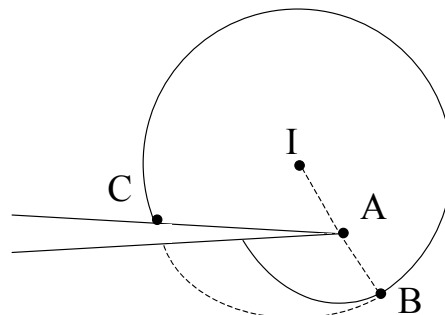


**Fig.IV-10: Domain of influence by the diffraction method**

The Finite Element Method is used as the constitutive block for the methods coarsely described below. Much of the theoretical and numerical developments of FE can be extended and applied in order to refine the accuracy of solutions for engineering problems.

#### **IV.B.7.b/H-, P-, HP-Version of FEM**

H-adaptivity denotes a refinement of the cell. This method subdivides the cell into smaller ones and increases by the same time the element density in regions of high-stress gradients while the P-adaptivity leaves the mesh density constant but increases the polynomial order of the element-shape function [2001-Stresscheck]. Reformulating a successfully running FE analysis model to a P-adaptive solution is less time consuming than remeshing the geometry. It is a powerful analysis tool but needs substantially

more processing time than the H-adaptive process. The HP-adaptive technique is a combination of both methods.

### IV.B.7.c/eXtended Finite Element Method (XFEM)

In a FE model, the elements near the crack tip and along the crack faces are enriched by asymptotic displacement fields. It was proven [1997-Fleming] that the use of discontinuous displacements along the crack produces a solution with zero traction along the crack faces (see Fig.IV-11).

In the eXtended Finite Element Method (XFEM) (also true for the Generalised Finite Element Method presented in the next section), a standard FE mesh is created without considering any internal discontinuities (such as cracks, voids, third bodies...) [2003-Karihaloo]. Then, these discontinuities are represented by additional displacement functions. In Fig.IV-11, nodes around the tip (circles) are enriched by crack tip functions while nodes along the faces (squares) are enriched with discontinuous functions. For example, the Heaviside jump function  $H(x)$  is a discontinuous function across the crack surface and is constant on each side of the face: +1 on one side and -1 on the other side.

The XFEM pays most attention to the enrichment of nodes to model the internal boundaries (cracks or inclusions) but shows a lack in the determination of accurate stress intensity factors. The SIFs are computed thanks to contour integrals via a post-processing procedure ([2003-Karihaloo]). This lack comes from the fact that only the first term of the displacement field is taken into account.

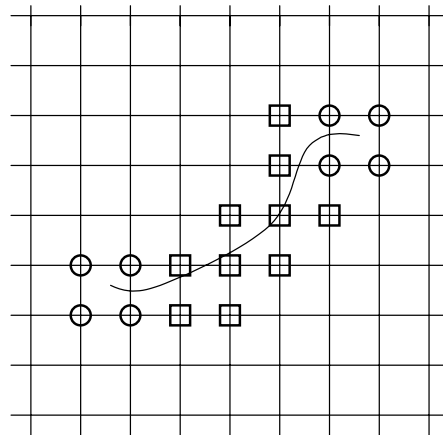


**Fig.IV-11: Uniform mesh with enriched nodes to model a crack**

However, this concept enables the integration of different types of singularities such as the cracks in bimaterial media [2003-Sukumar] (Fig.IV-12). In this case, the crack lies on element edges and no element partitioning is needed.

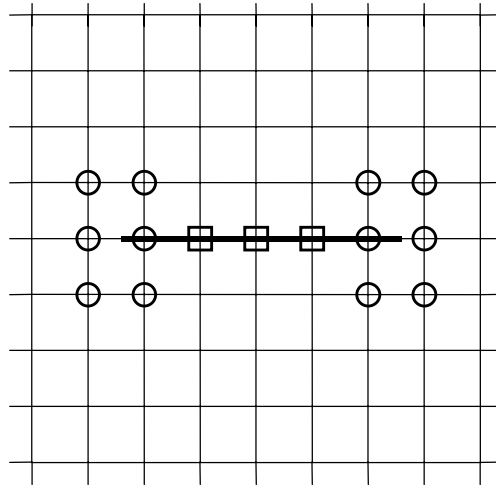


**Fig.IV-12: Enriched nodes for a bimaterial crack**

#### **IV.B.7.d/Generalised Finite Element Method (GFEM)**

The Generalised Finite Element Method (GFEM) is similar to the XFEM. The additional functions contain the analytically known or numerically computed handbook functions. Hence, the local and global solutions are enhanced within the PU method. However, the application is restricted within the range where these solutions were first computed. The P-adaptativity is allowed in the GFEM and provides accurate numerical solutions with relatively coarse meshes.

#### **IV.B.7.e/Boundary Element Method**

Deviation from FEM techniques, only the surface (or boundary) of the problem requires subdivision (see Fig.IV-13), thereby reducing the dimensionality of the problem and, thus, dramatically reducing the effort involved in obtaining a solution. The deep going analytical formulation of the method as boundary integral equation process with fundamental solutions ensure the high precision of the results [1997-Gaul].

The boundary integral equations are discretised through finite element on the boundaries. After this algebra formulation and the boundary conditions are sufficient to compute the unknown boundary quantities. The BEM let the possibility to compute the quantities at any point in the domain and not only at the discretised points.

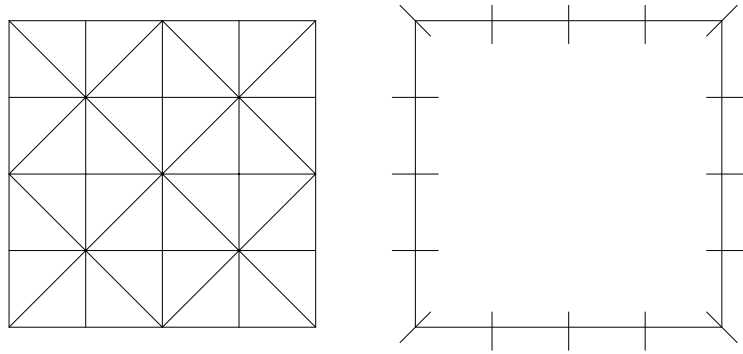


**Fig.IV-13: Discretisation with FE and BEM**

Numerical problems among other singularities in field quantities and the derivation of these closed to boundaries can be handled by convenient formulations. Other limitations are in the use of constitutive properties. They have to be homogeneous in the studied domain. Inhomogeneous domains are to be treated by a substructure technique.

Since this method is not so widely used as the FEM, the Boundary Element Method is for the moment an important complement to the Finite Element Method but can not replace it. Nevertheless there already exist softwares having implemented this method and which are employed in the framework of fracture mechanics.

## **IV.C/Conclusion**

*We saw the difficulties necessary to introduce a crack in a geometry. The FEM is the most widely used technique and has benefited from decades of experience in simulation and computational resources to be improved but the major problem remains that this technique relies on continuum theory, and then does not predict when fracture will occur.*

*As a consequence of the review of possible techniques, the work concentrates on the usage of the commercial package Abaqus, linked with Zencrack. But one should always keep in mind that computer modelling can not replace experimentation.*

---

---

# **Chapter V**

## EXPERIMENTAL AND NUMERICAL METHODS

## V/ Experimental and numerical methods

### V.A/Introduction

*In order to correctly predict the behaviour of a crack in a real component, the material parameters required by the underlying models need to be accurately determined. Thus, special experimental techniques need to be developed.*

*For this propose, we have to distinguish two different cases :*

- *The first one is the case where a crack is located in a homogeneous material. By now, our task will be to see if the crack :*
  - *Will grow slowly by means of a study under subcritical conditions, in which case one should be able to predict the time-to-failure of the device*
  - *Or if the crack will propagate suddenly like in the case of brittle failure.*
- *In the second case, a crack is already initiated at the interface between two different materials. Our propose is then to be able to say :*
  - *If the crack propagates along the interface*
  - *Or if it is deflected into the bulk, and in which direction.*

*The whole experimental process will be described which was used in order to study the crack behaviour in the case of homogeneous materials as well as in the case of interfacial cracks.*

*This process contains the handling of different sorts of specimens, the Compact Tension specimen (CT) to study cracks in homogeneous materials and the double cantilever beam (DCB) specimens to study cracks between two different materials. The experimental set-up for testing of specimens, the means used to record the results, and the way these data are processed will be listed. Ar the same time, the simulation techniques are introduced.*

## **V.B/Experimental work**

### **V.B.1/Objectives**

The main objective is to record the appropriate data in order to be able to predict the behaviour of a crack in a component under thermal and mechanical loads. Concerning the cracks in homogeneous materials, the interest focuses on only one type of specimen and two resins. And for interfacial cracks, we will proceed with double cantilever beam specimens formed by the assembly of one of these resins and a thermoplastic plate.

### **V.B.2/Preparation of specimens**

#### **V.B.2.a/Preparation of the resin**

Common to the two types of specimens, the resin is prepared by mixing the resin with a hardener, potted in a mould and then put in an oven for the gelification and curing.

The resin alone is preheated, before the hardener is added. The compounds are mixed together while the mould is preheated. Then the mixture is poured in a mould and put in the oven at about 70°C for the gelification phase for a couple of hours, the curing phase follows at a higher temperature for another couple of hours.

#### **V.B.2.b/Preparation of Compact Tension Specimens**

A very simple mould geometry is used for this kind of specimen. We cast the resin in the mould to get a plate with the dimensions 160x160x6 mm. This plate is then cut into smaller parts with a size of 24x27mm<sup>2</sup> and a notch is introduced.

#### **V.B.2.c/Preparation of Double Cantilever Beam Specimens**

This type of specimen needed to pay more attention during handling. Since it consists of the assembly of two different materials, the way to join the two materials need to be considered. Another type of mould was especially designed for these aims. For this purpose, thermoplastic plates with the dimensions 125x25x2mm<sup>3</sup> used as the "upper beam" of the double cantilever beam specimens were degreased with alcohol. The "lower beam" is furnished by a potted mass. The specimen-"family" was then constituted by different resin beam thicknesses of 2,4 and 10mm. In Fig.V-1, one mould type is depicted with a thickness of 4 and 10mm can be manufactured. Fig.V-2 shows a

specimen with a 4mm thick resin layer and a 2mm thick thermoplastic beam.

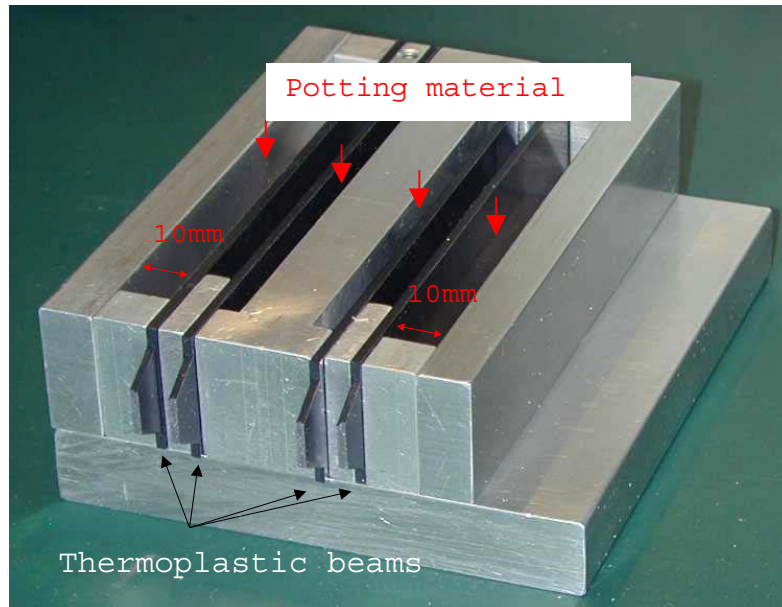


**Fig.V-1: Mould for double cantilever beam specimens**

To introduce a crack, in other words to produce pre-cracked specimens, each thermoplastic plate was covered at one end with a Teflon film and put into the mould.

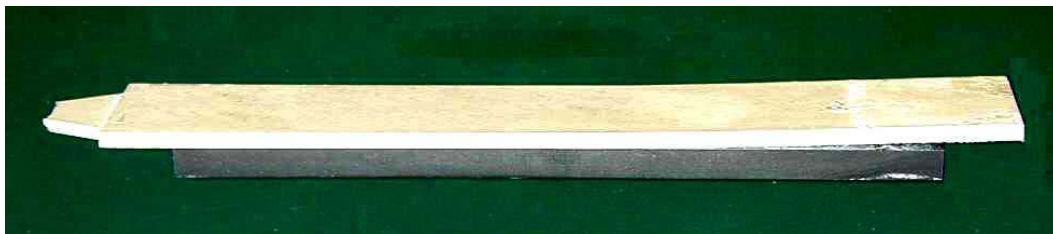


**Fig.V-2: Examples of a precracked double cantilever beam specimen (thickness of resin: 4mm, thermoplastic 2mm)**

Mould-release agent was put on surfaces in contact with the resin to ensure an easy demoulding.

### **V.B.3/Testing devices**

#### **V.B.3.a/Optical crack tracer in the case of Compact Tension specimen**

In order to measure the fracture toughness  $K_{Ic}$ , Compact Tension specimens are investigated (Fig.V-3). One may note the importance of data independent of the specimen size. To achieve this, it is essential that the plastic zone has to be smaller than the specimen size  $W-a$ ,  $a$  and  $B$ , where  $W$  is the width,  $a$  the crack length and  $B$

the thickness. This condition can be controlled by application of the ASTM Standard D5045-99 [1999-ASTM].

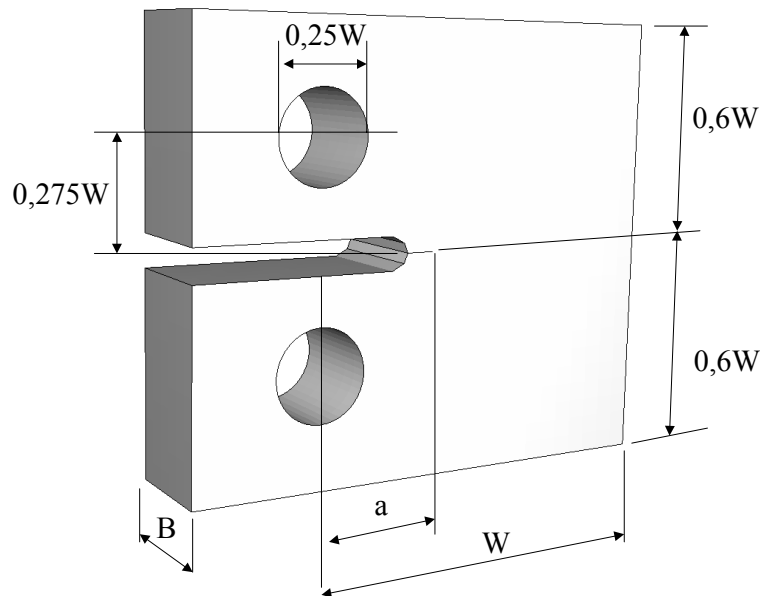


**Fig.V-3: Specimen configuration as specified in Test Method D5045-99**

Besides, the specimen size has to fit the domain size of application as well as to maintain the consumption of material as small as possible. For our purpose, a width of 20mm and a thickness of 6mm were chosen.

Since a "non-ideal" pre-crack leads to an overestimation of values from  $K_c$ , the introduction of a proper pre-crack is an essential step in the preparation of the test. A small v-shape notch was introduced at the tip of the "main" notch by tapping with a razor blade until the appearance of a crack. This leads naturally to a non-ideal pre-crack but then the specimen is loaded once or twice until crack propagation is noticed (detected by a drop of the force by 0,3%).

These tests are conducted on a tensile machine from Zwick. The force is monitored by a load-cell with a capacity of 1000N and displacement values come from the movement of the actuator.

To achieve the  $K_c$  measurement, an O.C.T.-device (Optical Crack Tracer) was used [2000-Uhlig]. The procedure is based on digital recording of images from the specimen surface (see Fig.V-4). The crack length is determined by a digital imaging software by treating the contrast difference in each image (see Fig.V-5). The  $K_c$  factor is computed from the force and the crack length according to the relation [1999-ASTM] (and for further details see Chapter II, Eq.II-27)

$$K = \frac{F}{B\sqrt{W}} f\left(\frac{a}{W}\right) \quad \text{Eq.V-1}$$

The cases of visco-elastic characterisation for different load rates and different temperatures were studied by Wittler [2002-Wittler]. He applied the principle of the master curve for visco-elastic behaviour to the fracture toughness and determined the limit of validity of such assumptions.

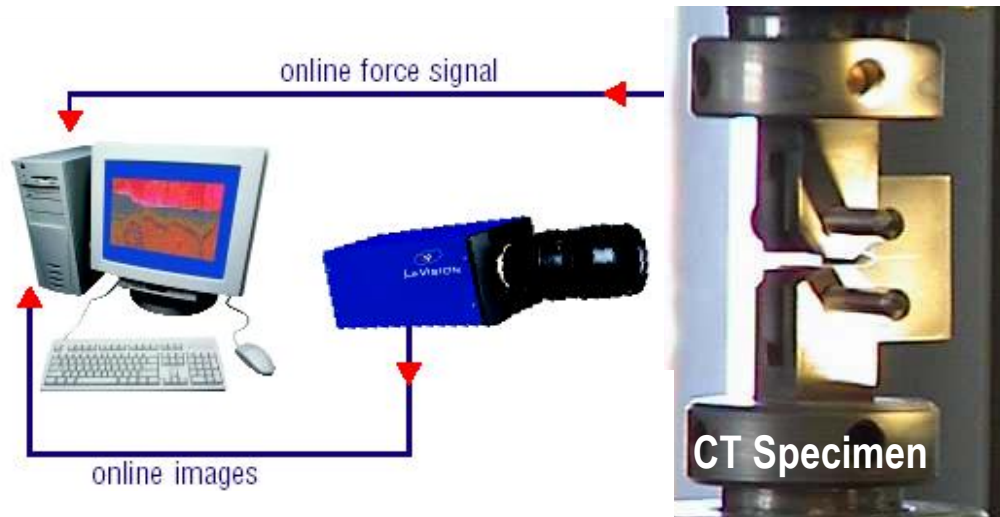


**Fig.V-4: Optical Crack Tracing**

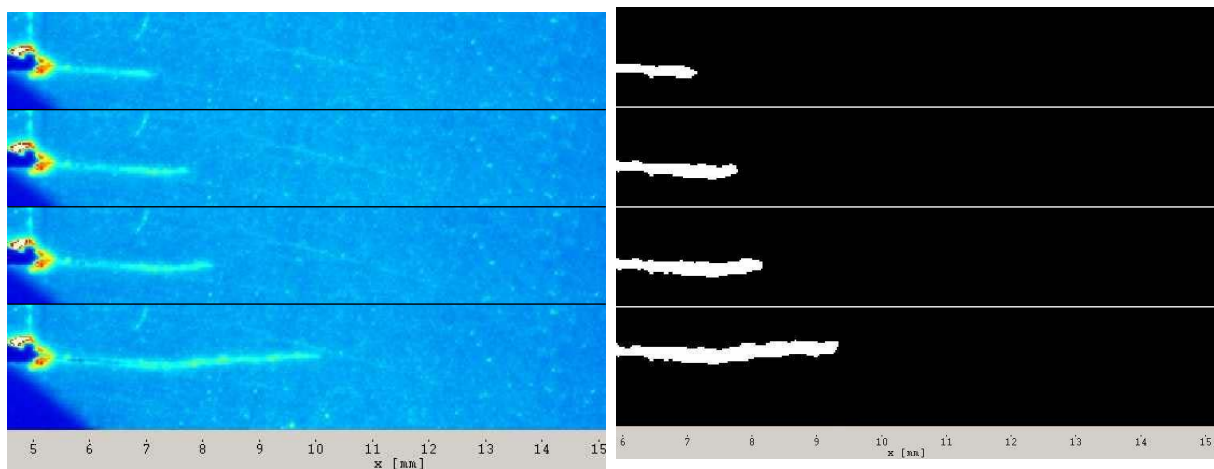


**Fig.V-5: Set of images recorded during a test and after post processed**

The crack length is determined for each image while the force is recorded at the same time. The relation from Eq.V-1 allows us to compute  $K_{Ic}$  and the following type of diagrams are then available (see Fig.V-6 and Fig.V-7).

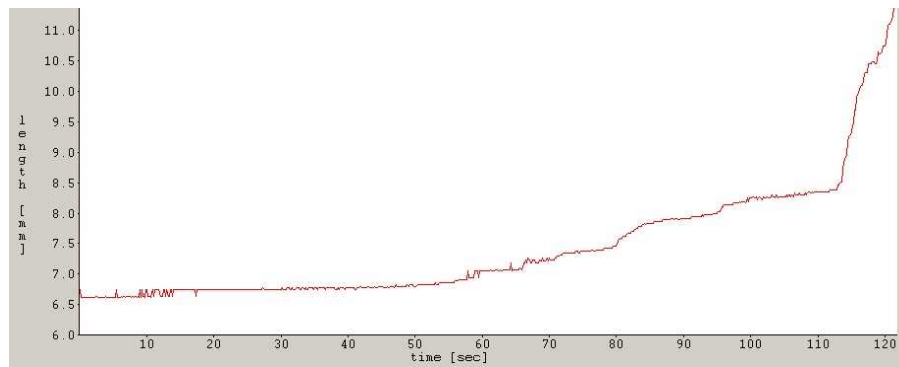


**Fig.V-6: Evolution of crack length of a CT specimen during a test**

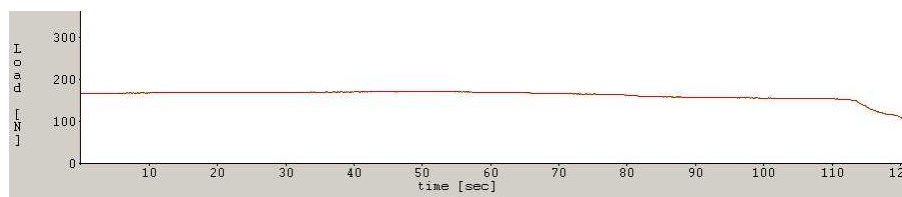


**Fig.V-7: Evolution of load applied on a CT specimen during a test**

### V.B.3.b/About subcritical crack growth

The knowledge of subcritical crack growth behaviour, also termed slow crack growth, may be necessary while designing structural components. In fact, under certain stress or environment conditions, imperfections, flaws or cracks can slowly extend and lead to time-dependent fracture. Cracking can therefore occur at loads below the fracture toughness  $K_{Ic}$ , and the threshold (for instance denominated  $K_I^*$ ) at which cracking starts depends widely on environmental conditions [2002-Wiederhorn]. However, under conditions leading to subcritical crack growth at  $K_I < K_{Ic}$  the dynamics of crack propagation can be uniquely described by the stress intensity factor  $K_I$  at the crack tip and a corresponding crack velocity  $da/dt$ , and the relation between  $da/dt$  and  $K$  can be written as

$$\frac{da}{dt} = A_I K^{n_I} \quad \text{Eq.V-1}$$

To measure the parameters  $A_I$  and  $n_I$ , the idea is to apply a constant load. Thanks to the OCT-device described above, the  $K_{Ic}$  is known. For a precracked specimen, the crack length is known. It is then possible to apply a force corresponding for instance to 90% of the fracture toughness. The crack growth rate can be calculated by measuring the final and initial values of crack length and the time during which the force is applied. This experimental approach is particularly useful for determining the  $da/dt=f(K)$  at low crack speed and therefore the test can be repeated several times on the same specimen [1975-Beaumont].

### V.B.3.c/Double Cantilever Beam Specimens

#### Presentation

The aim of this part of the work is to determine the behaviour of interface cracks. The literature investigation leads us to the choice of double cantilever beam specimens similar to those described in the Asymmetric Double Cantilever Beam (ADCB). The reason for this choice is that ADCB specimens allow a wide variation in loading conditions, realised by a special testing device which was developed in this work (Fig.V-8).

The particularity of this device is the allowable variation of the orientation. It will help us to test the specimens in such different manners that with one type of geometry we can afford to reach a wide range of mixed mode angles and to be able to determine the interfacial toughness curve for a given couple of materials.

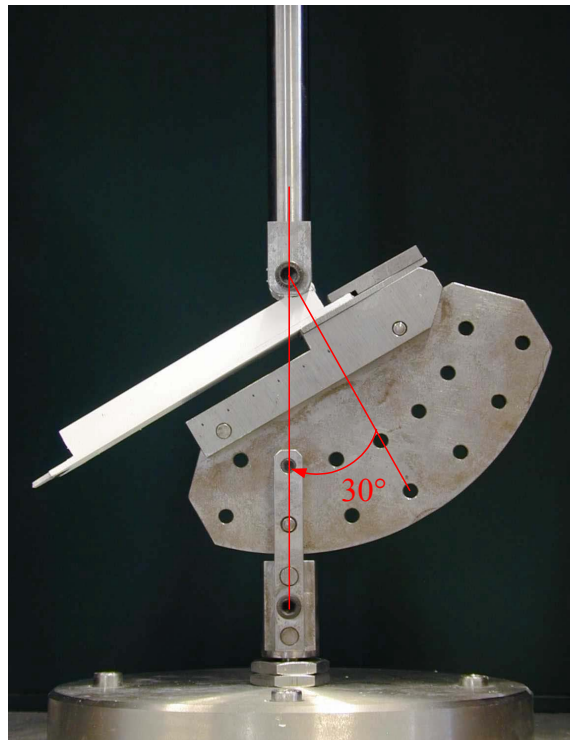


**Fig.V-8: Testing device for bimaterial specimen (configuration +30°)**

The specimen is clamped on the pre-cracked side and a block is glued on the top of the specimen (not visible in the Fig.V-8 but present in Fig.V-9) which enables the loading of the specimen. An important remark should be made here: the position 0° should not be confused with the ADCB configuration. Although the load is always applied in the normal direction to the crack plane, the reaction force in the ADCB is along the same axis as the applied force while in the configuration 0° it is with a certain angle. This leads to a different load condition and mixed mode.

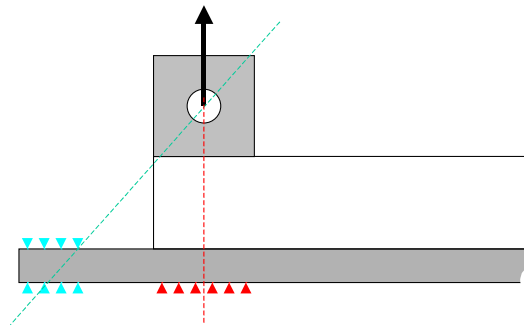


**Fig.V-9: Modelling the difference between the ADCB and the configuration 0°**

The tests are conducted using a uni-axial loading frame in the Texture-Analyser from Stable Micro Systems as the expected critical loads are very small in magnitude. All tests are run under controlled displacement loading. The displacement rate is in a range of 0,01 to 0,05mm/min for all tests and the experimental displacements are acquired during the tests by the displacement of the traverse. The resulting load is measured by a 2500N load cell capacity. The approximate resolution is 1 $\mu$ m for the applied displacement and 0,01N for the measured load. In this part, tests for one material couple (thermoplastic/resin) for different specimen geometry and loading conditions are reported.

#### Measurements

For measurement of interface specimens, the same optical measurement device for the crack length is used again here as in case of the bulk specimens to determine the crack length after each load-unload cycle. The value of the force or the displacement is then used for an experimental determination of the interfacial fracture toughness. The final evaluation is provided by numerical simulations which deliver  $K_{I}$ ,  $K_{II}$  and the mixed mode angle.

#### Data processing

In the chapter II-D-2-b, the "Area method of Data Reduction" (AMDR) to compute the interfacial energy release rate  $G$  was already introduced. The specimen is loaded until either a crack advance is noticed (or is heard) or a load drop is recorded. It is then unloaded and immediately reloaded. As written below, the test is recorded and the crack length is extracted (Fig.V-10). However, depending on the assembly of materials, the contact surface (or the interface) may not offer enough contrast, especially if both materials are of the same colour, or on the contrary a too high contrast (see for instance the specimen in place in Fig.V-8) to detect an eventual crack tip. For this reason, the specimen surface pointing towards the digital camera is sprayed with a dye to obtain a uniform coloured surface state. The crack creates a trace in the dye layer and is then easier to detect. However, digital image processing with the help of different filters from the measured

image sequence taken during crack propagation is always profitable if a high precision in the crack length determination needs to be achieved (Fig.V-11).

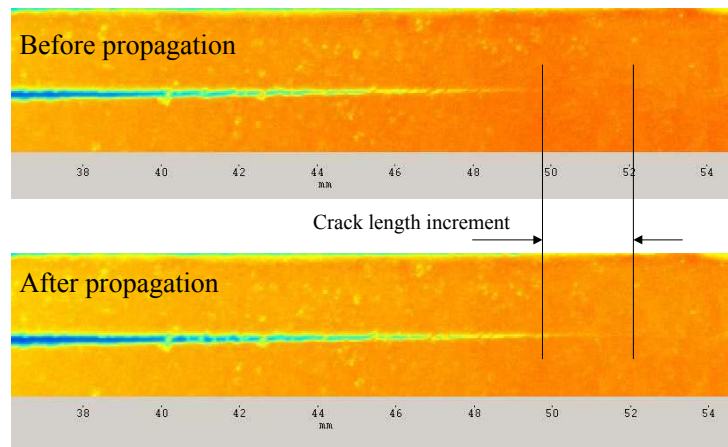


**Fig.V-10: Crack detection for double cantilever beam specimens**

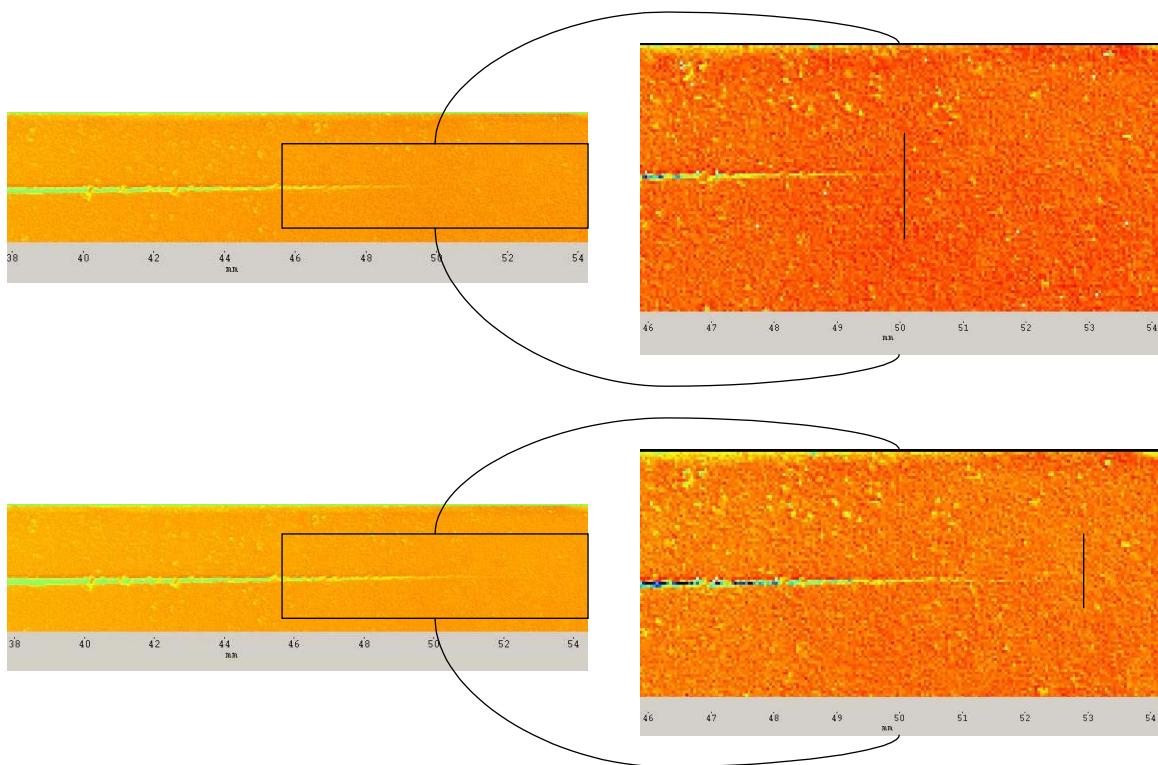


**Fig.V-11: Crack detection with filters: example on the Laplace Edge Crack Detection, crack tip at 50,07mm before crack advance and at 52,94mm after crack advance**

### Validity of the tests

For a specimen with a lower beam of 10mm thickness for the resin and an upper beam of 2mm thermoplastic, tested under an angle of  $0^\circ$ , a sequence of load deflection curves as depicted in Fig.V-12 can be obtained. Clearly the response is linear.

A diagram as given by Fig.V-12 allow us to extract for each test:

- the slope (corresponding to the inverse of compliance)
- the maximal force and displacement
- and the analysis of the video sequence additionally yields the crack length.

From the maximal force and displacement, thanks to the AMDR the energy release rate can directly be computed. The problem of this method is that the results depend strongly on the precision of each data source. This can lead to a great scatter of the results, and sometimes a negative energy but it helps us to receive a first estimation of the ERR.

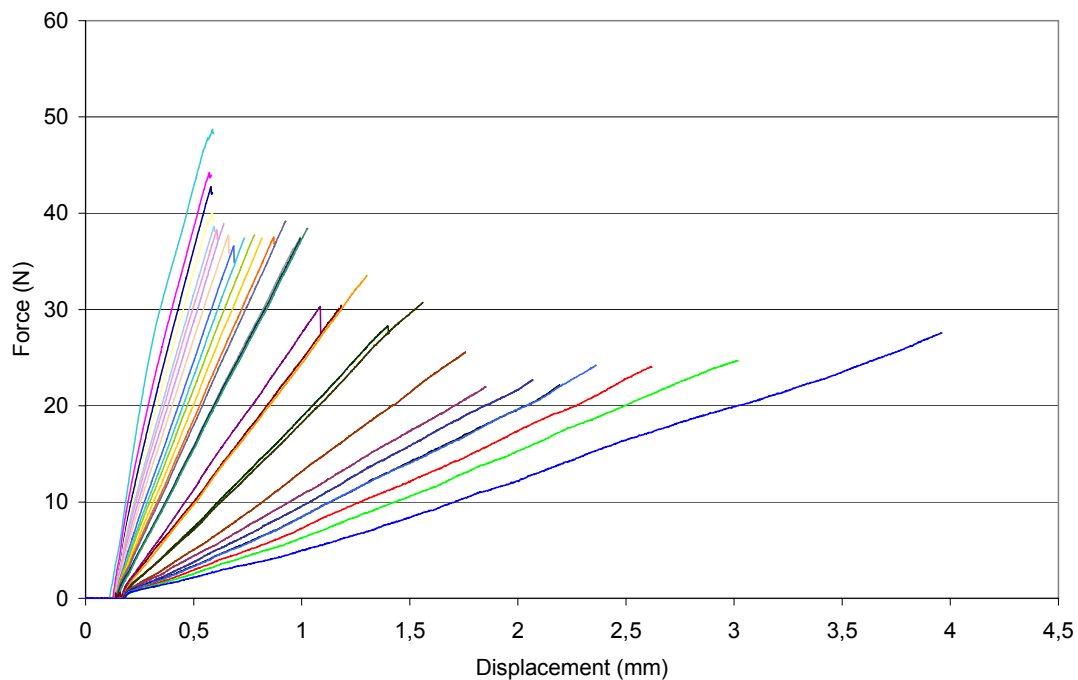


**Fig.V-12: Force-displacement curves for a typical test**

From the force and displacement curve, we get the compliance. For each crack length, we have a compliance value. It is possible to interpolate the set of compliance data by a polynomial function [2003-Surcin]. When comparing the results between a third order and a second order polynomial fit, it is found that the second order polynomial function is fully satisfying (see Fig.V-13). With this analytical function, it becomes easy to derive the compliance

according to the crack length and to introduce the derived function into the computation of the ERR.

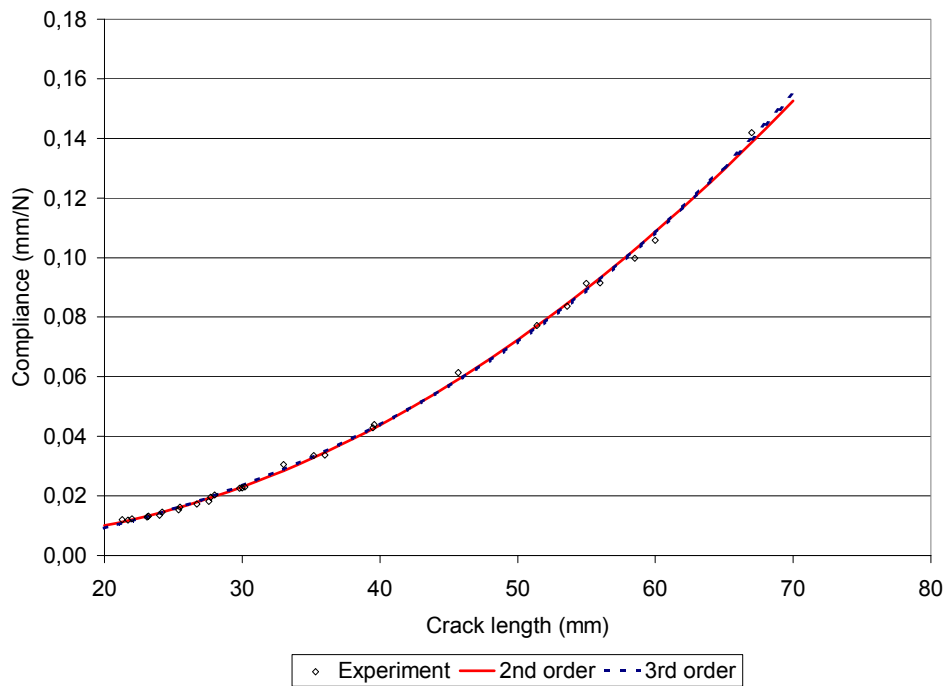


**Fig.V-13: Comparison between 2<sup>nd</sup> order and 3<sup>rd</sup> order polynomial interpolation function for the compliance**

The Area Method of Data Reduction delivers a first approximation of the specimen energy release rate. As shown in the Fig.V-14, the AMDR may not be really reliable and depends strongly on the precision of the different sources of data. On the contrary, the linear response of the specimen allows a satisfactory determination of the compliance and let the Compliance Method be used as second method to obtain a basis for comparison.

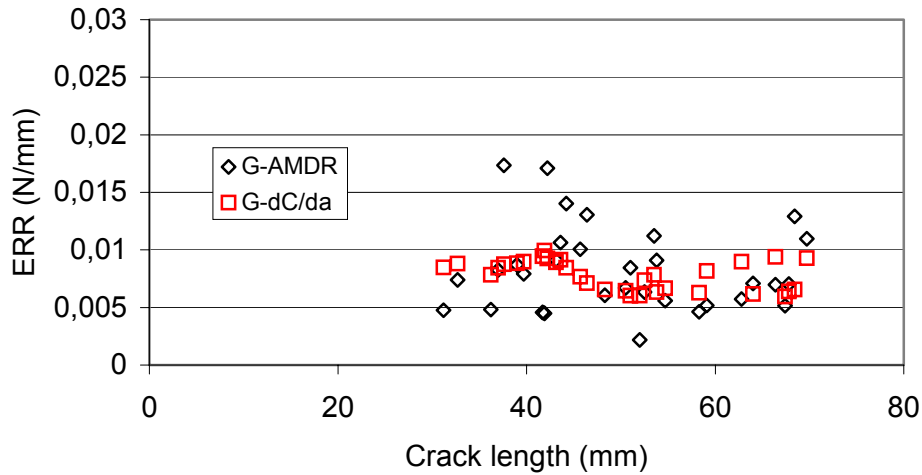


**Fig.V-14: Comparison between the AMDR and the compliance methods**

It can be assumed that the ERR is independent of the crack length, since the interface is supposed to be homogeneous over the entire specimen. The compliance method leads in fact to interfacial fracture energy which is virtually constant for the whole range of crack length. In order to control the validity of this assumption, a reverse approach is taken.

If the ERR is constant, then the force as a function of crack length can be derived from the formula  $G=(P^2/2B)dC/da$ ,

$$P = \sqrt{\frac{2BG}{A_1a + A_2}} \tag{Eq.V-2}$$

with B the specimen width, A1 and A2 two coefficients corresponding to the derived compliance according to a 2<sup>nd</sup> order polynomial.

Obviously, a similar expression is obtained with the compliance following a 3<sup>rd</sup> order polynomial. It should be noticed that the compliance formula comes from the slope of the loading curve and not directly from the maximal displacement and force. However, the results in Fig.V-15 clearly show that the measured maximal forces as a function of a crack length follow the trend predicted by Eq.V-2. This indirect proof is applied since no reference data are available for the type of interfaces under investigation. The method offers a way to control the results and to check if they are valid or not.

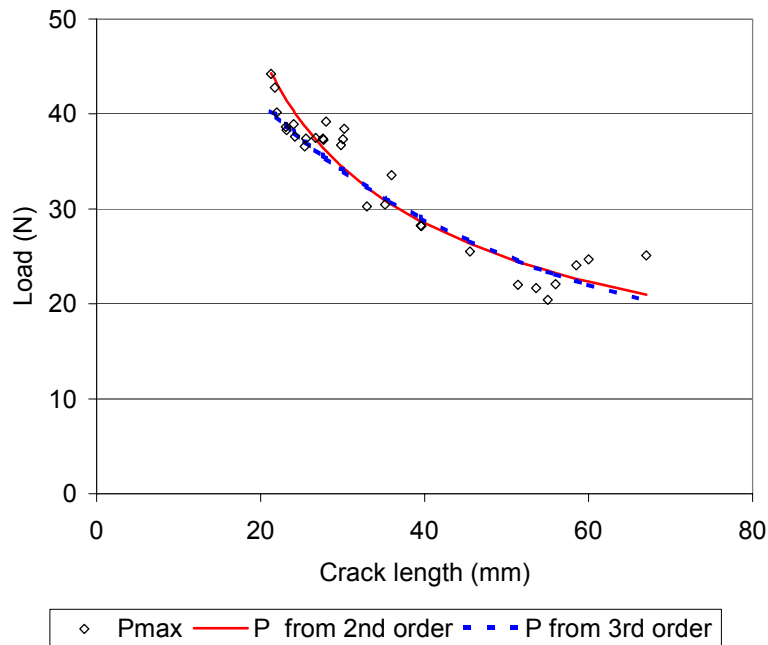


**Fig.V-15: Comparison between the force applied and the force extrapolated**

Measurement flowchart

Based on the measurement that were done in this work, the following flowchart was applied (see Fig.V-16).

- For the  $i^{\text{th}}$  crack length  $a_i$ , the specimen was loaded until a crack advance was noticed (when a drop in load-displacement curve was noticed, or when the crack advance was heard or when the crack advance was visible).
- Then the specimen was unloaded. The maximal force  $P_{\text{max},i}$  and the maximal displacement  $d_{\text{max},i}$  are extracted as well as the new crack length  $a_{i+1}$ .

If the specimen can support a new load (depending on the crack length increments recorded so far) then new measure is restarted. If not the data are processed. At this point, the three methods (Area Method of Data Reduction, the Compliance Method and the numeric simulation) can be applied to compute the energy release rate.

- On the experimental side, The AMDR and the Compliance Method are used directly with the experimental data to compute a value of the ERR and see if both values are comparable. This experimental mean value is then used in the reverse test to control the validity of the test.
- On the numerical side, the maximal force and associated crack length are implemented in a model to compute the corresponding J-integral as well as the associated stress intensity factors  $K_1$  and  $K_2$ . Lastly, the mixed mode angle is computed with  $K_1$  and  $K_2$ .

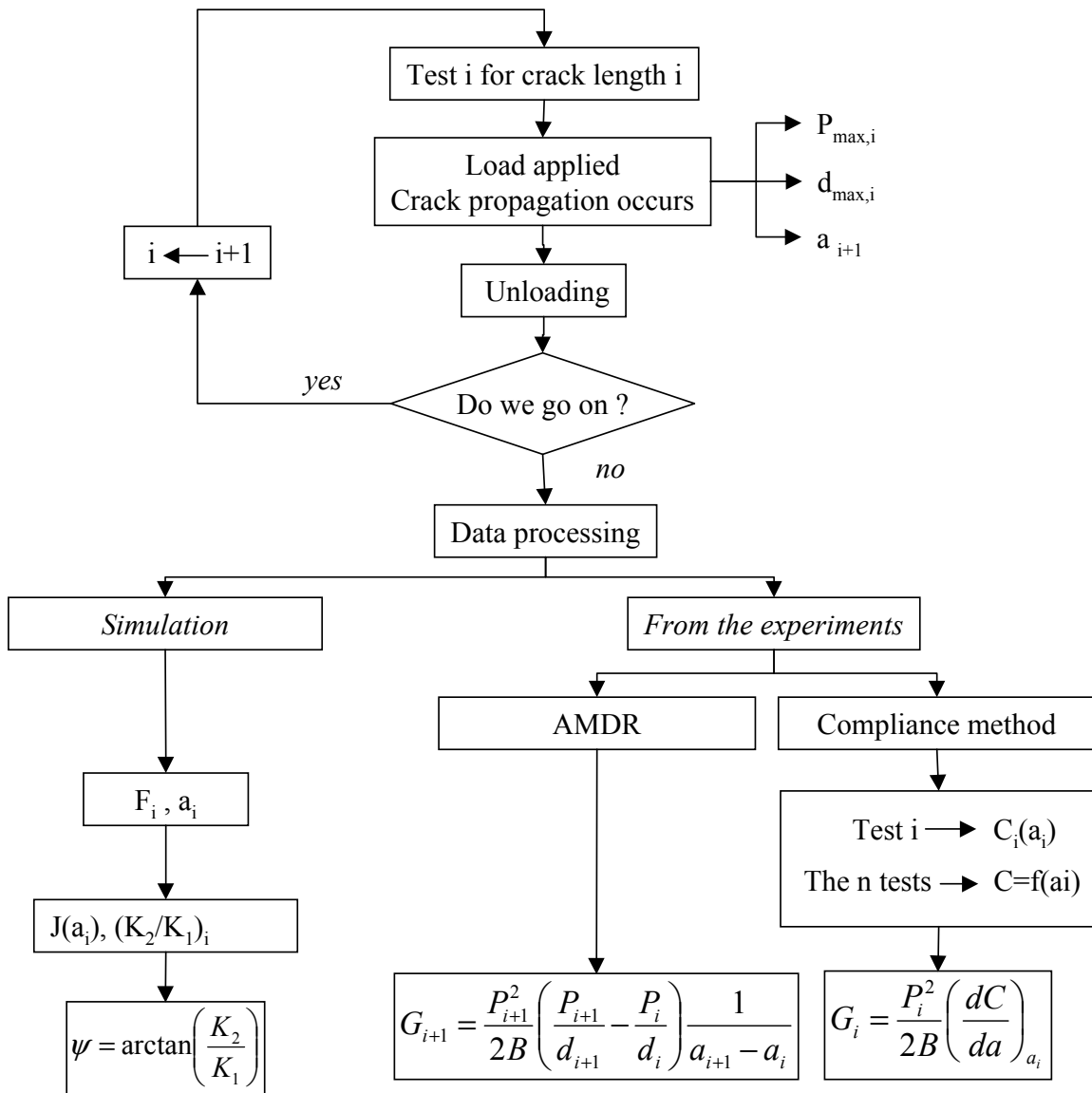


Fig.V-16: Measurement flowchart

## V.C/Numerical modelling

### V.C.1/Objectives

The methods for the numerical simulation of cracks in homogeneous materials and at interfaces used in this work will be described.

### V.C.2/Cracks in homogeneous materials

As indicated in the chapter 3, the commercial software Zencrack version 7.3 is utilised in combination with Abaqus, version 6-4.1, to predict the crack propagation. From a virgin mesh in conjunction with data describing the crack (length, form of the crack front, propagation law), Zencrack creates a new mesh and starts the Abaqus job. Once the computation is finished, Zencrack post-processes the results. The program evaluates the stress conditions at the crack tip and updates the mesh with the new crack front position if a crack growth is requested. The procedure is described in Fig.V-17.

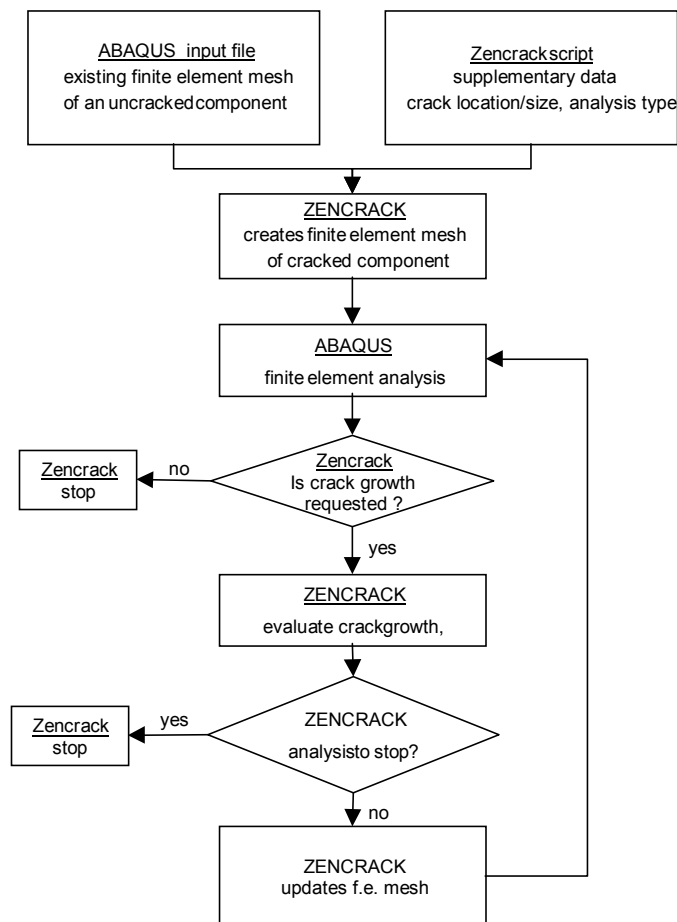
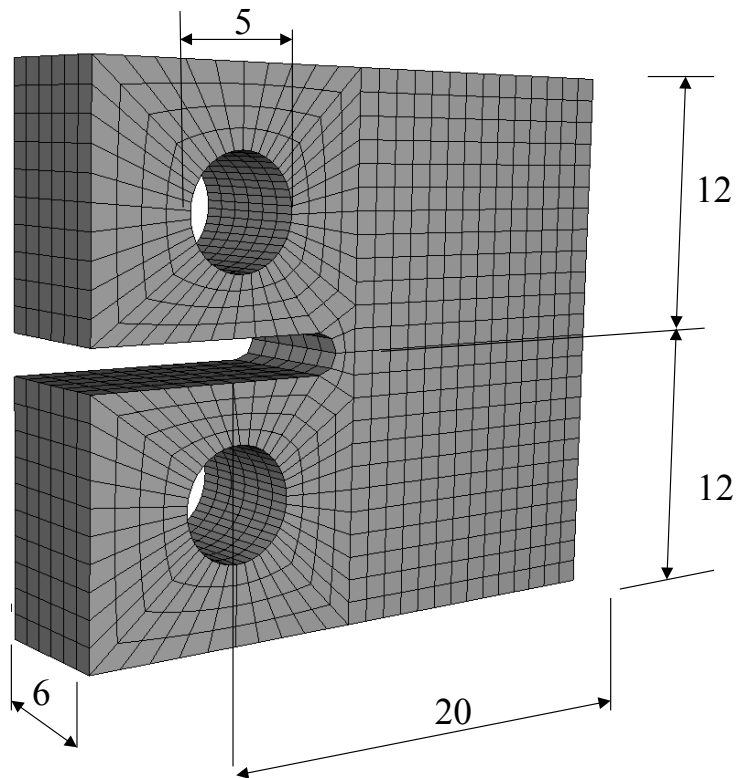


Fig.V-17: Overview of the crack growth scheme

Following the ASTM-Standard, the virgin model of a compact tension specimen is dimensioned with a width  $W$  of 20mm and a thickness  $B$  of 6mm as depicted in Fig.V-18. The model was meshed with the brick element type C3D8. In order to specify the crack size, one has to define the crack length. In order to create the crack faces, pairs of elements from the virgin mesh located between the notch and the desired crack front position must be picked out and specified in the Zencrack-script. Then, elements along the crack front are replaced with crack blocks, and the crack front position is specified by the ratio of the crack length in the element divide by the element length. Fig.V-19 depicts an example of a crack block being used to model a straight crack front. This particular one replaces one Abaqus element by 151 elements with 5 elements in the depth.

In addition, if the elements along the crack front undergo a distortion leading to numerical errors, Zencrack allows a new mesh to be generated with these elements being "relaxed", that is to say by shifting elements such that their distortion is diminished.



**Fig.V-18: Dimension of the CT model**

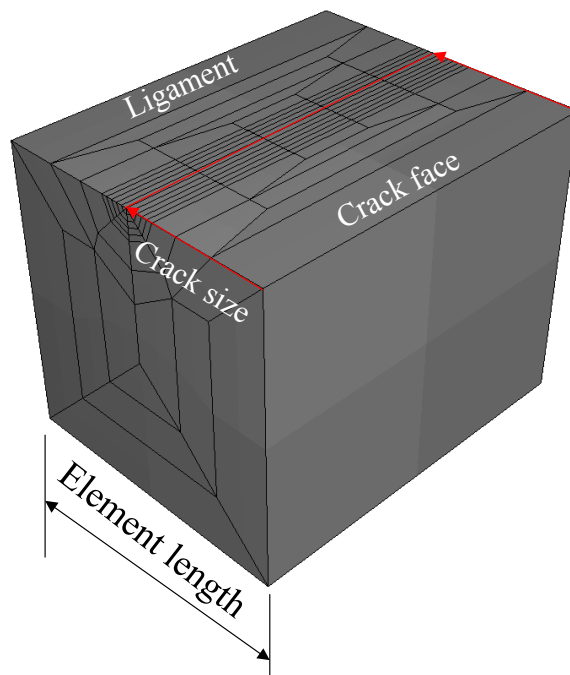


**Fig.V-19: Zencrack crack block, type st151x5.sup**

Fig.V-20 depicts a specimen mesh for a crack length of 9,74mm with elements being relaxed. Fig.V-21 shows as an example a cracked mesh. If one focuses on the crack front, one sees the crack block and the different contours of elements along which the  $J$  integral is evaluated. Zencrack is also able to deal with non-planar propagation (Fig.V-22(a), (b) and (c)) and can handle more than one crack at a time (Fig.V-23(a) and (b)).

### **V.C.3/Interfacial cracks**

If requested, Zencrack can process results coming from the simulations with Abaqus, but one of the main limitations lies in the fact that, for the versions up to now, the program deals only with cracks in bulk materials. But the ability for Zencrack to generate cracked meshes will be very helpful for the treatment of interfacial cracks.

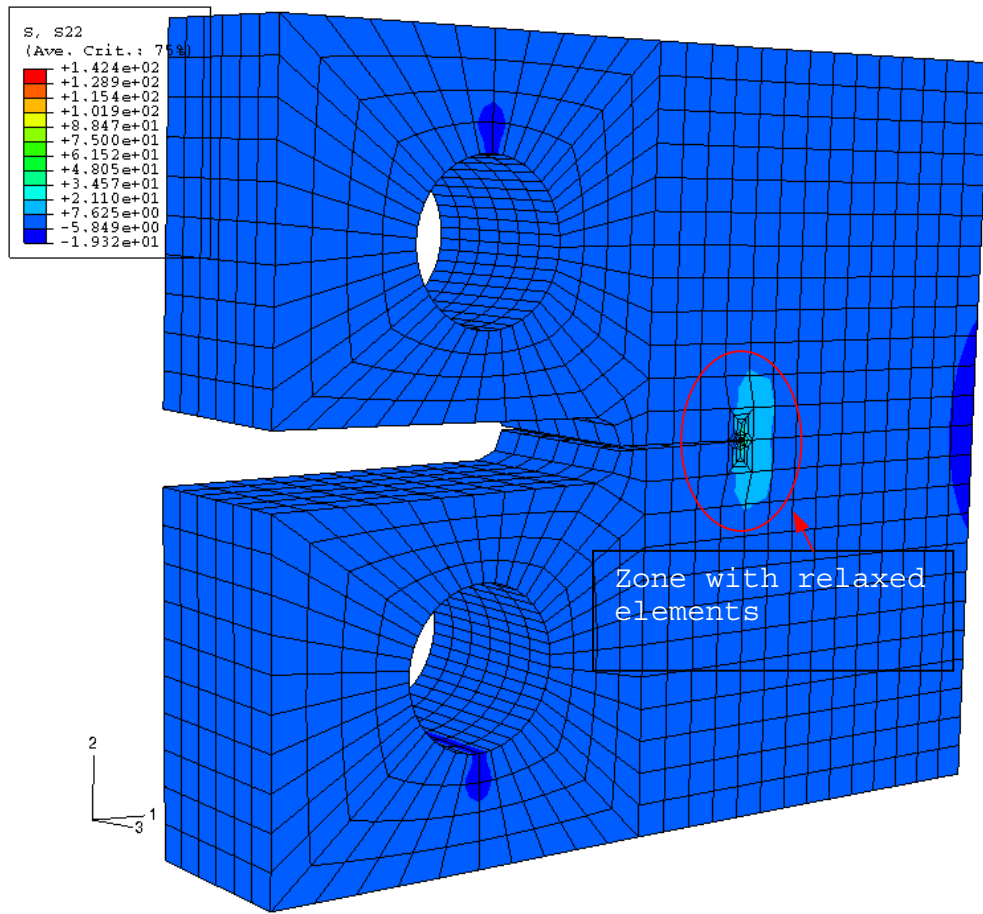


Fig.V-20: CT model with a crack length of 9,74mm under a tensile force of 85N

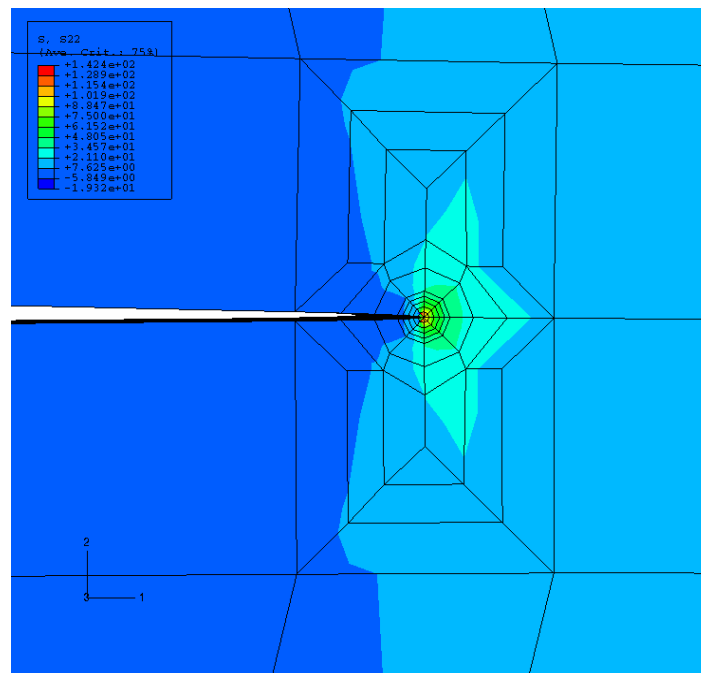
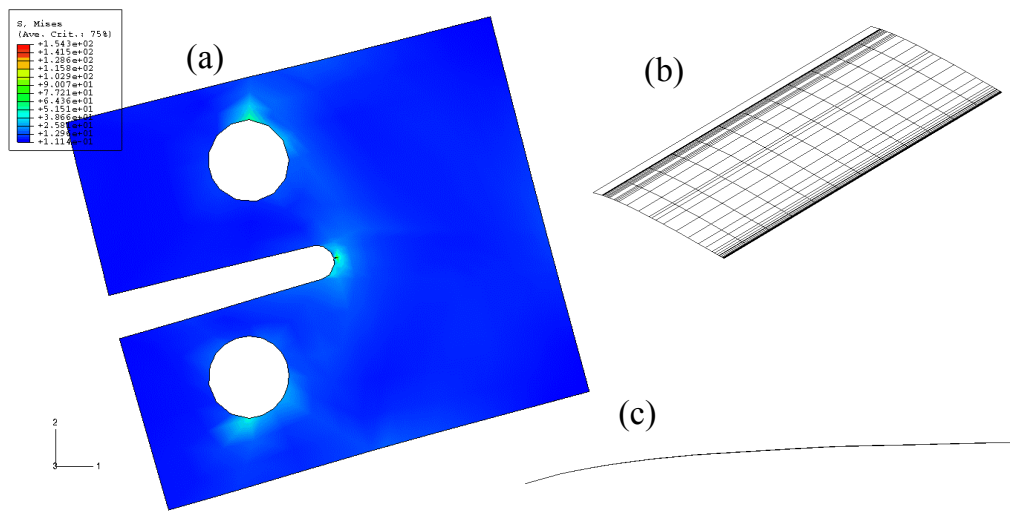
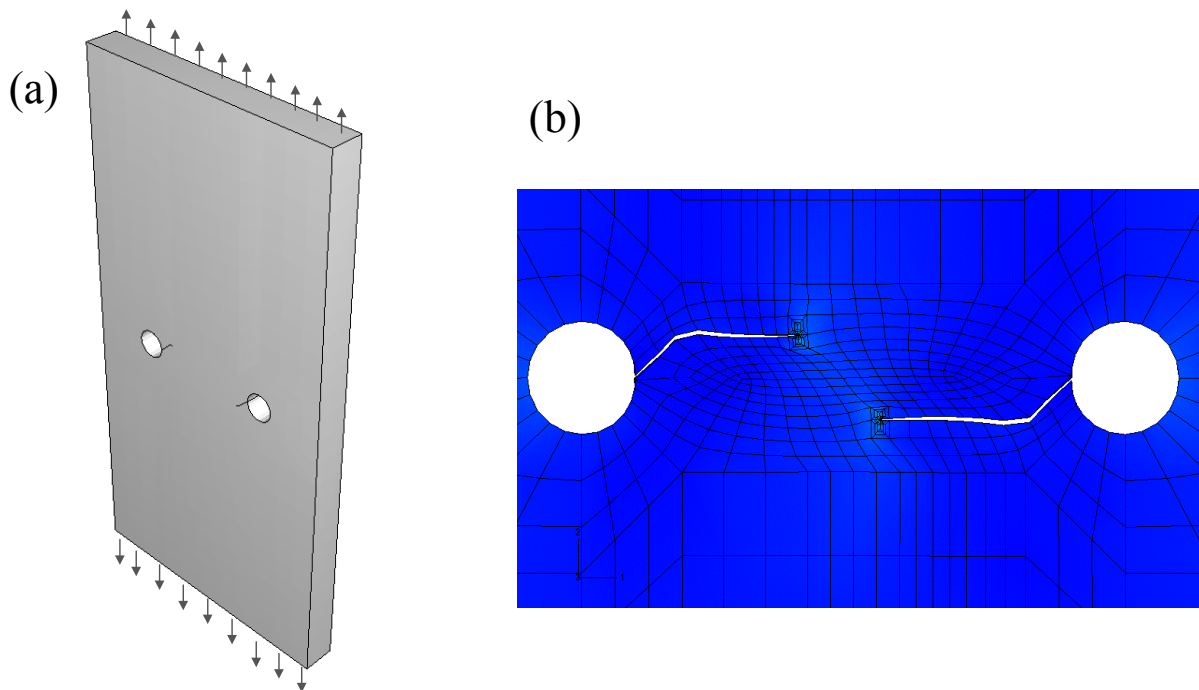


Fig.V-21: Focus on the crack tip



**Fig.V- 22: CT specimen, inclination of 15°. (a) Cracked specimen; (b) Crack advance; (c) Crack profile**



**Fig.V- 23: Model of the plate with two holes, (a) initial state and (b) final state**

The uncracked model of the asymmetric double cantilever beam specimen (ADCB) used in this study is parameterised such that crack lengths measured during the tests are easily implemented in the numerical analysis (see Fig.V-24), as well as the associated forces. Zencrack is used here only as a meshing tool, and the cracked input file is slightly modified to give as an output not only the J integral but the K-factors too.

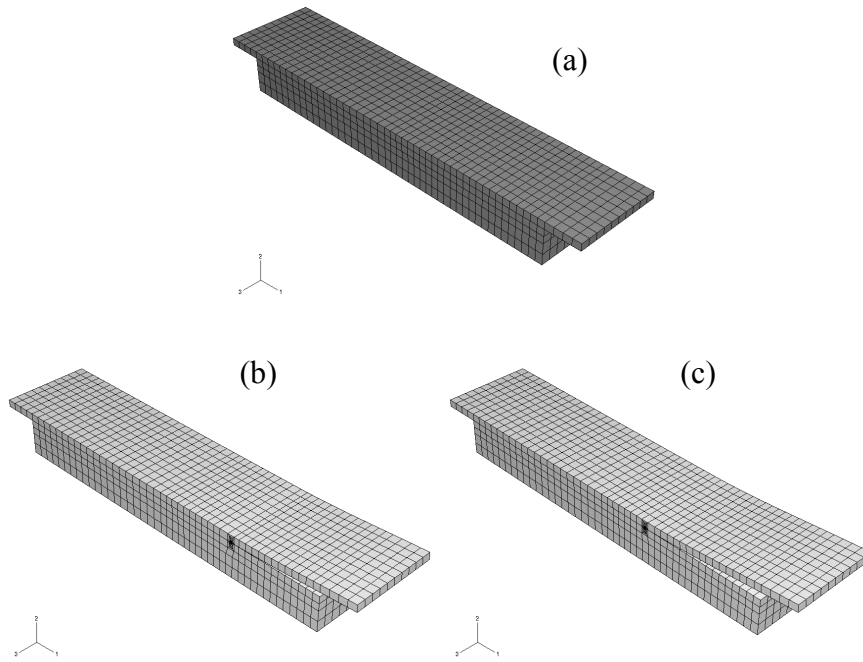


**Fig.V-24: Zencrack used as meshing tool. (a) the uncracked model of an ADCB specimen, lower beam of 10mm thickness; (b) with a crack length of 31,47mm and (c) with 40,24mm**

Thanks to the Abaqus keyword `*CONTOUR INTEGRAL`, it is possible to get the  $K_1$  and  $K_2$  value along the crack front as well as the ERR computed from the formula

$$J = \frac{1-\beta^2}{E^*} (K_1^2 + K_2^2) + \frac{1}{2G^*} K_3^2 \quad \text{Eq.V-3}$$

where  $\beta$  is the Dundur's parameter and

$$\frac{1}{E^*} = \frac{1}{2} \left( \frac{1}{E_1} + \frac{1}{E_2} \right); \quad \frac{1}{G^*} = \frac{1}{2} \left( \frac{1}{G_1} + \frac{1}{G_2} \right); \quad \bar{E} = \frac{E}{1-\nu^2}; \quad G_i = \frac{E_i}{2(1+\nu_i)} \quad \text{Eq.V-4}$$

Abaqus makes a distinction between cracks in homogeneous materials and cracks "lying on the interface between two different materials". It is explicitly written in the documentation [2004-Abaqus] that the  $K_1$  and  $K_2$  do not correspond to  $K_I$  and  $K_{II}$  and therefore it is possible to compute the mixed mode angle by taking the ratio  $K_2/K_1$ .

The crack-block which is used (see Fig.V-19) allows us to replace one Abaqus standard element with a crack block containing 151 elements, including 6 element rings (or 6 element contours). The path independence for  $J$  is controlled along the contours 2 to 6. This is to avoid inaccuracy from the first contour (also recommended by Abaqus [2004-Abaqus]).

## V.D/Statistical approach

### V.D.1/objectives

In order to obtain a better understanding of the statistical information provided by gathered data, a special approach is taken. For the analysis, the Weibull distribution is chosen to describe the set of results and the statistical approach is based on a bootstrap method [1997-Bootstrap].

### V.D.2/Weibull distribution

The Weibull distribution is widely used in the reliability analysis of components. It is based on the description of the set of data by a two-parametric function for the cumulative failure probability.

$$F = 1 - \exp\left(-\left(\frac{K}{K_0}\right)^m\right) \quad \text{Eq.V-5}$$

where  $m$  denotes the Weibull modulus and  $K_0$  is the scaling parameter, here it can be called the scaling toughness. For  $K=K_0$ , the cumulative failure probability equals  $F(K_0)=1-1/e=0,632$ . In other words, the toughness is lower or equal to  $K_0$  with a probability of 63,2%. The cumulative failure probability expresses the probability that the variable  $X$  takes a value less than or equal to  $x$ :

$$F(x) = \Pr(X \leq x) \quad \text{Eq.V-6}$$

The advantages of such a formulation are its mathematical simplicity, the amenability to graphical analysis and its wellknown ability to fit most lifetime data with a great confidence [2004-Nist]. The Weibull plot is given by:

$$\text{Ln}\left(\text{Ln}\left(\frac{1}{1-F}\right)\right) = f(\text{Ln}K) \quad \text{Eq.V-7}$$

and the approximation of the failure probability utilised here is:

$$F_a = \frac{i-0.5}{N} \quad \text{Eq.V-8}$$

The experimental Weibull data are compared with a fit of the Weibull distribution obtained by the maximum likelihood method.

### V.D.3/Maximum likelihood

The maximum likelihood method built so as to maximise the chance that a model fits a given data set.

Even if a model provides an accurate description of statistical data, it is important that occasional outliers be discarded from the fit. Instead of minimising a residual between the model and all the data points, a maximum likelihood estimation therefore aims at maximising the probability that the model reproduces most, but not all the data points.

The likelihood function L is defined as

$$L = \prod_{i=1}^N \left( \frac{dF(K_i)}{dK} \Big|_{K_i} \right) \quad \text{Eq.V-9}$$

where N is total number of samples.

The maximum likelihood of the Weibull modulus is

$$\frac{dLn(L)}{dm} = 0 \Leftrightarrow \frac{1}{m} = \frac{\sum_{i=1}^N (LnK_i - K_i^m)}{\sum_{i=1}^N K_i^m} - \frac{1}{N} \sum_{i=1}^N LnK_i^m \quad \text{Eq.V-10}$$

and for the scaling toughness

$$\frac{dLn(L)}{dK_0} = 0 \Leftrightarrow K_0^m = \frac{1}{N} \sum_{i=1}^N K_i^m \quad \text{Eq.V-11}$$

Eq.V-10 and Eq.V-11 are estimated with an iterative method such as the Newton's method.

### V.D.4/Bootstrap method

The Bootstrap method is a non-parametric method invented in 1957 by B. Efron [1997-Bootstrap]. The aim of this method is to determine the confidence for parameters of a data distribution (see Fig.V-25). It is a powerful method since it is independent of assumption on the distribution function.

A Bootstrap sample is a random set drawn from the original data set with replacement. If the original data set contains twenty samples (or for instance twenty measured values), a random number generator, here the Monte Carlo algorithm, is used to create a virtual data set constituted by twenty samples, each sample can be picked various

times since the selection is performed with replacement. Then, the Weibull parameters are estimated.

By this Monte Carlo procedure, there can be created as many bootstrap samples as required, in this work typically thirty thousand times. That is to say, thirty thousand estimations for the Weibull parameters are available and are processed in order to represent the frequency of occurrence for the Weibull modulus and the scaling toughness. From the cumulative probability of the thirty thousand values of the scaling toughness, a confidence interval can be obtained, i.e. the scaling toughness can for example be determined with 95% confidence.

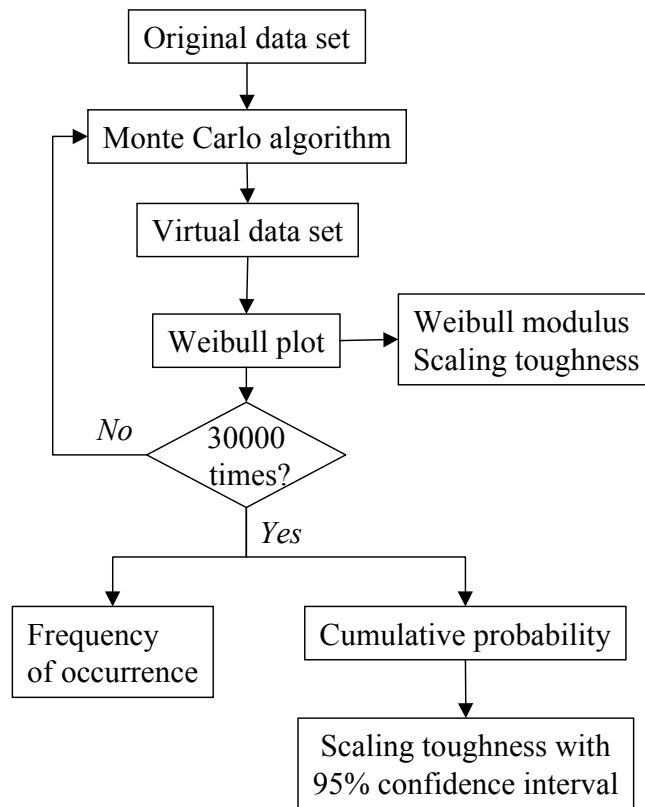


**Fig.V-25: Flowchart for Bootstrap method**

## **V.E/Conclusion**

*The way the different specimens are manufactured has been presented. At the same time, the complete data processing, from acquisition to implementation in numerical models has been highlighted. The data acquired during the measurements can be processed via different methods to determine the interfacial energy release rate.*

*One of the methods, the Area Method of Data Reductions delivers immediately a mean value for a set of data, but the scatter in the results depends on the precision of the measurement. The Compliance method delivers more reliable results since the specimen response to the loading case is almost linear. Besides, a test to control the quality of the measurements and to ensure its validity was arranged. Both methods will be applied in the following part. The way Zencrack is used for both crack situations, i.e. in the bulk material or at the interface between different materials is noted and statistical tools for the estimation of the results reliability are described.*

---

---

# **Chapter VI**

## EXPERIMENTAL RESULTS

## **VII/ Experimental results**

### **VI.A/Introduction**

*The chapter presents results on the fracture toughness of potting materials obtained by CT specimen. One goal is to provide a method to ascertain reliable information on the fracture toughness and the scatter of the results. Another target is to establish a method to measure the subcritical crack growth. Experimental investigations are supplemented by simulations of crack growth.*

*The second part deals with investigation of interfacial fracture toughness. A method is presented to measure the energy release rate on double beam specimens submitted to different types of loads. Further numerical simulations are performed and a comparison is made with experiments to validate the numerical models and to extract the mixed mode angle, the goal being to obtain the interfacial fracture toughness curve for a material combination.*

## VI.B/Homogeneous materials

From a reliability point of view, determining the confidence of results can improve the lifetime prediction of devices. The better the material characteristics are known, the more reliable are the simulation results. The determination of the confidence of the obtained results is focused on here.

### VI.B.1/Fracture toughness as a function of crack length

Two materials which differ singularly in their mechanical performance are selected and about twenty CT specimens for each material have been tested.

For material 1, the mean value for the fracture toughness was determined to be  $1,325 \text{ MPa}\sqrt{\text{m}}$ , with a standard deviation of 10,6% (see Fig.VI-1). For material 2, the fracture toughness is  $1,001 \text{ MPa}\sqrt{\text{m}}$  with a standard deviation of 2,2% (see Fig.VI-2).

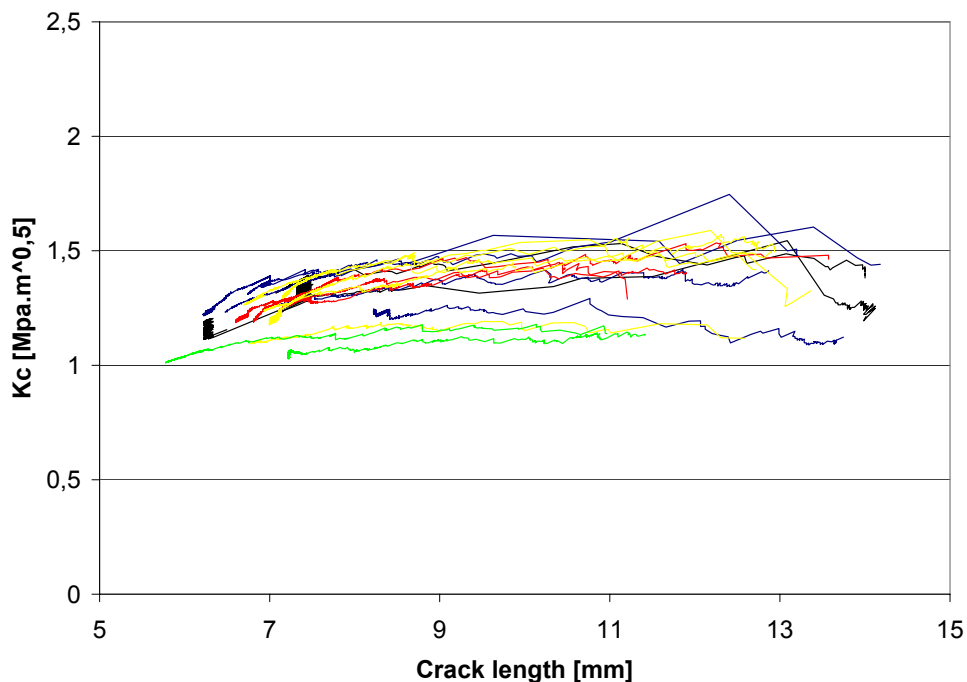


Fig.VI-1:  $K_c$  measurement for material 1

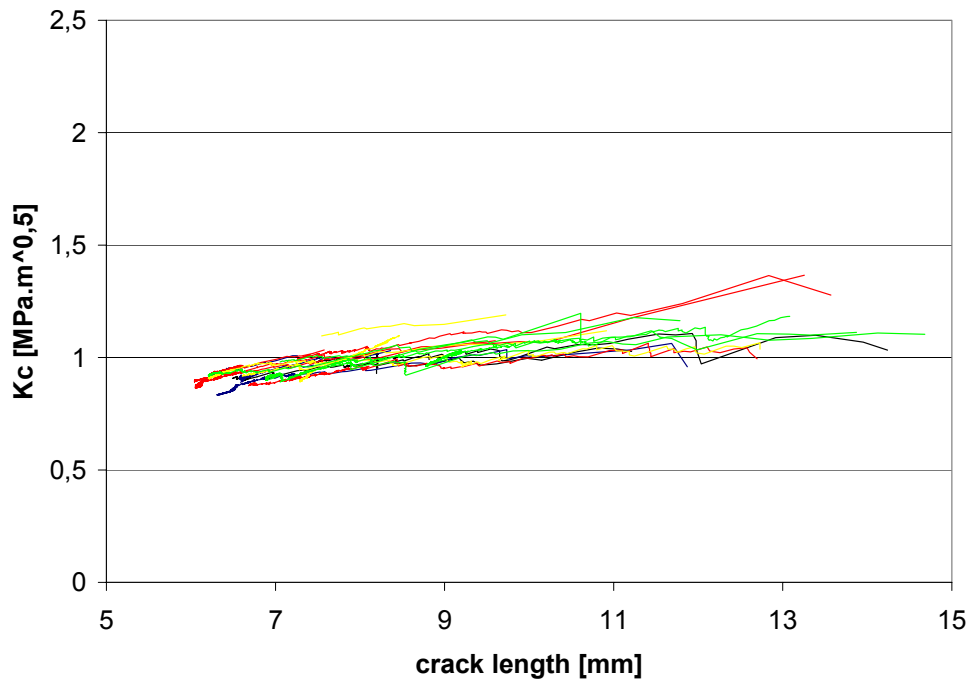


Fig.VI-2:  $K_c$  measurement for material 2

### VI.B.2/Statistical analysis

The data gathered during the experiments led on CT specimens are post-treated here by means of the bootstrap method.

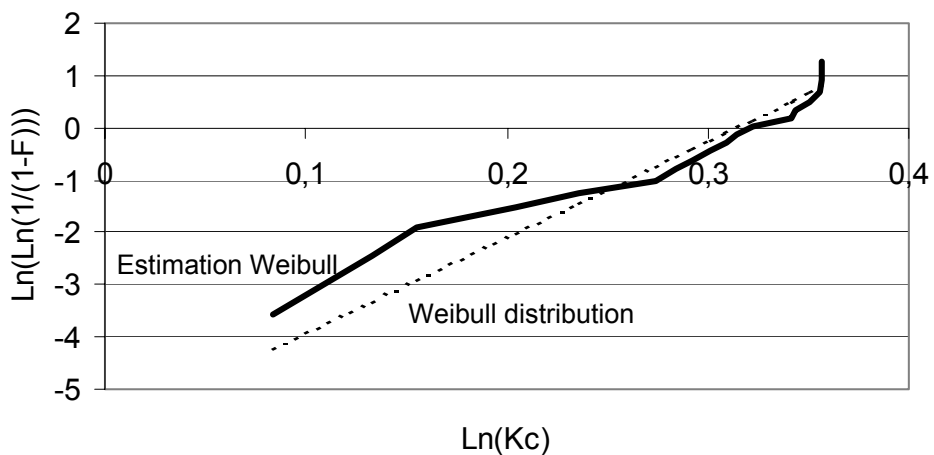
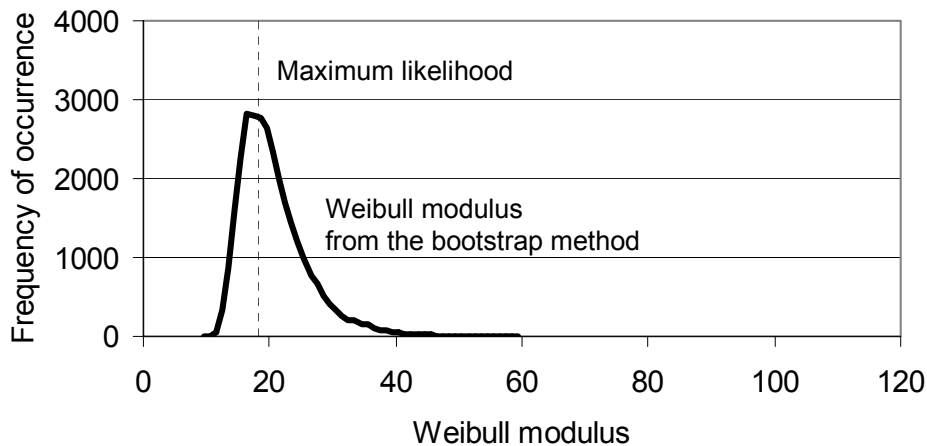


Fig.VI-3: Comparison between Weibull distribution and estimation for material 1

Since the Weibull distribution depicted in the Fig.VI-3 fits reasonably well to the estimation, it can be concluded that this data set can be described by the 2 parametric Weibull distribution. In the case of the material 1, a Weibull modulus of  $(m=18,41)$  and a

scaling toughness ( $K_0=1,369 \text{ MPa}\sqrt{m}$ ). This means that the toughness is lower or equal to  $1,369 \text{ MPa}\sqrt{m}$  with a probability of 63,2%.

Next, the Bootstrap method described previously is applied in order to estimate the accuracy of the Weibull parameters. Fig.VI-4 and Fig.VI-5 depict the frequency of occurrence of the Weibull modulus and the scaling toughness for material 1 based on 30.000 bootstrap samples. For comparison, the maximum likelihood estimated for the original data set is also plotted as the vertical dotted line. It is evident that the scaling toughness is provided with higher accuracy than the Weibull modulus.



**Fig.VI-4: Bootstrap method applied to the Weibull modulus for material 1**

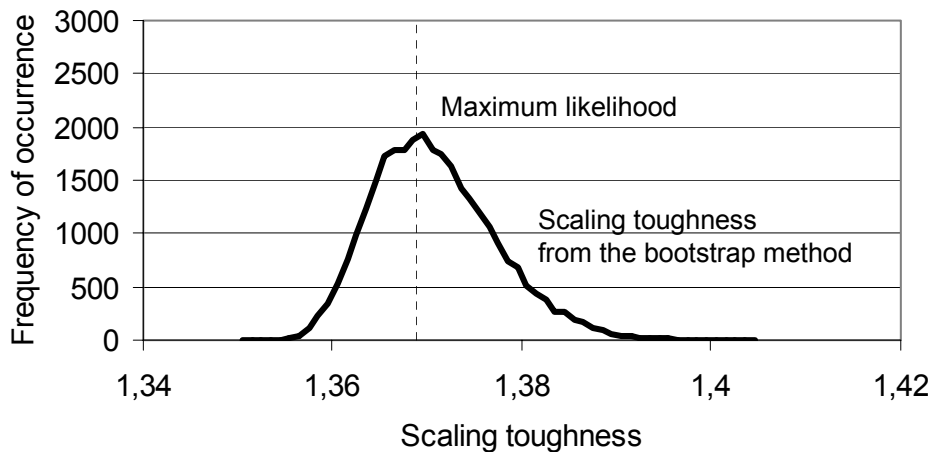


**Fig.VI-5: Bootstrap method applied to the scaling toughness for material 1**

At this point, it is possible to determine the 95% confidence interval for both parameters, namely by determining the values of the distribution function for which a cumulative probability of 2,5% and 97,5% are reached (see Fig.VI-6).

The Weibull modulus is then equal to 18,41 with a 95% confidence interval of [12,51 - 33,51]. And the scaling toughness is 1,369  $\text{MPa}\sqrt{m}$  with a 95% confidence interval [1,359 - 1,372].

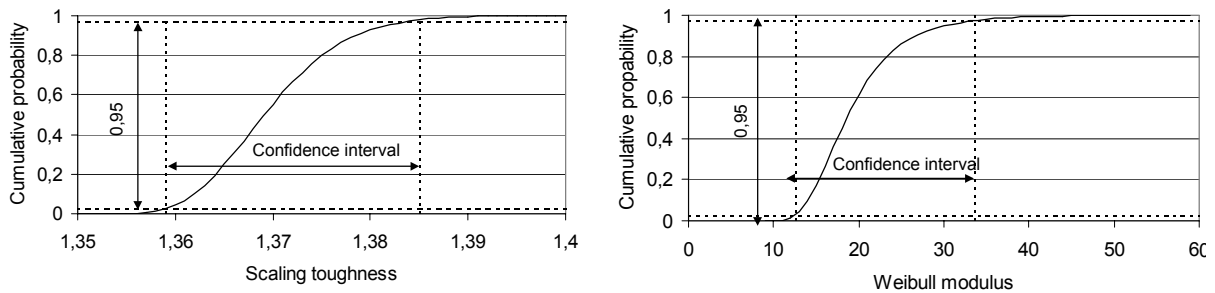


**Fig.VI-6: Cumulative likelihood for the Weibull parameters of material 1**

The same analysis is performed for the second material. The Weibull distribution plotted in Fig.VI-7 fits well the estimated failure probability and for this material a Weibull modulus of 40,63 and a scaling toughness  $K_0=0,997 \text{ MPa}\sqrt{m}$  are determined via the maximum likelihood method.

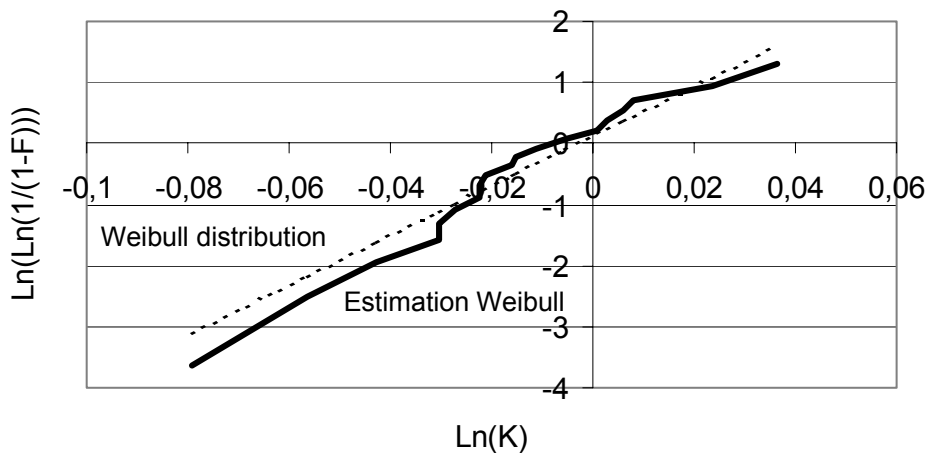


**Fig.VI-7: Comparison between Weibull distribution and estimation for material 2**

The bootstrap method is applied and the frequency of occurrence of the Weibull modulus is plotted in Fig.VI-8. On the same diagram, the limits of the 95% confidence interval are represented and determined to be [32,46 - 70,00] for the Weibull modulus.

The magnitude of the Weibull modulus delivers information on the reliability of the data set. The higher the modulus, the more reliable is the material under consideration. In this case, it proves that the material 2 really shows less scatter.

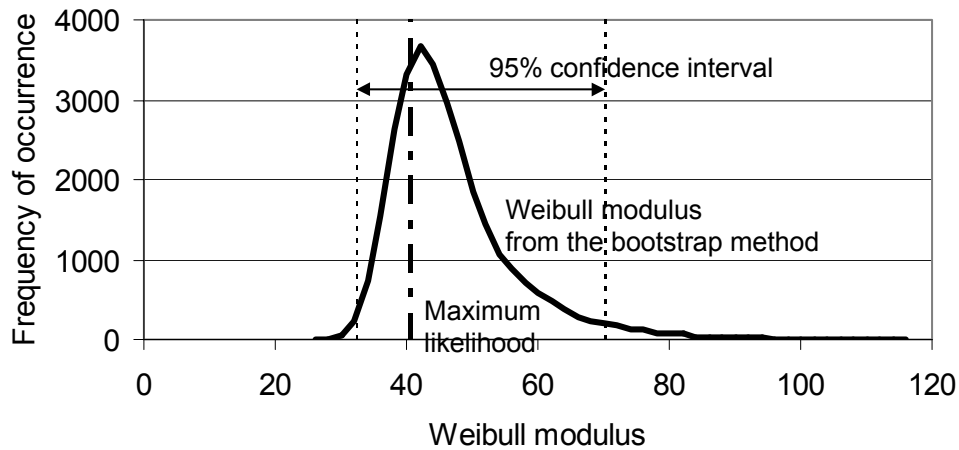


**Fig.VI-8: Bootstrap method applied to the Weibull modulus for material 2**

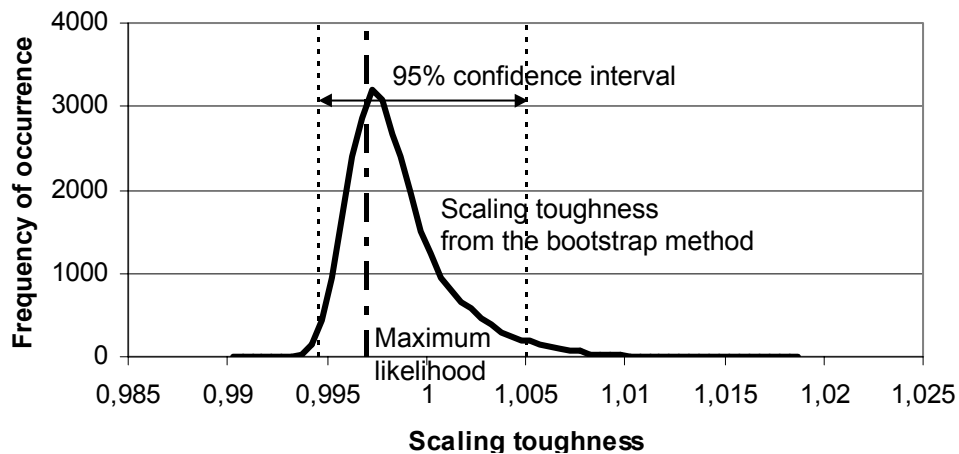


**Fig.VI-9: Bootstrap method applied to the scaling toughness for material 2**

Fig.VI-9 depicts the bootstrap method applied to the scaling toughness. The maximum likelihood is then to be 0,997 with the 95% confidence interval of [0,995 - 1,005].

The comparison between both materials can be combined in Table VI-1.

		Maximum likelihood	2,50%	97,50%	Relative error
material 1	$K_0$	1,359	1,359	1,372	0,01
	$m$	18,41	12,51	33,51	1,14
material 2	$K_0$	0,997	0,995	1,005	0,01
	$M$	40,63	32,46	70,00	0,92

**Table VI- 1: Bootstrap method applied to the determination of the fracture toughness**

The "relative error" in the Table VI-1 is calculated with the width of the confidence interval devised by the maximum likelihood. Example for the fracture toughness is given by:

$$Relative\ error = \frac{K_{97,5} - K_{2,5}}{K_{max\ likelihood}} \quad \text{Eq.VI-1}$$

Obviously the fracture toughness of both materials is known with the same relative error. But the reliability of results of material 2 is higher compared to material 1, definitively since the relative error of the Weibull modulus is lower for material 2 than for material 1. Therefore, crack growth experiments are concentrated on material 2.

## Simulation

A comparison between the results coming from the ASTM-standard and the simulations led with Zencrack running in parallel with Abaqus will take place.

For a given crack length (9,4mm) and under a given load (P=75N), the ASTM-standard delivers a value for K of 24,68 MPa $\sqrt{m}$ . The model used for the simulation is presented in Fig.VI-10.

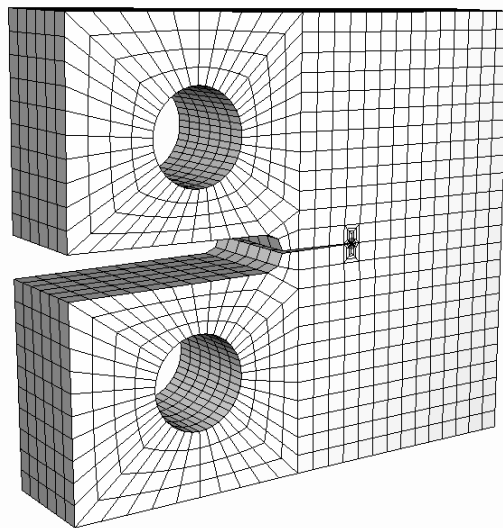


**Fig.VI-10: 3D model of CT specimen**

One has to recall that plane strain and plane stress states correspond only to idealised 2D cases (see chapter I-B-3-b). In plane stress, the out-of-plane stress is unable and respectively the displacement in plane strain. However, the Poisson's ratio still plays a role in plane stress and plane strain as shown in Eq.VI-2

$$\varepsilon_x = \frac{1-\nu^2}{E} \left( \sigma_x - \frac{\nu}{1-\nu} \sigma_y \right), \quad \varepsilon_y = \frac{1-\nu^2}{E} \left( \sigma_y - \frac{\nu}{1-\nu} \sigma_x \right), \quad \text{Eq.VI-2}$$

and  $\sigma_z = \nu(\sigma_x + \sigma_y)$  in plane strain

$$\varepsilon_x = \frac{1-\nu^2}{E} \left( \sigma_x - \frac{\nu}{1-\nu} \sigma_y \right), \quad \varepsilon_y = \frac{1-\nu^2}{E} \left( \sigma_y - \frac{\nu}{1-\nu} \sigma_x \right), \quad \gamma_{xy} = \frac{2(1+\nu)}{E} \tau_{xy}$$

and  $E\varepsilon_z = -\nu(\sigma_x + \sigma_y)$  in plane stress

In 3D, these conditions are not fully fulfilled, neither at the edge of the specimen nor in the middle, what leads to some confusion when one wants to make comparisons between results and material characteristics. Besides, a numerical artefact in FE simulations is to set the Poisson's ratio to zero when defining the material parameters if one wants to avoid through-thickness effects. But this artefact has no physical meaning since it corresponds neither to plane stress nor to plane strain conditions.

Fig.VI-11 depicts the comparison between results of a FE simulation and the ASTM-D5045-99. The standard helps to determine K value under plane strain conditions. The ERR can be obtained by

$$G = \frac{K^2(1-\nu^2)}{E} \quad \text{Eq.VI-3}$$

The curved form of the J integral data along the front is due to the influence of the lateral contraction of the specimen on the stress state. If the Poisson's ratio is set to 0, the through-thickness effect is suppressed and the J integral data are flat. However, one may think that, one approximates results on the free surface by plane stress conditions and that plane strain conditions apply in the middle of the specimen. But the value coming from the standard do not corroborate such a hypothesis. The data set "G from ASTM" corresponds to a plane strain state and the value in the middle of the specimen does not equal the plane strain value. If the mean value of the "J-Abaqus" is plotted, it approximates the G of ASTM with more or less satisfaction.

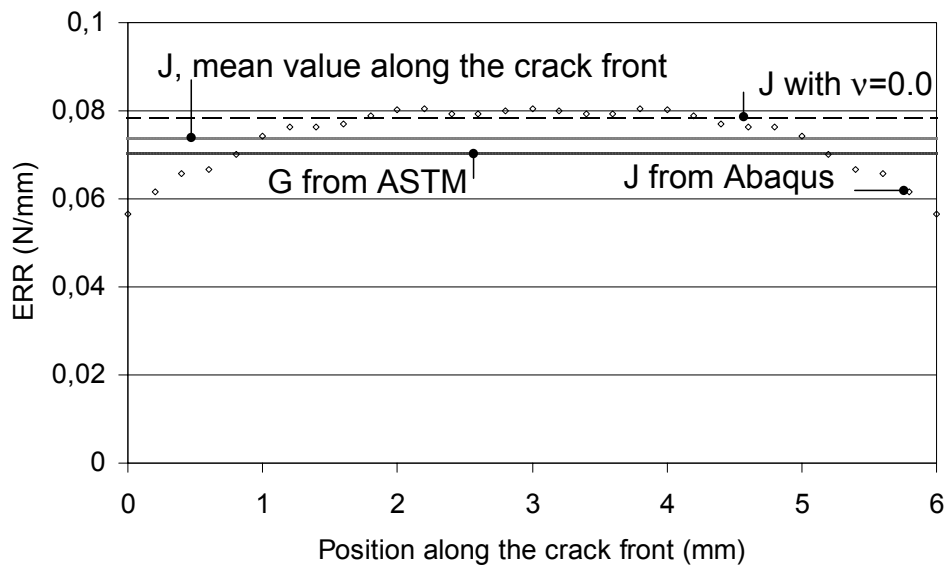


**Fig.VI-11: Comparison of ERR values delivered by the simulations and ASTM-Standard for a given crack length and a given force**

The other case to consider is when the crack length varies. The force is still constant to 75N and the crack length varies between 9 and 13mm. The trends of curves in Fig.VI-12 confirm that values taken at the free surface and at the middle bound the standard solution.

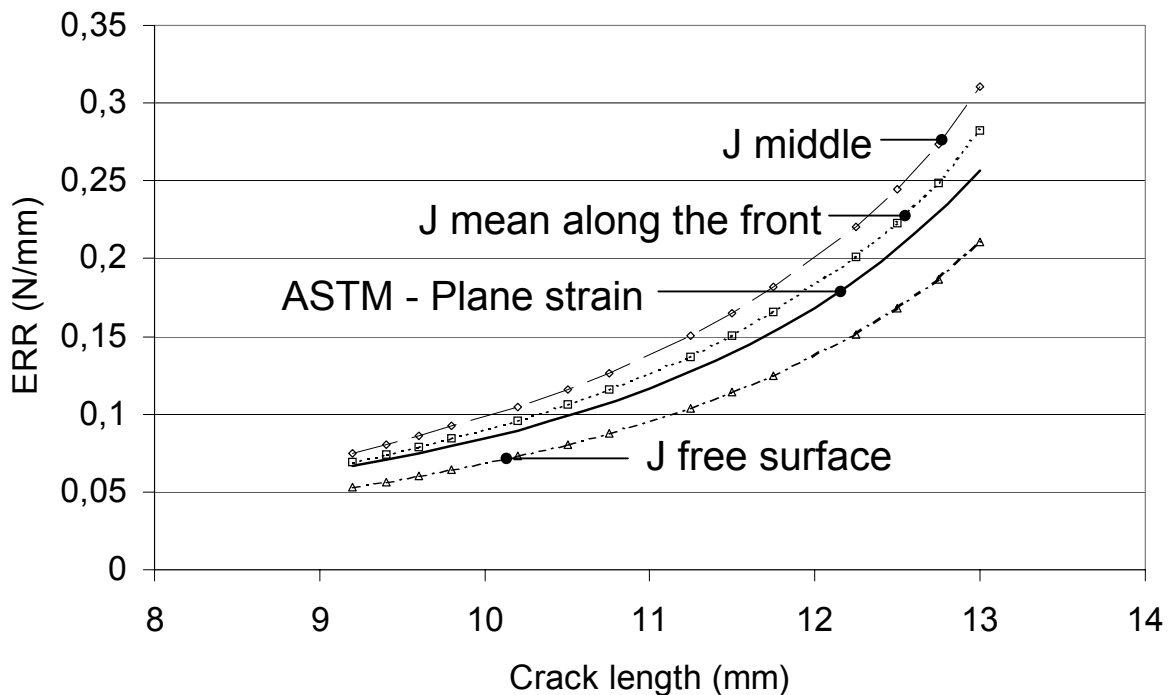


**Fig.VI-12: Comparison of ERR values for a given force**

This investigation shows that the simulations on the case of the CT specimen are satisfying but highlights the fact that one has to interpret with special attention the results provided by the simulations if they have to be compared with experimental values.

### VI.B.3/Subcritical crack growth

#### VI.B.3.a/Experimental data

As described in the chapter V, a sustained load corresponding to a value  $K$  lower than the fracture toughness is applied to the CT specimen during a long time. The load is sustained in the order of magnitude of 40 minutes. The crack length is measured and the crack advance divided by the time gives the crack propagation velocity for the given  $K$ . Fig.VI-13 depicts an example of a such measure. The load is plotted depending on the time and the monitored crack length evolves slowly.

The "hesitations" concerning crack length data come directly from the image recording. Since the digital camera does not record the real colours but the intensity of light received on the CCD captor, the crack tip can "move" from one image to the next in the range of one or two pixels.

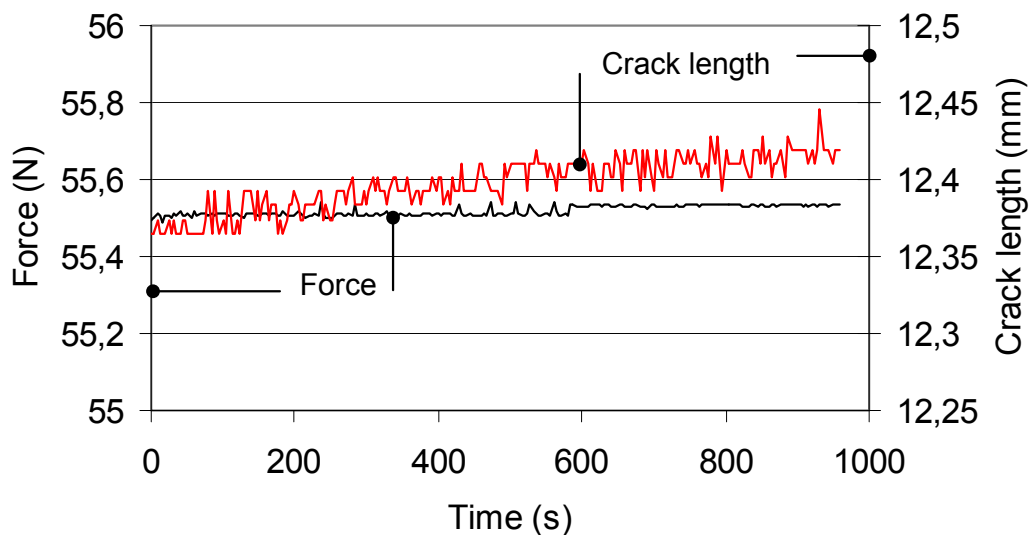


**Fig.VI-13: Sustained load and crack advance on CT specimen**

Here, the precision of our system is reached since a precision of one pixel corresponds to  $9\mu\text{m}$ . However, a crack advance is noticeable if the generally rising trend is considered. Moreover the force signal has slightly varied while the crack slowly propagates, although the testing frame should control the force during the crack advance

### VI.B.3.b/Data processing

Knowing the initial crack length helps in the choice of the force to apply. Since the fracture toughness is known, it is easy to calculate the force corresponding to 90% or 95% of the  $K_{Ic}$ . Knowing the time and the crack length increment during the test gives a crack propagation velocity  $da/dt$  for the applied  $K$ .

Such measurements are repeated. When a distinct crack advance was noticed during a test, the applied force was diminished for the next test. This ensures to stay below the critical force. By repeated measurements, data for the crack growth law  $da/dt=f(K)$  can be collected (see Fig.VI-14).

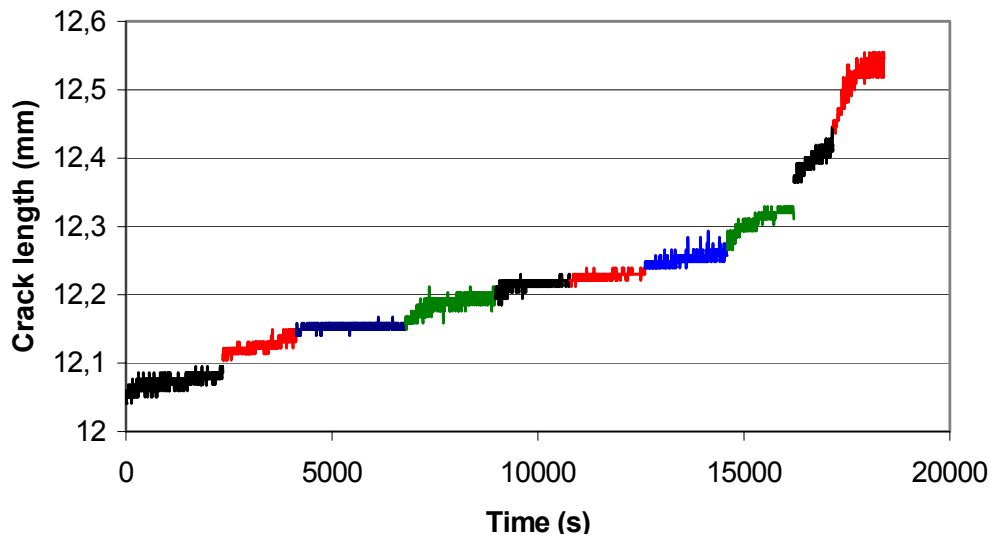


**Fig.VI-14: Crack length increment for repeated tests under sustained loads**

The plot in Fig.VI-15 yields an estimation for the Paris law of material 2 at room temperature.

$$\frac{da}{dt} = 1,0 \cdot 10^{-7} K^{36} \quad \text{Eq.VI-4}$$

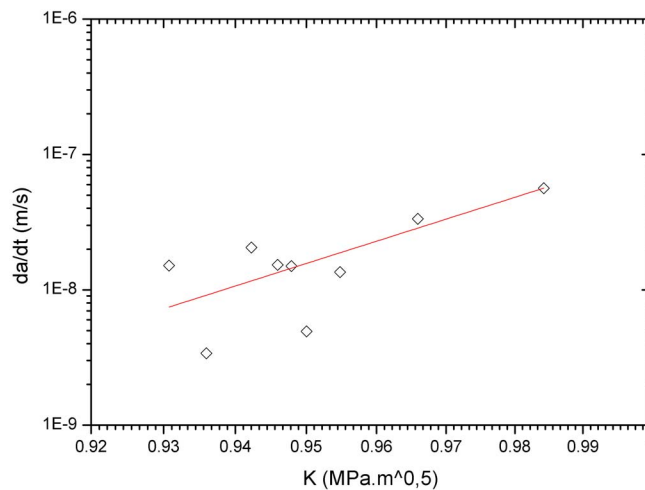


**Fig.VI-15: Subcritical crack growth curve for material 2 (logarithmic plot)**

Beaumont showed that a form of poly(methyl methacrylate) (PMMA) presented a power of  $K$  from 25 [1975-Beaumont]. Subcritical crack growth can also be considered as a singular case of cyclic fatigue where the loading case varies from 0 to  $K$  and the  $dN$  (increment in number of cycles) is replaced by  $dt$  (time increment). This law could be compared with values from Hertzberg and Manson [1980-Hertzberg]. They reported growth rates for different polymer materials under cyclic loading. Polycarbonate and polystyrene showed a power of  $\Delta K$  ranging from 4 to 6, while epoxy resin showed a power of 30. Fig.VI-16 depicts these curves. "Macro" stands for macroscopic growth rate and "micro" for measurements from the fatigue striation spacing.

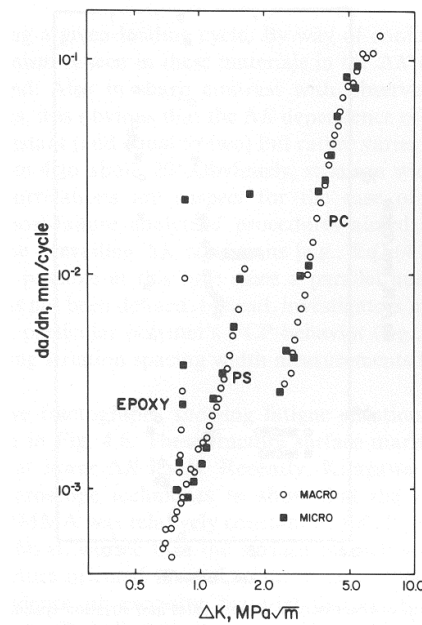


**Fig.VI-16: Comparison of growth rates in epoxy, polystyrene and polycarbonate [1980-Hertzberg]**

Other polymer materials such as poly(vinyl chloride) (PVC) showed a power of 2,4 and poly(methyl metachrylate) (PMMA) about 6 [1984-Williams] under cyclic fatigue.

### VI.B.3.c/simulation

The Paris law is then implemented in Zencrack. In the example given in Fig.VI-17, an initial crack length of 12,1mm is defined. The sustained load is applied and the crack length is represented versus time.

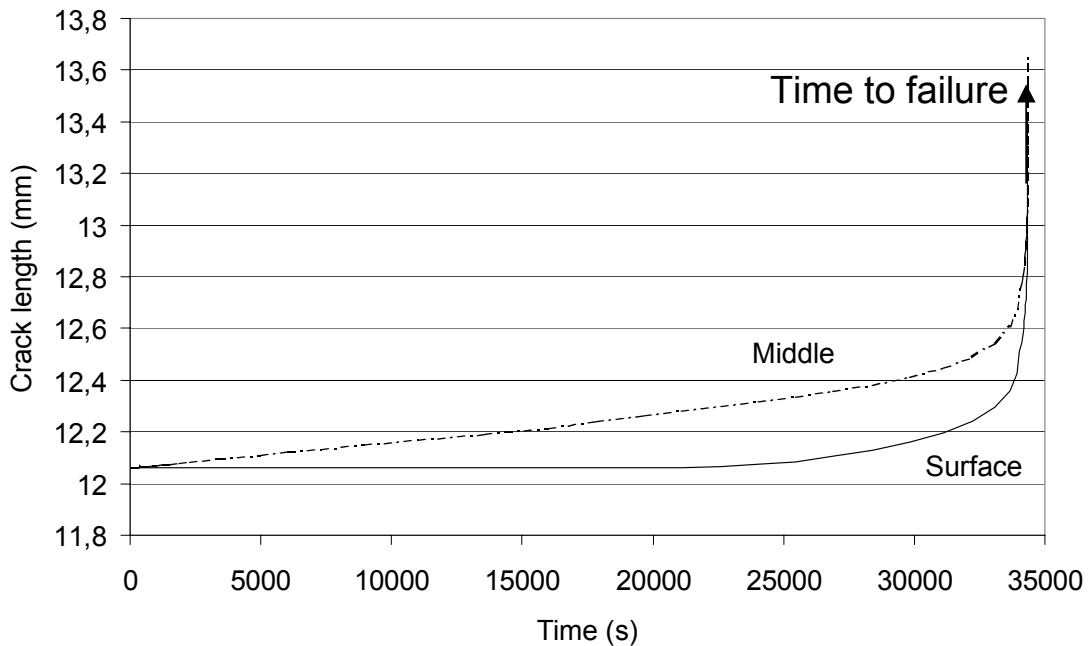


**Fig.VI-17: Evolution of crack length under sustained load**

In Fig.VI-17, the curve "middle" stands for the evolution of the displacement of the node in the middle of the specimen, which gives the evolution of the crack length. Following the conclusions related to the Fig.VI-11, since the K distribution is higher in the middle of the specimen, the resulting crack velocity is then higher too, leading to a more important displacement than at the free surface of the specimen.

At a certain time, the so-called "time-to-failure" under the given load, the critical stress intensity factor is reached, leading to a very high acceleration of the crack velocity. With this method, the time to failure can be calculated, provided that accurate experimental crack growth data are available.

Fig.VI-18 depicts the growth profile plots provided by Zencrack after an analysis. The initial open part of the crack is represented and the lines represent the growth profile. One finds again in (a) the difference between the middle and the free surface of the

specimen in the different crack front shapes whereas in (b), where  $v=0.3$ , crack fronts are straight.

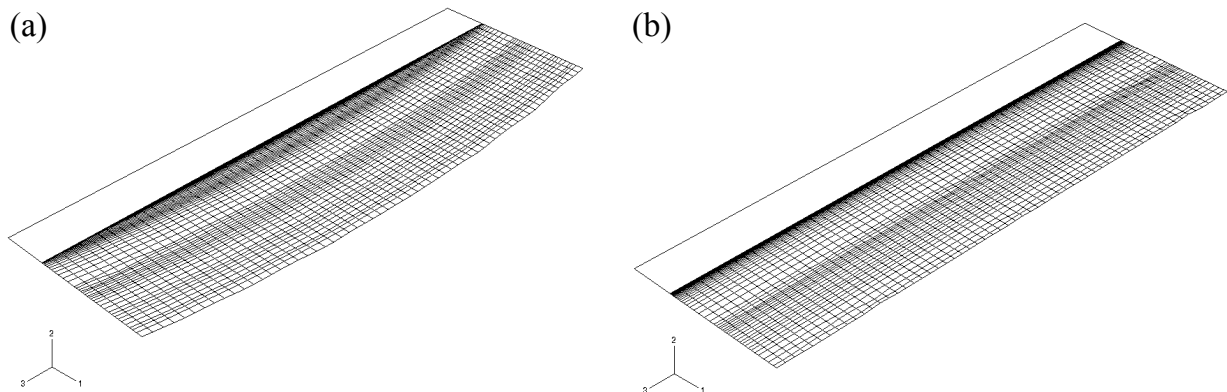


**Fig.VI-18: Crack growth profiles of a crack in a CT specimen under sustained load; (a) with  $Nu=0.3$  and (b) with  $Nu=0.0$**

Fig.VI-19 depicts the initial and the final state of the simulation. In Fig.VI-19(a), the mesh was modified by Zencrack around the crack tip to represent the exact crack length. During the propagation simulation (Fig.VI-19(b)), the crack front was moved from one set of element locations to the other when the length increment implied a great distortion overcoming the mesh quality parameters.

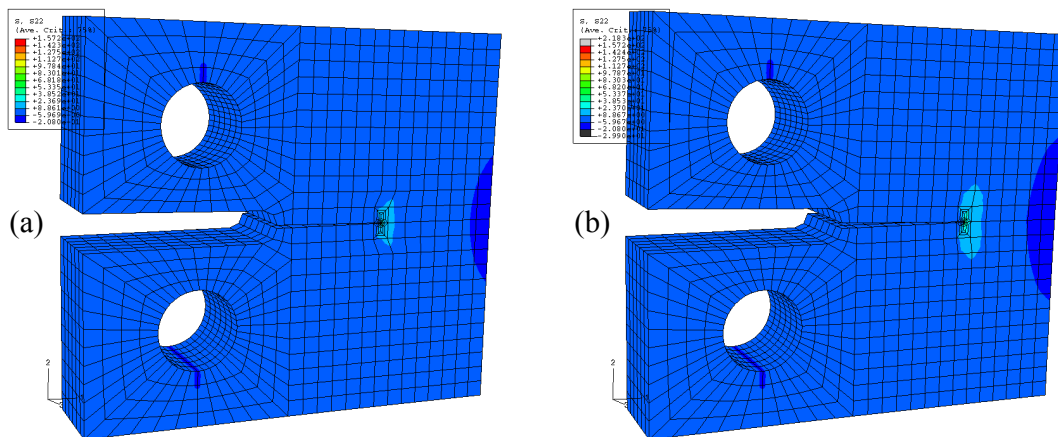


**Fig.VI-19: Model of CT specimen; (a) initial state and (b) final state**

## VI.C/Cracks between two different materials

### VI.C.1/S3PB 10mm/2mm

Test were performed on homogeneous specimens with a lower beam of resin with a 10mm thickness. The specimen was placed in a conventional three-point-bending device.

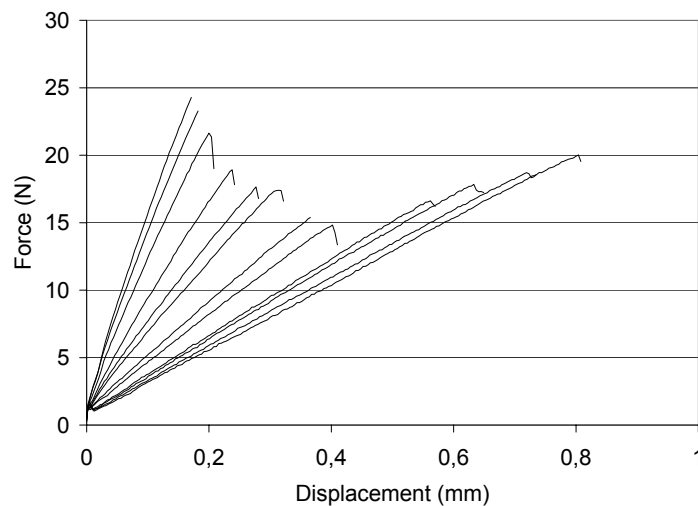


**Fig.VI-20: Typical response for 10mm/2mm double cantilever beam specimen**

One can note two trends in the load-displacement curves in Fig.VI-20. In the first half of the test series, the critical load tends to decrease while it rises again for the last tests. The first trend is observed for crack length smaller than one half of the specimen (for crack length prior to 55mm) and the second trend occurs when the crack reaches the specimen half. This trend can be explained by the load distribution under three point bending. Fig.VI-21 depicts the evolution of the crack length during the load/unload cycles.

After the total separation of the specimen, one beam was investigated under an optical microscope in order to characterise the interface. The different crack front positions can be clearly distinguished as well as the "thumbnail" shape of crack front (Fig.VI-22). Since it is not possible to record *in vivo* such a crack front distribution, and in order to simplify the evolution of the crack shape, the assumption of a perfectly linear crack front is made.

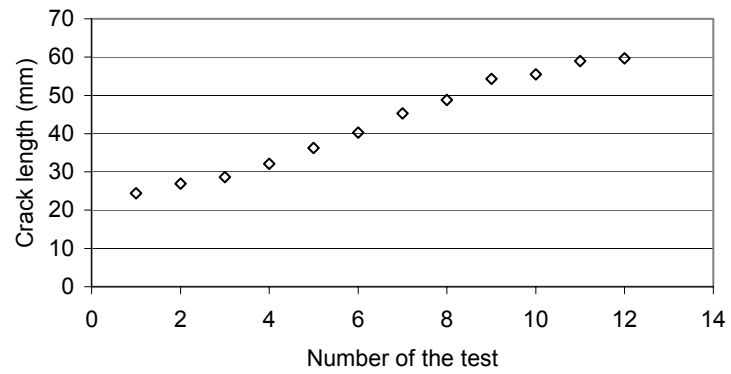


**Fig.VI-21: Evolution of crack length after each loading condition**

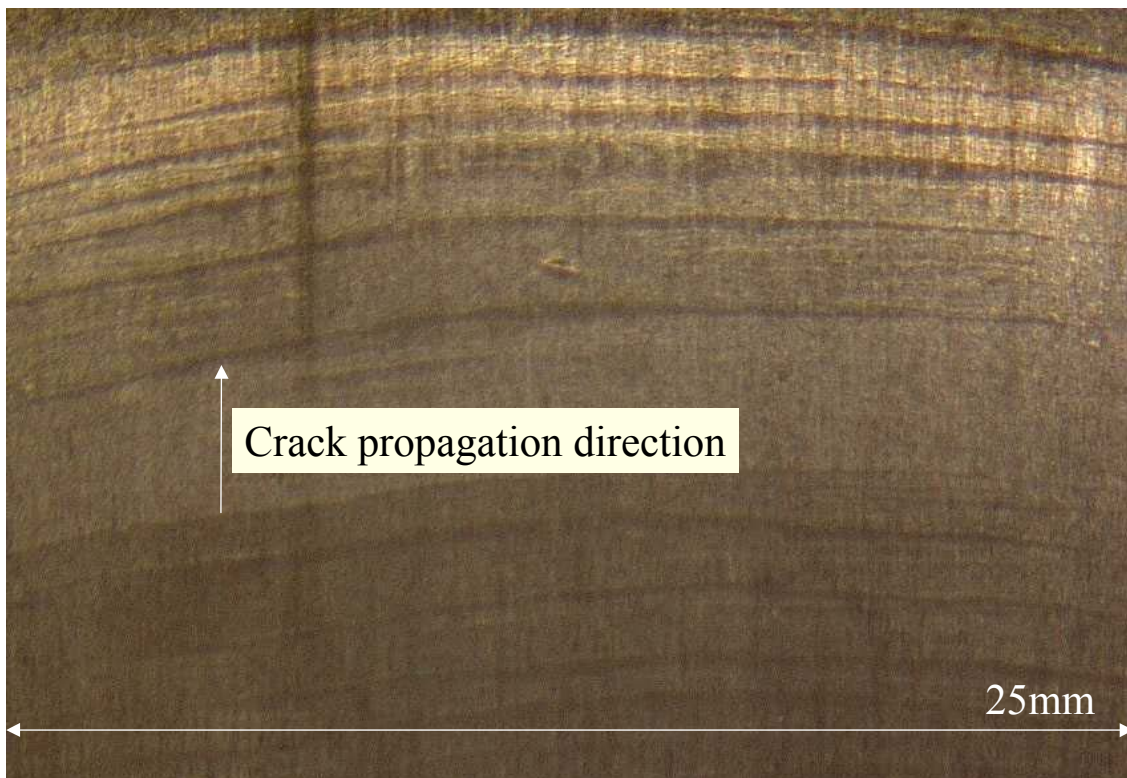


**Fig.VI-22: Propagation paths on contact face**

From the load-displacement curves, the compliance is calculated from the slope of each curve. After testing of different specimens, the compliance as a function of crack length can be obtained by a polynomial fit for a geometry with a 10mm beam (Resin) and a 2mm beam (thermoplastic material) (Fig.VI-23).

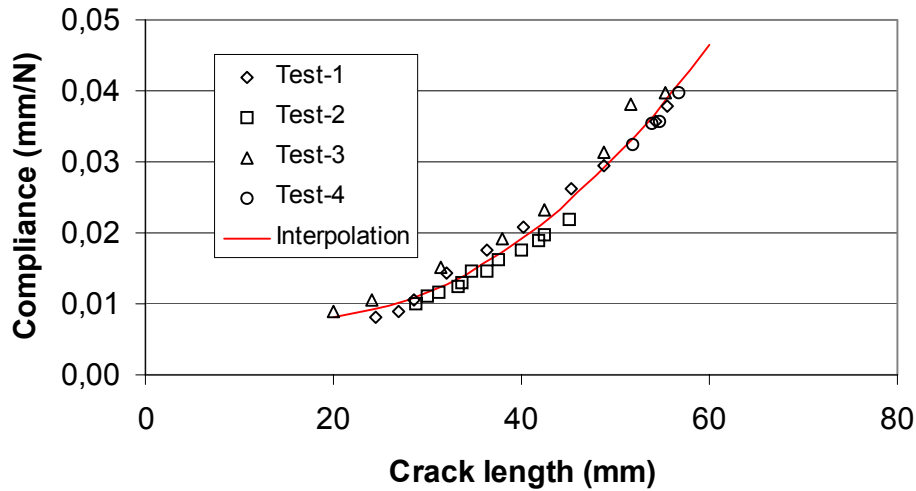


Fig.VI-23: Compliance from different tests for the S3PB 10mm/2mm

At this point, it is possible to compute the ERR and to compare the results coming from the Compliance Method (Chapter III-C-2-a) and the Area Method of Data Reduction (see Chapter III-C-2-b). Fig.VI-24 points the main disadvantage of the AMDR, namely a large dispersion. The mean value for the AMDR is 0,0054 N/mm with 29% relative error while the Compliance Method gives an approximated value of 0,0051 with "only" 20% error.

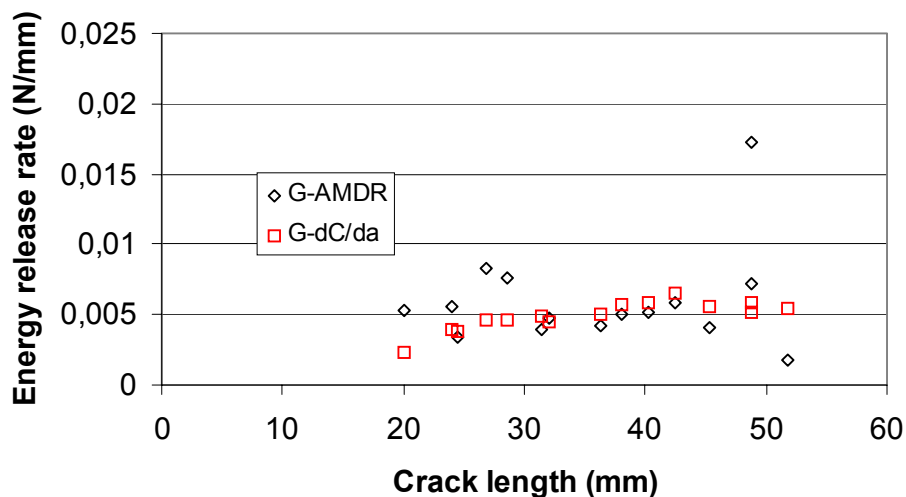


Fig.VI-24: Comparison between the AMDR and the Compliance Method

However, the fact that any knowledge of material parameters is necessary to reach these results is underlined. To control the validity of such tests, a reverse test has been developed (Fig.VI-

25). Under the assumption of a constant critical energy release rate, one can determine the force which would have been necessary to apply.

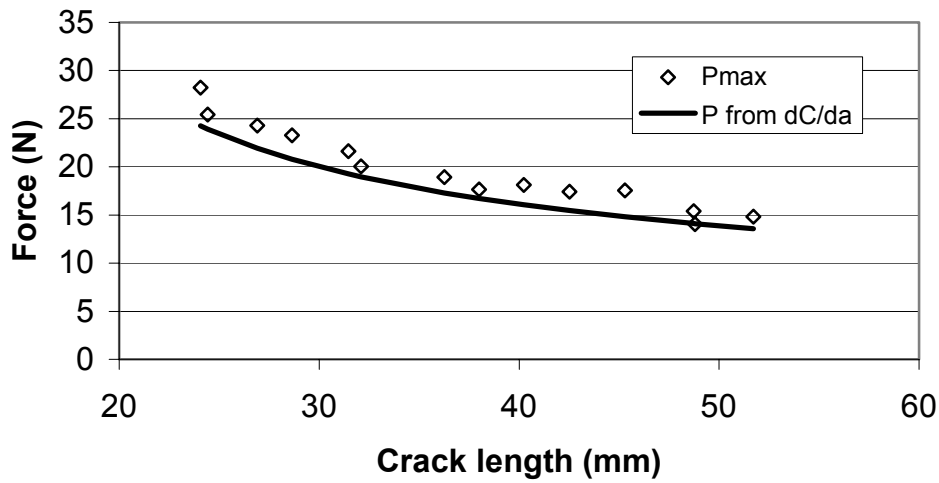


Fig.VI-25: Reverse test

The deviation between the measured force and the "ideal" force, represented in the Fig.VI-25, lies below 7,5%, which suggests that the determination of the ERR by means of this procedure is sufficiently reliable. With the knowledge of the crack length and the corresponding force, numerical simulations are performed to investigate the mixed mode angle.

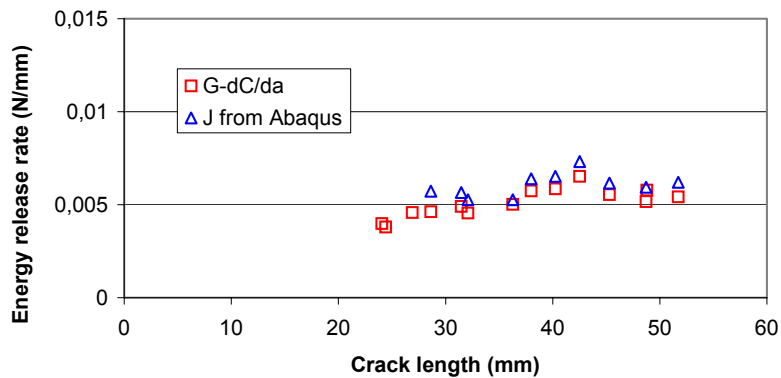
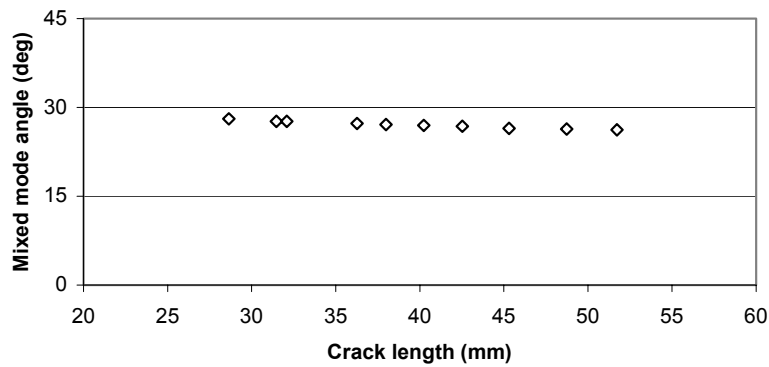


Fig.VI-26: Energy release rate computed with Abaqus

Fig.VI-26 depicts a comparison between the ERR determined by the Compliance method and the J integral delivered by Abaqus. Both results are superposed. It proves that the simulation agrees well with the experiments and that the values of  $K_1$  and  $K_2$ , consequently the mixed mode angle, correspond to the type of loading.

As depicted in the Fig.VI-27, the mixed mode angle (MMA) evolves linearly with the crack length. But its trend allows us to consider it as constant. The value of  $27,1^\circ$  (2% error) has been determined and associated with the ERR 0,006 N/mm.



**Fig.VI-27: Mixed mode angle extracted from the simulations for 10mm/2mm**

If the ERR is represented in function of the mixed mode angle as in Fig.VI-28, it can be concluded that the energy release rate is constant for this type of test and that an ERR of 0,006 N/mm has to be brought to let a crack propagate between this thermoplastic and this resin under a loading condition of 27,1°.

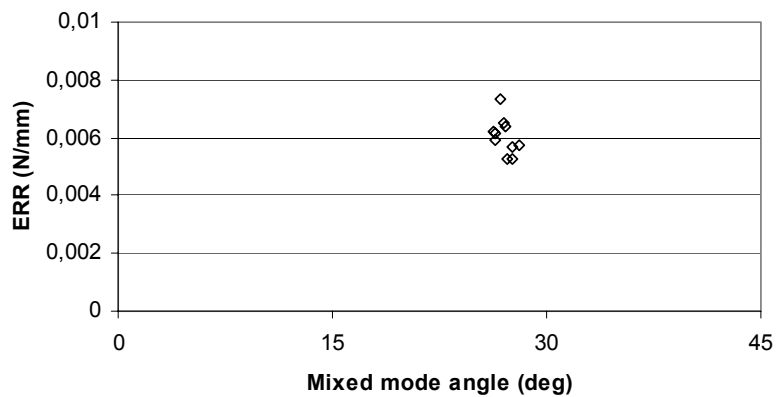


**Fig.VI-28: ERR depending on the mixed mode angle**

It should be mentioned that the results of the simulation depend on the knowledge of the elastic constants for both materials, and an error in the estimation of these properties leads necessarily to an error of the computed critical energy release rate.

At this point where the methodology was highlighted, the same data process is applied for each following configuration. At least three specimens were tested and only the pertinent results are depicted. At the end of this part, a sensitivity analysis is performed and a discussion takes place in Chapter VII.

### VI.C.2/S3PB 4mm/2mm

Fig.VI-29 depicts the compliance curve coming from the S3PB test for a specimen of 4mm thick resin beam.

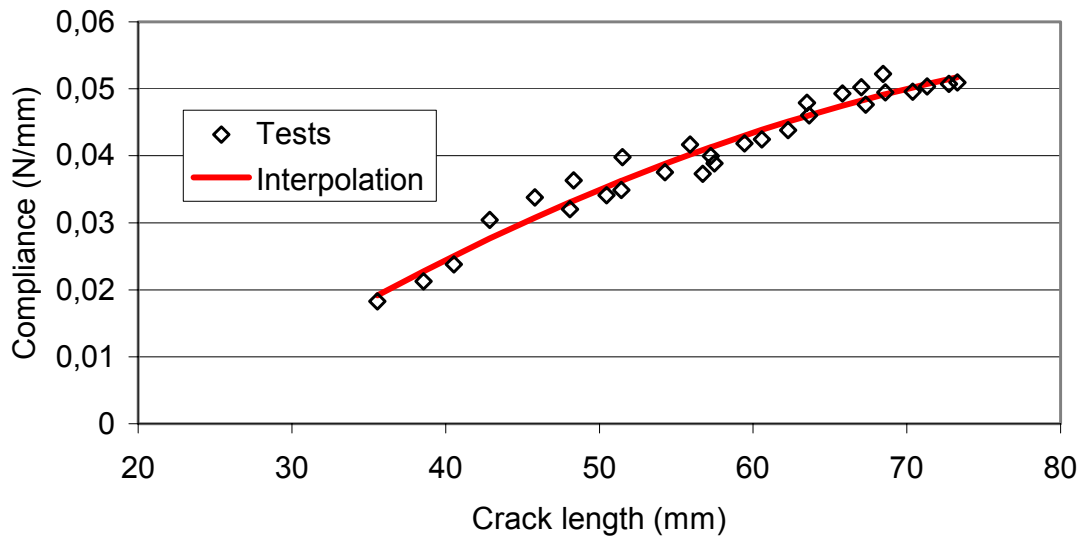


Fig.VI-29: Compliance curve for the S3PB 4mm/2mm

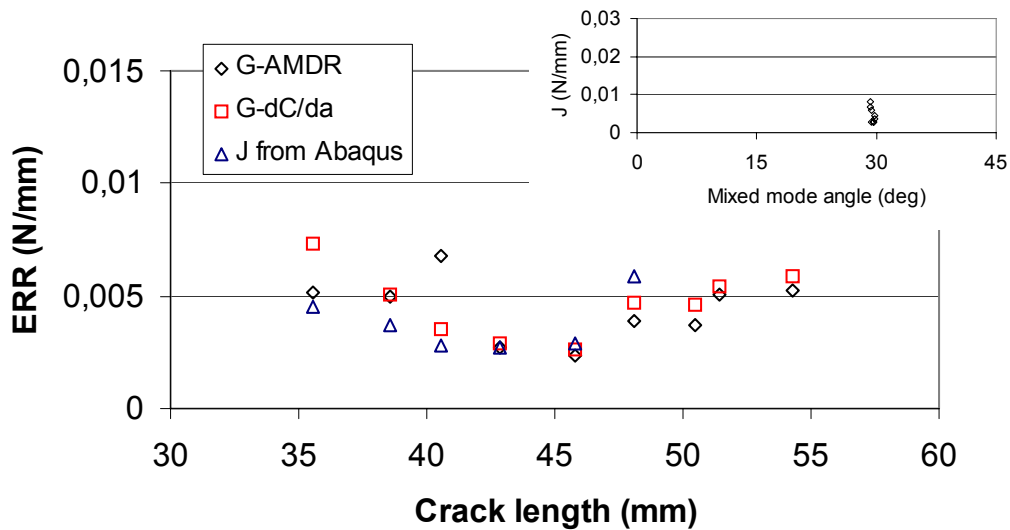


Fig.VI-30: Comparison of the ERR provided by the three methods for the S3PB 4mm/2mm, a mixed mode angle of 29,6 is noted

As depicted in the Fig.VI-30, a mixed mode angle of 29,6° is obtained, and the energy release rate necessary for the crack to grow is 0,0052 N/mm, determined with a standard deviation of 27%.

### VI.C.3/S3PB 2mm/2mm

Fig.VI-31 and Fig.VI-32 depict the most relevant results of the experimental test on specimen of 2mm/2mm under three points bending.

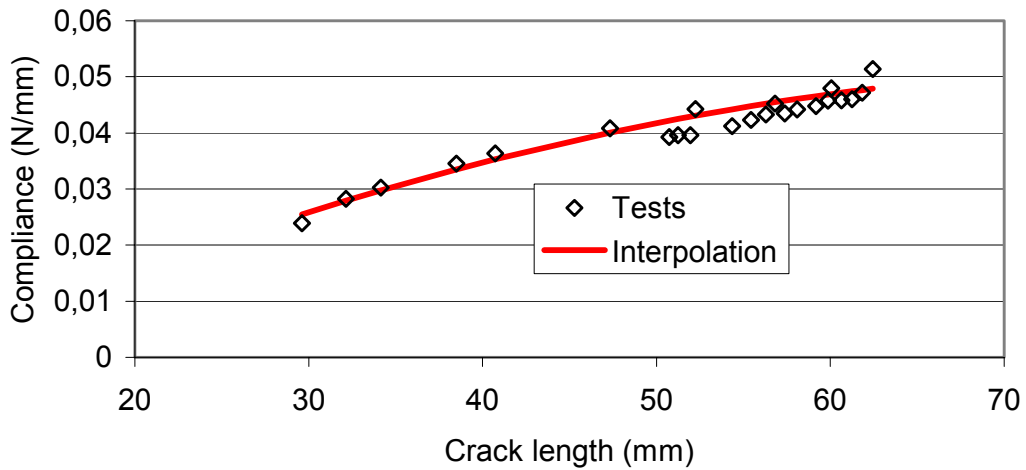


Fig.VI-31: Compliance curve for the S3PB 2mm/2mm

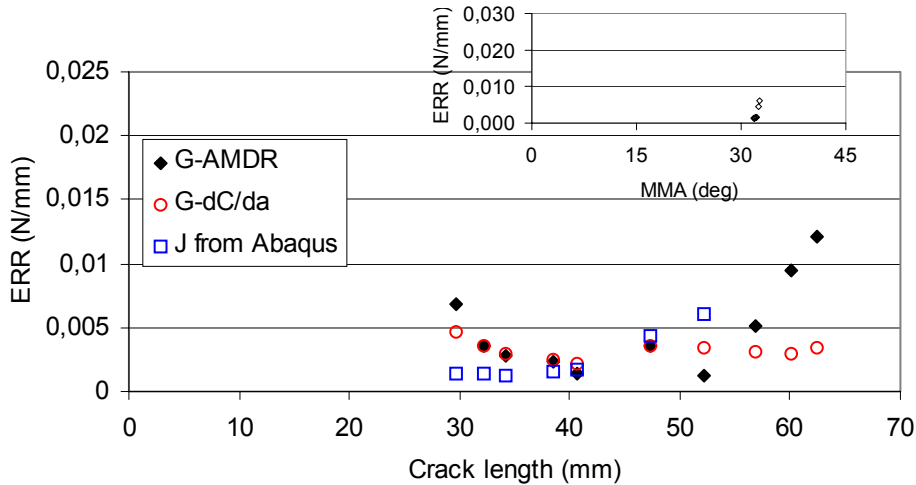
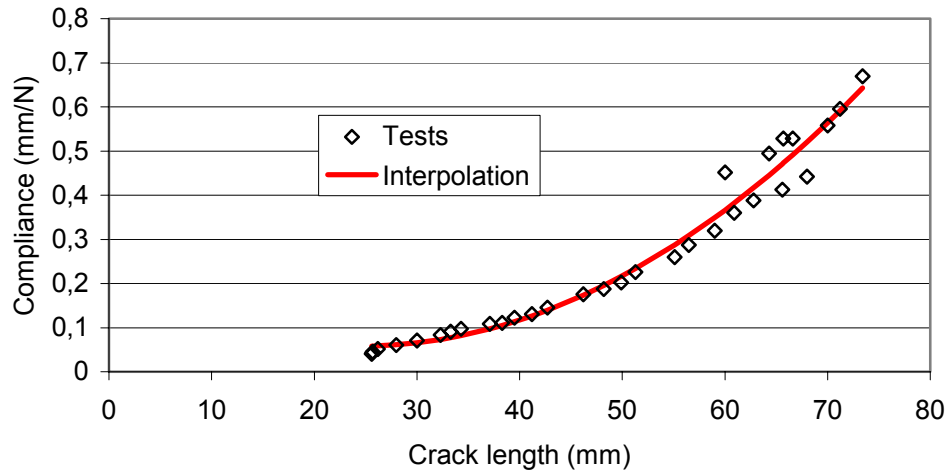


Fig.VI-32: Comparison of the ERR for three different methods

For this test, a MMA of 32,1° is obtained, and the energy release rate necessary for the crack to grow is 0,0025 N/mm, with a standard deviation of 8%.

### VI.C.4/Angle of 0°, 2mm/2mm

For a specimen of 2mm/2mm tested with the special device under a physical angle of 0°, the compliance curve in Fig.VI-33 and the ERR showed in Fig.VI-34 are obtained.



**Fig.VI-33: Compliance curve for the specimen 2mm/2mm tested with the special device under a physical angle of 0°**

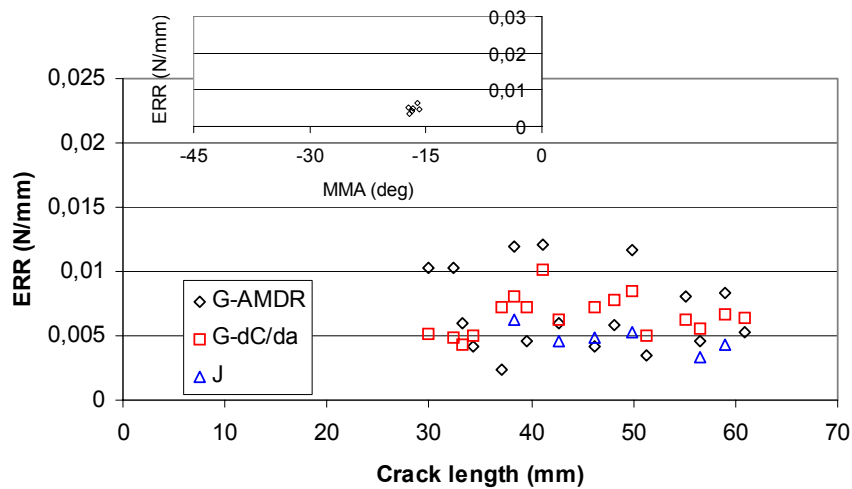


**Fig.VI-34: Comparison of the ERR provided by three methods and the associated mixed mode angle**

For this test, the MMA is -16,6°, and the associated energy release rate is 0,0048 N/mm, with a standard deviation of 20%.

### VI.C.5/Angle of 0°, 4mm/2mm

Fig.VI-35 depicts the compliance curve obtained by testing specimens of 4mm/2mm with the special device under an angle of 0°.

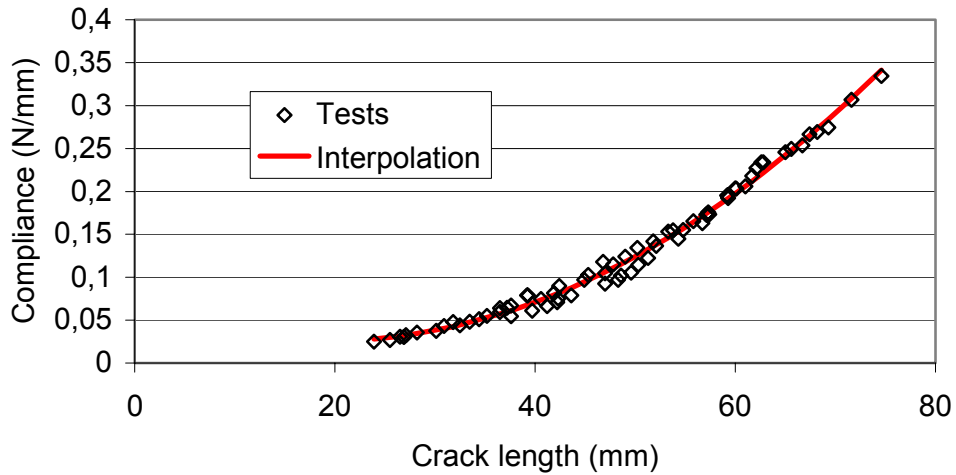


Fig.VI-35: Compliance for the specimen 4mm/2mm under 0°

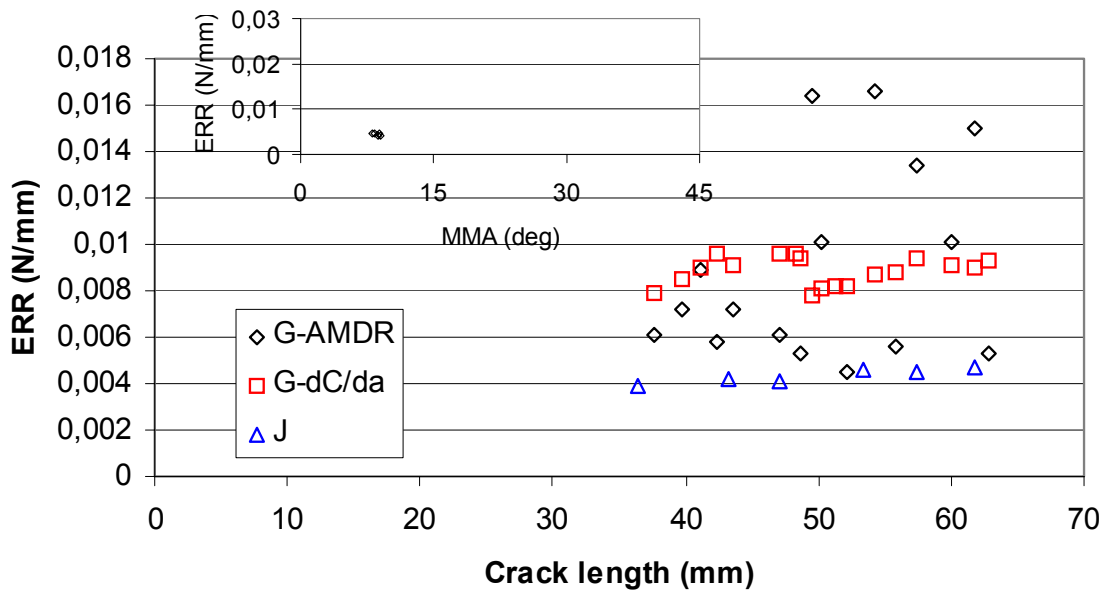


Fig.VI-36: ERR for a 4mm/2mm under 0°

As shown in Fig.VI-36, a mixed mode angle of 8,4° is obtained, and the energy release rate necessary for the crack to grow is 0,0088 N/mm, with a standard deviation of 12%.

### VI.C.6/Angle of 0°, 10mm/2mm

Fig.VI-37 and Fig.VI-38 depict the experimental results of the 10mm/2mm geometry under a physical angle of 0°.

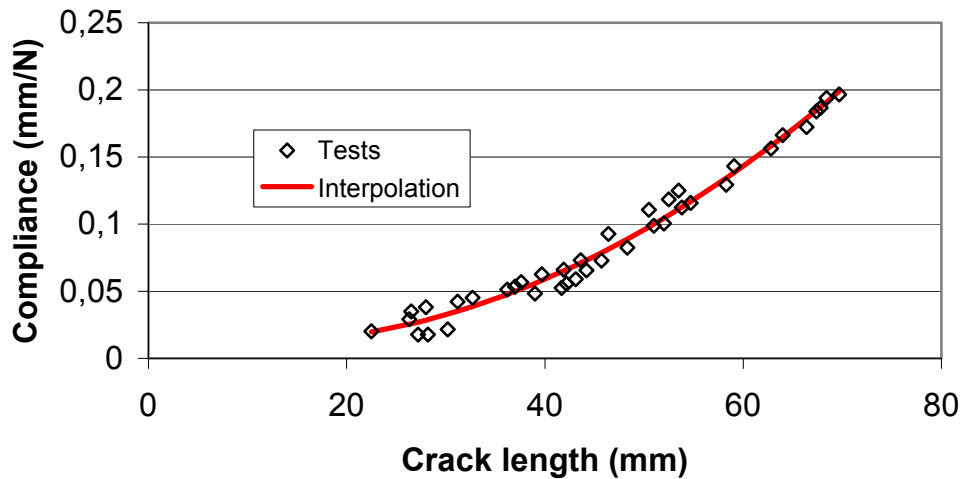


Fig.VI-37: Compliance of the 10mm/2mm geometry under 0°

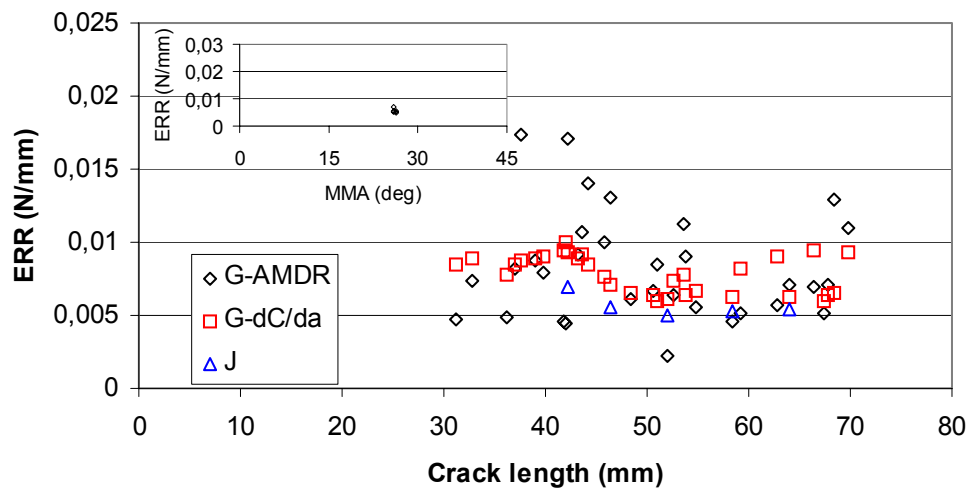


Fig.VI-38: ERR of the 10mm/2mm geometry under 0°

For this test, a mixed mode angle of 26,1° is obtained, and the energy release rate necessary for the crack to grow is 0,0056 N/mm, with a standard deviation of 14%.

### VI.C.7/Angle of 15°, 10mm/2mm

The 10mm/2mm geometry is tested under a physical angle of 15°. Fig.VI-39 and Fig.VI-40 show the results.

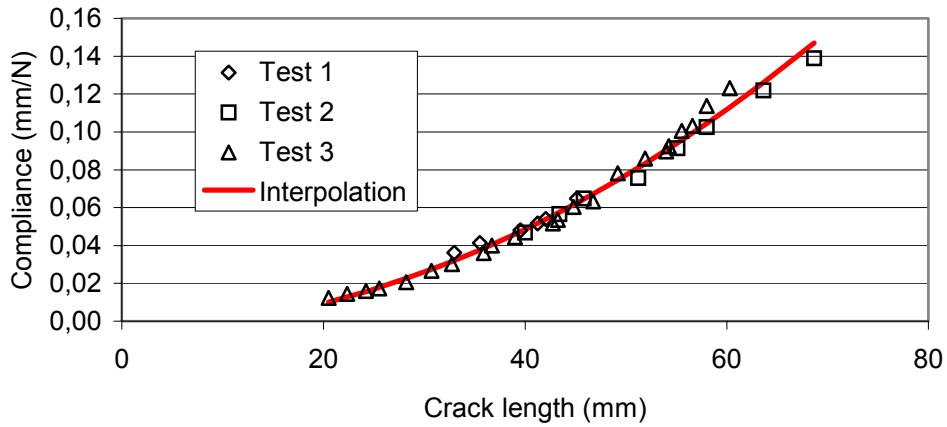


Fig.VI-39: Compliance curve for the 10mm/2mm geometry under 15°

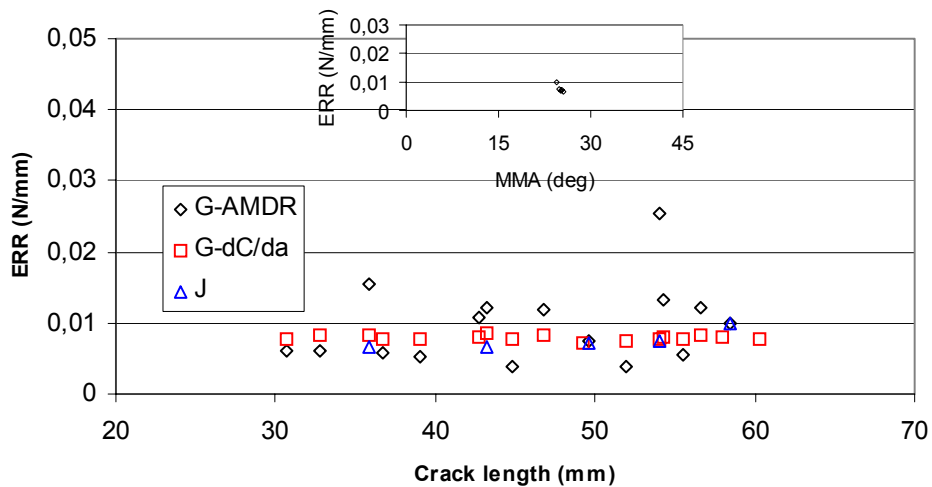


Fig.VI-40: ERR results for the 10mm/2mm under 15°

For this test, a mixed mode angle of 25,1° is obtained, and the energy release rate necessary for the crack to grow is 0,0076 N/mm, with a standard deviation of 17%.

### VI.C.8/Angle of 30°, 10mm/2mm

The device is here oriented such that the specimens are tested under a physical angle of 30°. Fig.VI-41 depicts the measured compliance and Fig.VI-42 the comparison of the three methods to compute the ERR.

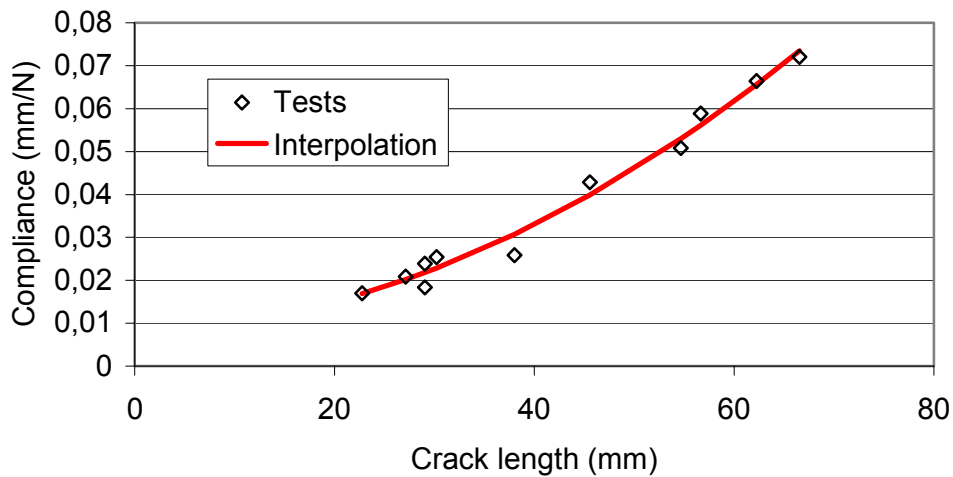


Fig.VI-41: Compliance of the 10mm/2mm under 30°

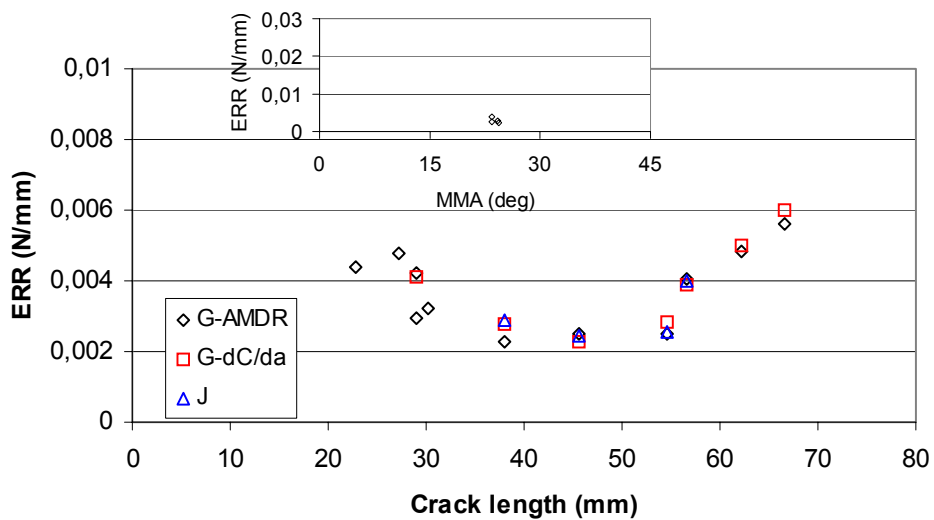
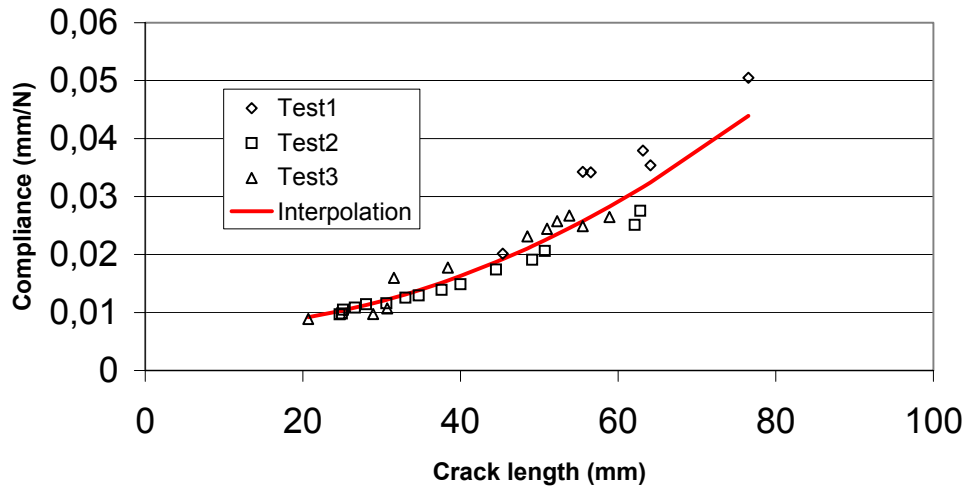


Fig.VI-42: ERR of the 10mm/2mm for 30°

For this test, a mixed mode angle of 23,9° is obtained, and the energy release rate necessary for the crack to grow is 0,0030 N/mm, with a standard deviation of 24%.

**VI.C.9/Angle of 45°, 10mm/2mm**



**Fig.VI-43: Compliance of the 10mm/2mm under 45°**

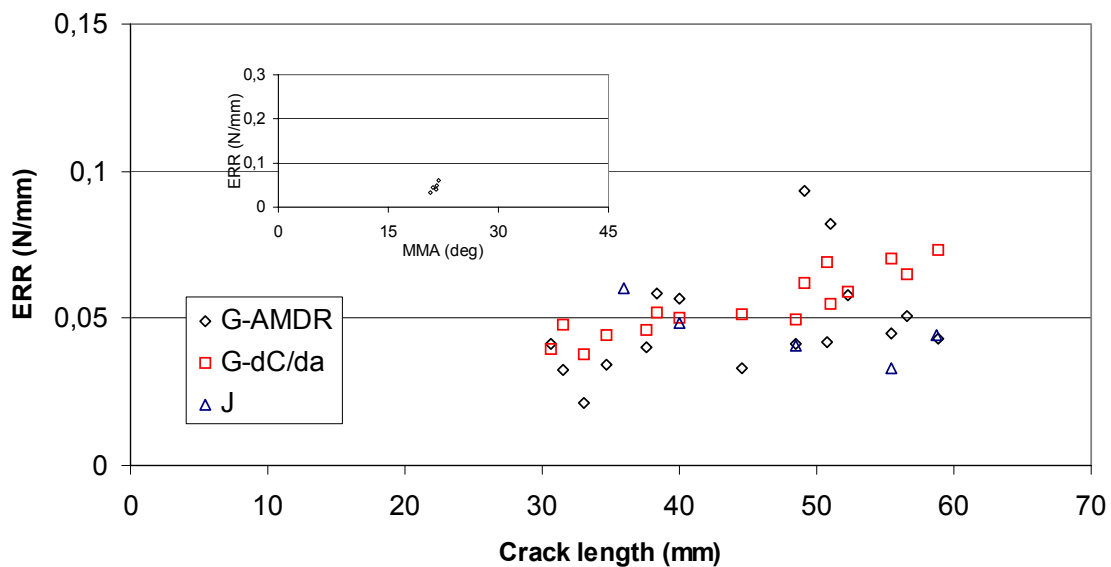


**Fig.VI-44: ERR of the 10mm/2mm under 45°**

Specimens with the geometry 10mm/2mm tested under a physical angle of 45° show a compliance as depicted in Fig.VI-43. The ERR provided by the three methods are represented in Fig.VI-44. For this test, a mixed mode angle of 21,3° is obtained, associated with an ERR of 0,0455 N/mm, with a standard deviation of 22%.

### VI.C.10/Sensitivity analysis

A first sensitivity analysis has already been performed numerically. The influence of specimen geometry and material combination have been studied [2003-Leblanc]. The above results can sum up the variation of different parameters on experimental results. Firstly, concerning the tests on the symmetric three points bending, the thickness of the resin beam has varied. The resulting mixed mode angles are plotted in the Fig.VI-45. In the case of the S3PB, increasing the resin thickness leads to diminishing the mixed mode angle, i.e. reducing the contribution of mode II in the crack tip stress state.

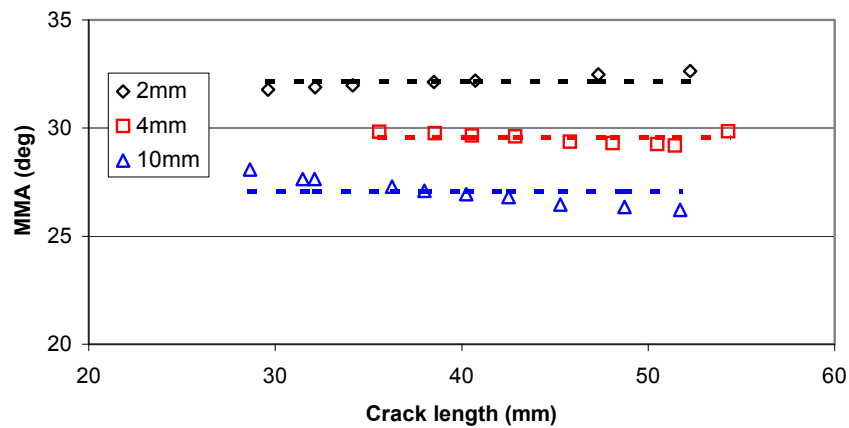


**Fig.VI-45: Variation of the mixed mode angle with the resin layer thickness under 3 points bending**

Secondly, while keeping the physical loading angle constant to 0°, one lets the resin layer thickness vary. In this case, the mixed mode angle increases with the resin layer thickness as showed in the Fig.VI-46.

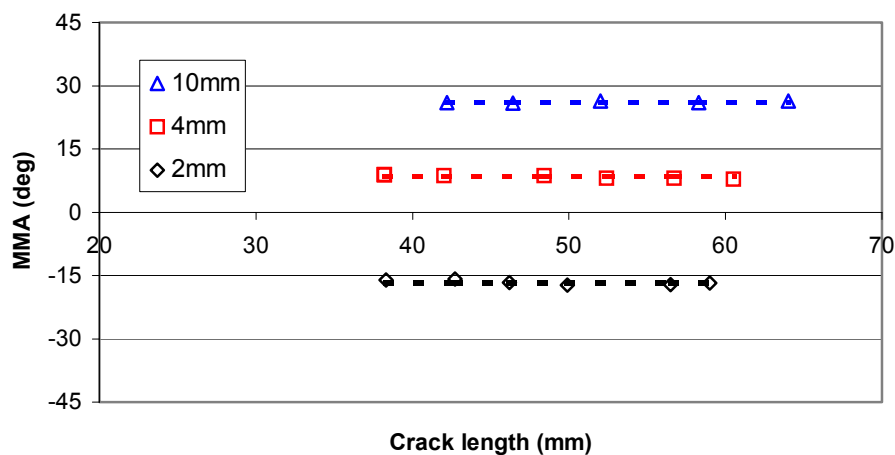


**Fig.VI-46: Variation of the mixed mode angle with the resin layer thickness under a physical angle of 0°**

Finally, when the resin thickness is held constant and when the physical angle varies, the mixed mode angle depicted in the Fig.VI-47 tends to diminish slightly while the thickness increases.

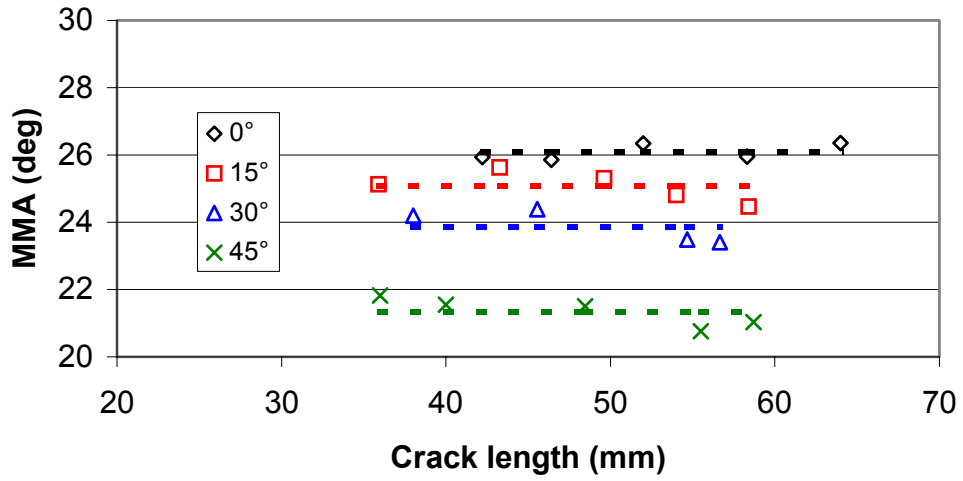


**Fig.VI-47: Variation of the mixed mode angle with the physical angle, the resin thickness being constant and equal to 10mm**

### VI.D/Interfacial fracture energy curve

The ultimate result to present is the interfacial fracture energy curve resulting from the measurement campaign (Fig.VI-48) in conjunction with the numerical analysis. A trend could be depicted in this curve. But one has to be very careful with interpretations.

The point corresponding to a MMA of  $21,3^\circ$  comes from the  $45^\circ$  configuration. The relative high difference with the other points come from that this configuration was tested first. Thereafter, the experimental procedure was improved since the tools used for the experiments were better understood. The finding that the specific fracture energy is almost independent of the mixed mode angle is surprising. The correlation between  $G$  and  $\psi$  has, therefore, to be further investigated.

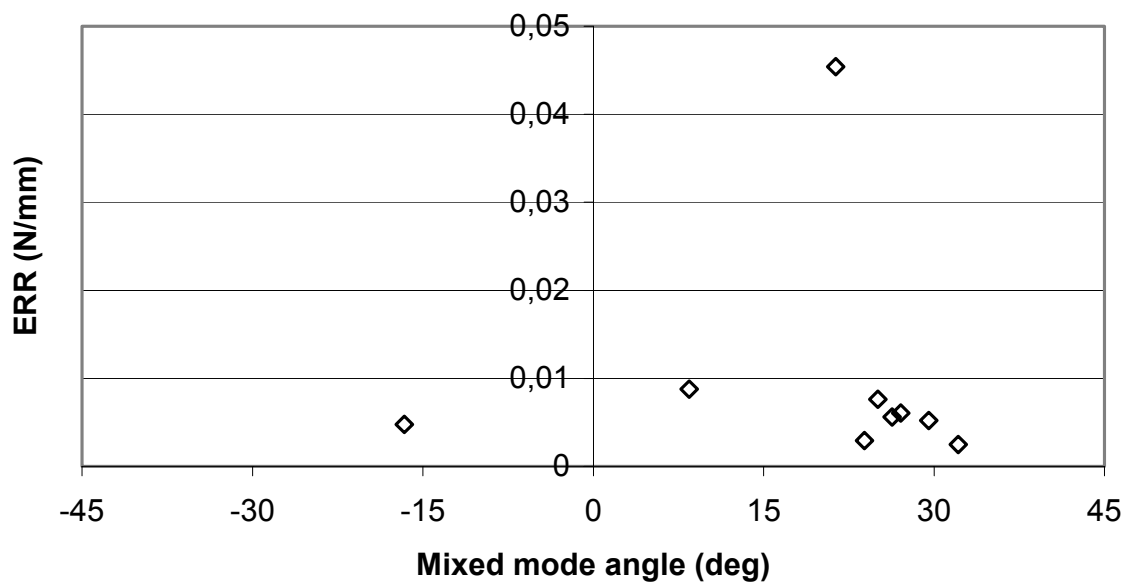


Fig.VI-48: Interfacial fracture energy curve

---

---

# **Chapter VII**

## DISCUSSION



## VII/ Discussion

The choice of producing a FE analysis, in the fracture mechanics framework has to be highlighted.

### VII.A/About the fracture toughness

#### VII.A.1/Location of the crack

The first question to answer is to know where the crack has to be introduced in the model. This may come from pictures of real components which were tested and failed or the critical locations may be identified from a damage mechanics analysis. Secondly, one has to fix the initial crack length. If the crack was already detected and if the component has not failed, then the length is defined by the dimensions depicted on the micrograph. If such a picture is not available, one may fix the initial crack length equal to the characteristic length of flaws contained in a material. It can be the size of a particle or the size of an air bubble.

It is also possible to fix the initial length depending on the fracture toughness from Eq.VII-1. Suppose that the stress to failure  $\sigma_f$  is known, it is then possible, with the help of some scaling parameters  $Y$ , to determine a length corresponding to the  $K_c$ . For example,  $Y=\sqrt{\pi}$  for a straight crack in infinite specimen cracks and  $Y=2/\sqrt{\pi}$  for a penny crack in an infinite body. Then the simulation will say if the  $K$  arising in the crack domain is critical or not. If not, subcritical crack growth could occur.

$$a_0 = \left( \frac{K_{Ic}}{Y\sigma_f} \right)^2 \quad \text{Eq.VII-1}$$

#### VII.A.2/Type of mesh

Then comes the question of the mesh generation. As seen earlier in chapter IV, the mesh has to be produced with brick elements. This is a practical solution if the geometry is simple, for instance, if the geometry presents a topology suitable for a block structured mesh.

If not, there exists the possibility to isolate the crack domain, to mesh it with block elements and the rest of the geometry automatically with tetrahedrons.

A third possibility as a FE analysis technique is the submodelling. An analysis will be performed on the whole component, considered as the global model, and results are transposed, or interpolated, to a

local part of the model, the submodel, which is meshed finer and will contain the crack.

### VII.A.3/Material parameters

Obviously, as treated in this work, the material parameters play an important role. The influence of the fracture toughness in conjunction with the exponent of the propagation law on the time-to-failure is investigated. Four cases have been distinguished. They are depicted in the Fig.VII-1.

With the cumulative probability  $F$  (Chapter V, Eq.V-6), one determines lower and upper bounds for the maximum likelihood fit of the fracture toughness. The lower bound will be determined by the cumulative probability of 2,5% (i.e. the fracture toughness is lower or equal to the maximum likelihood fit with a probability of 2,5%, when  $F=0,025$ ) and the upper bound will be determined by the cumulative probability of 97,5% ( $F=0,975$ ).

The time-to-failure  $t_f$  is given by the equation from chapter II:

$$t_f = \frac{2[(K_{I1}^{2-n_I} - K_{Ic}^{2-n_I})]}{[(n_I - 2)A_I Y^2 \sigma_0^2]} \quad \text{Eq.VII-2}$$

Case (a): case of a material with a low scatter and a high exponent

The case (a) concerns the influence of the knowledge of  $K_{IC}$  on the time-to-failure. The exponent  $n_I$  of the subcritical crack growth law will be 36 and the coefficient  $A_I$  equal to  $1,0 \times 10^7$  (Chapter 5, Eq.VII-4). The scaling factor  $Y$  equals  $\sqrt{\pi}$  for a straight through crack and the applied stress equals 12,5 MPa (it corresponds to a force of 75N applied along the 6mm thickness of the CT specimen). The initial crack length will be fixed to 9,4mm, which corresponds to an initial  $K$  of  $0,781 \text{ MPa}\sqrt{m}$ .

From material 2 comes:

$$F(K) = 1 - \exp\left(-\left(\frac{K}{0,997}\right)^{40,63}\right) \quad \text{Eq.VII-3}$$

Then,

$$F=0,025 \Rightarrow K_{0,025}=0,911 \text{ MPa}\sqrt{m}$$

$$F=0,975 \Rightarrow K_{0,975}=1,026 \text{ MPa}\sqrt{m}$$

$$\Delta K=0,115 \text{ MPa}\sqrt{m}.$$

Case (b): case of a material with a high scatter and a high exponent

The case (b) deals with a larger width of the interval of  $K$ . From material 1 comes

$$F(K) = 1 - \exp\left(-\left(\frac{K}{1,369}\right)^{18,41}\right) \quad \text{Eq.VII-4}$$

Then,

$$F=0,025 \Rightarrow K_{0,025}=1,121 \text{ MPa}\sqrt{m}$$

$$F=0,975 \Rightarrow K_{0,975}=1,470 \text{ MPa}\sqrt{m}$$

$$\Delta K=0,345 \text{ MPa}\sqrt{m}.$$

This  $\Delta K$  is applied to the maximum likelihood fit of  $K_0$  for material 2 ( $0,997\text{MPa}\sqrt{m}$ ) in order to compare the influence of the width of the confidence interval. This yields the values  $K_{0,025}=0,823$  and  $K_{0,975}=1,171 \text{ MPa}\sqrt{m}$  as lower and upper bounds.

The case (c) stands for a material with a low scatter and a high exponent. It shows the influence of the exponent in the subcritical crack growth law. The exponent considered here comes from subcritical tests on PMMA [1987-Kausch] and is equal to 25, with the  $\Delta K$  of case (a). Case (d) corresponds to a material with a high scatter and a low exponent. It uses the exponent of case (c) and the width  $\Delta K$  of case (b).

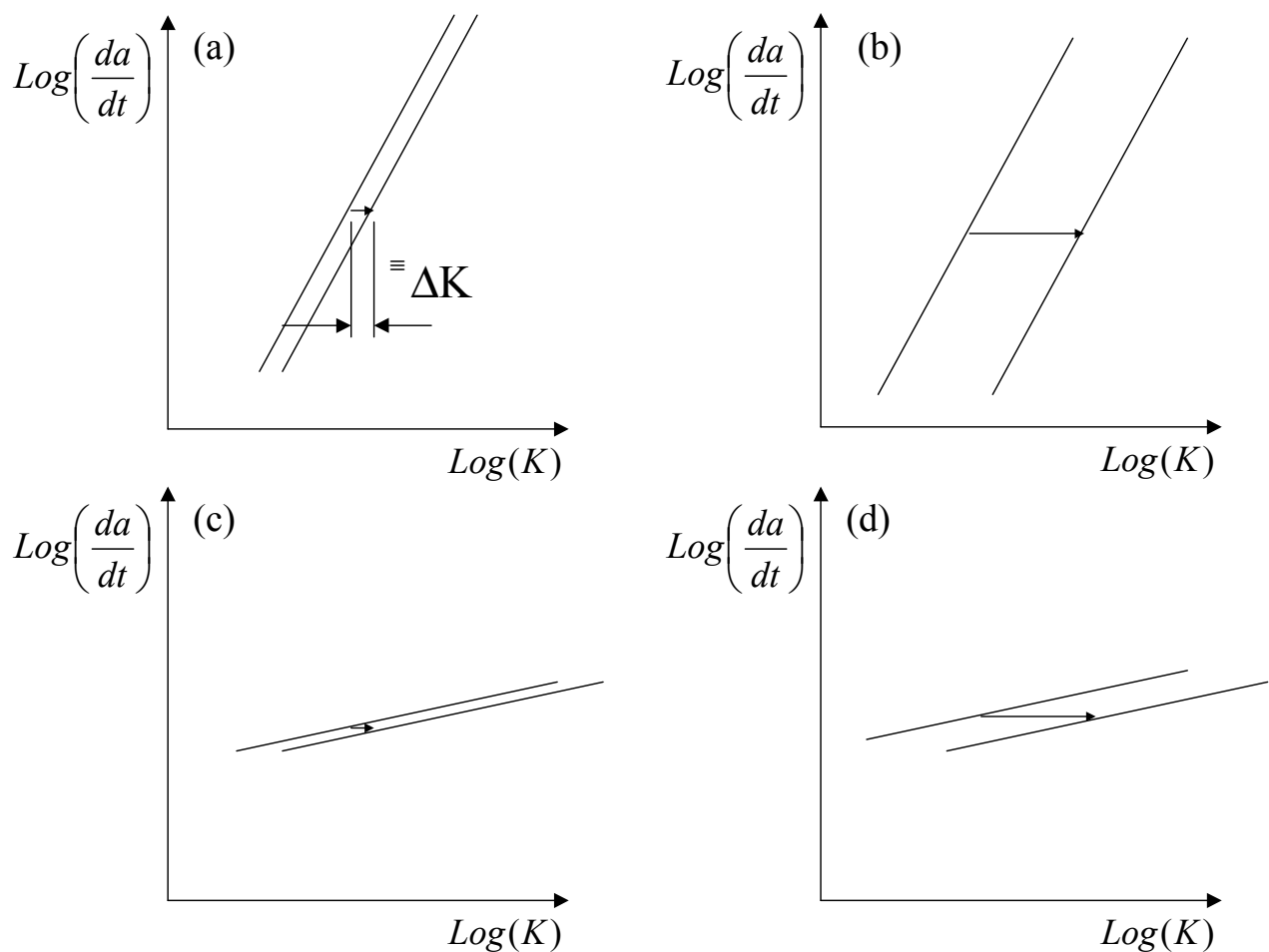


Fig.VII-1: Cases to be considered

For each case, two times-to-failure are calculated. One corresponding to the lower bound  $t_{f,lower}$ , and one corresponding to the upper bound,  $t_{f,upper}$ . The quantity  $\text{Log}(t_{f,upper}/t_{f,lower})$  is depicted in Fig.VII-2 for each case. In the case of a high exponent, the time-to-failure can vary by a factor of 100 until 500000 times, depending on the scatter of the fracture toughness. For a lower exponent, the variation ranges from 50 to 100000 times. It means that simulations performed with a material with a high scatter, no matter the exponent, can not be considered as reliable since the predicted lifetime can vary by a factor of 500000.

A procedure in the case of a material with large scatter and a high exponent in the crack propagation law can be to fix the allowed stress intensity factor to the lower bound of the 90% or 95% confidence interval  $K_{low,90\%}$ . After having computed the loading case and determined the  $K_{load}$  occurring at the crack tip, this value is compared with the lower bound. In the case  $K_{load} < K_{low,90\%}$ , one will say that the load represents no danger for the cracked component. In the other case, the crack will be considered as critical. Such a procedure can be likewise followed when the order of magnitude of the exponent in the propagation law is relative high.

Another approach can be chosen when the fracture toughness is known with a high reliability. One decides to use two different exponents in the propagation law and to perform some simulations with each of these exponents and to check the difference in the results.

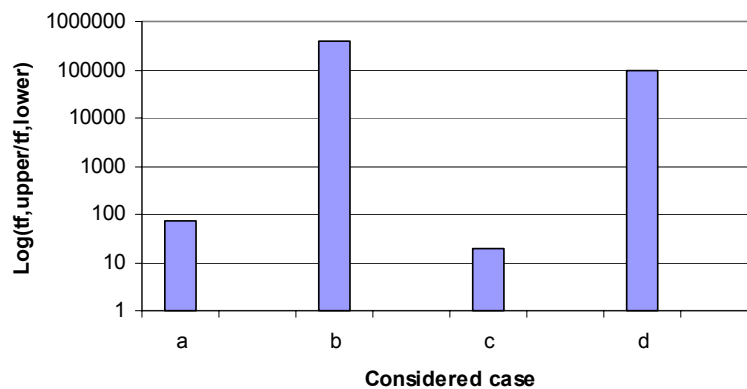


Fig.VII-2: Comparison between four cases for the time-to-failure

### VII.B/About the interface investigation

Based on the wide range of tests performed until now, one may note that the Area Method is easy to perform. One measures the crack lengths and load-displacement curves for at least six loading-unloading cycle to get a minimum of five values for the ERR. It is also noted that the AMDR is applicable in cases where the specimen response to the load is mainly linear and the interfacial crack advance is stable. The first condition is fulfilled for each test configuration reported here while the second is fulfilled only for ADCB configurations, according to Auersperg et al [2001-Auersperg].

In practice, always more than eleven cycles can be taken per specimen. This allows us to get enough points to achieve an accurate interpolation of the compliance curve. As a matter of fact, the compliance method can be applied in any case and we are able to compute the energy release rate for each configuration.

In general, it seems that the interfacial fracture toughness values obtained using the AMDR are of the same order of magnitude as those obtained through the Compliance Method or the finite-element analysis. As already mentioned, the trend of the obtained curve is not comparable to those in the literature. However, since the ERR values between the simulations and the experiments agree quite well, we presume that this trend describes the behaviour of the studied interface specimens. Naturally, further investigations will be performed to validate these results.

As outlined by Sundararaman and Sitaraman [1999-Sundararaman], the effect of the finite width of the specimen should be taken into account. The waves on the fracture surface clearly show the particular form of the crack front and prove that the mixed mode angle and/or the ERR vary along the crack front, which is confirmed by the simulations.

Fig.VII-3 shows the evolution of the mixed mode angle and of the J-Integral along one half of the crack front. Boundary effects affect drastically the J-Integral distribution and the profile of the crack front form (often described by a "thumbnail" form) can be found to be the same in experiments and in simulations (Fig.VII-3(b)). However the effect if the free boundary is minimised by the large ratio width/thickness. Besides, the uncertainty in the determination of the critical ERR is increased by variation of the interface adhesion from specimen to specimen but this undesired manifestation coming from manufacture can be overcome by increasing the number of measurements.

Further parameters should be considered, amongst others the residual stresses from manufacturing, the viscoelasticity of the resin and the anisotropy of thermoplastic. Residual stresses can affect the results in the sense of shrinkage. Since we cool the resin after potting, shrinkage takes place during this stage and could play a role by bending the thermoplastic plate. Bending deformed specimens were observed for 2mm thick resin layer, and this effect tends to be reduced when increasing the resin thickness.

For the sake of simplification and since Abaqus allows to compute the  $K_I$  for interfacial cracks only under the assumption of a linear elastic case, viscoelasticity of the resin and anisotropy of the thermoplastics are not taken into account. Viscoelasticity could play a role through the relatively slow displacement rate and the repetition of the loading and unloading. But the low magnitude of the applied force and time let us suppose this effect can be reasonably neglected. In the same way, the anisotropy can be neglected, since the elastic properties do not strongly depend on the direction. A way to account for the non-linear material behaviour would be to implement a subroutine to be used with Abaqus which will compute the ERR via the Modified Crack Closure Technique presented in part III (B-6-b).

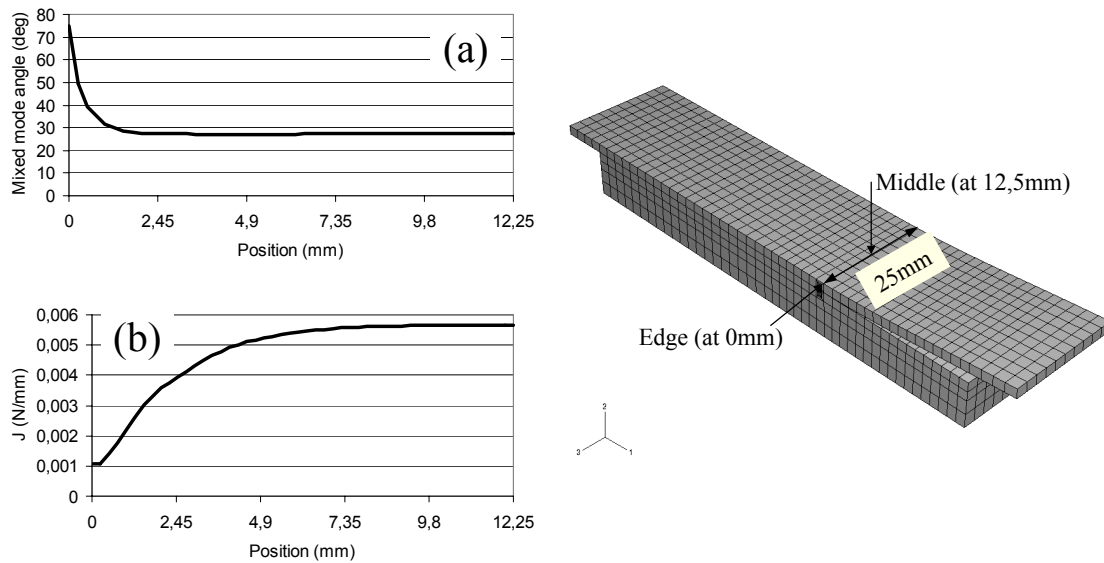


**Fig.VII-3: Magnitude of: (a) the Mixed mode angle and (b): the ERR along the crack front**

Results presented in the previous part need to be completed by further investigations, especially with negative physical load angles and other bending tests like the Single Leg Bending. The practicability of such tests was demonstrated but not presented.

However, we have to note that all the work on interfacial fracture toughness determination is based on the investigation of a relatively weak interface. This is unfortunately not always the case. One may have to deal with stronger interfaces which can not be measured by the presented methods. Sometimes the interface was tougher than one or both materials, which led either to crack kinking out of the interface plane (see for instance Fig.VII-4) or to a non uniform propagation (Fig.VII-5).



**Fig.VII-4: Crack kinking out of the interface plane**

Strong interface by itself is not necessarily a problem. However, if the interface is very strong, such that it does not lead to failure, it might not be necessary to determine the critical ERR for such material couples. If we are asked if the interface resulting of such a material combination presents a risk for the reliability, the answer will be that the risk comes from one of the materials in presence and not from the material combination. Further investigations inspired by the works of He and Hutchinson [1989-He] or Leguillon [2001-Leguillon] on the topic of crack deviation and/or penetration need to be performed.

Another case to consider is a non uniform propagation in the interface plane (see Fig.VII-5). Here is a combination of two effects observed after having taken the picture on the right: on one side a crack clearly started in the thermoplastic (side where the length is noted 15600 $\mu$ ) while on the other side the crack has continued to grow along the interface. Residual stresses from manufacturing may be the cause of this phenomenon.

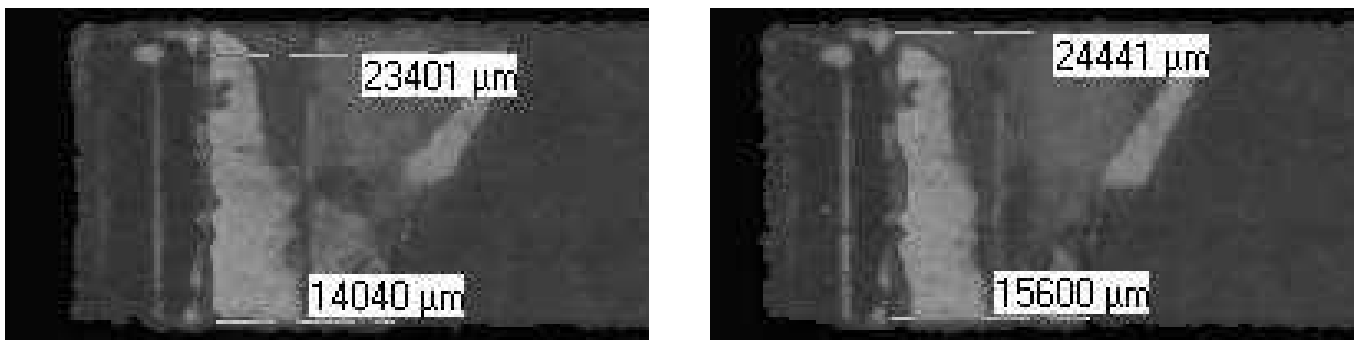


**Fig.VII-5: Ultrasonic micrographs of an example of non uniform propagation**

From a numerical point of view, if one wants to study the delamination and assess the behaviour of the interfacial crack, one will run the simulation and pick out the value for  $K_1$  and  $K_2$  at the tip, by then the interfacial energy release rate  $G_{\text{computed}}$  is known. The mixed mode angle  $\Psi_{\text{computed}}$  is then computed and compared to interfacial fracture energy  $G_c$  for the given mixed mode angle. The interface crack propagates if  $G_{\text{computed}} > G_c(\Psi_{\text{computed}})$ .

The final stage in the crack behaviour analyse is reached when both materials (above and below the crack) are characterised depending on the mixed mode angle. Besides, assuming the interfacial fracture energy depending on the mixed mode angle is also known, one will be able to determine the direction of propagation of the crack. With the criterion  $G_{\text{computed}} > G_c(\Psi_{\text{computed}})$ , one is able to assess if the crack propagates along the interface. In the case where the interface resists the propagation, a criterion such as He and Hutchinson's

$\frac{G_c(\psi)}{G_{lc}^{(2)}} < \frac{G_d}{G_p}$  can be applied to determine if the crack will penetrate in a material.

# **Chapter VIII**

## CONCLUSION AND PERSPECTIVES

## VIII/ Conclusion and perspectives

Reliability becomes a major objective in the industry, and improved methods were developed during the last decades. In order to increase the reliability of a product, the automotive industry is interested in the advantages provided by numerical simulations during the development. Cracks often appear as a major cause of failure of products in service and there exists a need to understand the phenomena occurring when a product contains a crack. A methodology to investigate the behaviour of cracks in homogeneous materials and at the interface between different materials has been addressed.

In this work, the concepts of linear elastic fracture mechanics developed during the past decades have been presented.

Different fracture criteria have been highlighted, among them the energy release rate and the stress intensity factors.

A method to determine these criteria in the case of homogeneous materials has been found in a standard of the American Society of Standard and Technology.

The determination of the crack behaviour can be achieved by a propagation analysis when a propagation law is available.

Then the case of the crack lying at the interface between different materials is addressed.

The concepts involved in homogeneous materials have been adapted in order to describe the specifics of the stress state created at the crack tip when such a configuration is present.

The stress intensity factors have another meaning in the case of interfaces, and the mixed mode angle needs to be defined if one wants to achieve a description of the stresses.

The case of the crack leaving the interface plane needs to be considered.

In the domain of the simulation, there exist different methods to proceed to numerical analyses and to model a crack.

The most common is the finite element method but others like the boundary element method and meshless methods tend to catch up their delay.

The finite element method is the most widely used method, and complementary tools offer many possibilities in the domain of crack growth prediction.

In order to determine the characteristic quantities required to perform a fracture mechanics analysis, experimental procedures to measure the fracture toughness of homogeneous materials and the crack propagation law were presented. This is realised thanks to the coupling between a tensile machine and a digital camera to process images recorded during a cracking test. A special testing device was developed to investigate the interfacial fracture energy under different mixed mode angles.

Fracture toughness has been measured for two different materials and a statistical analysis has been performed to supply information on the reliability of the measured results.

It came out that the materials parameters can be described by a Weibull distribution. The materials responses present different behaviour, and the scatter in the results delivers information on how reliable these material properties are.

The subcritical crack growth of a material has been measured at room temperature and the law has been implemented in a finite element software.

Numerical simulations performed on a compact tension specimen deliver satisfactory results and they have been compared to analytical solutions provided by a standardised procedure. They are found to be in good agreement.

The measured subcritical crack growth law implemented in the finite element software, enhanced by a commercial software dedicated to fracture mechanics simulations and propagation simulations allow analyses to be performed, by which the crack path can be predicted.

The device especially developed for interfacial crack investigations, in conjunction with varying specimen geometry allows us to explore a wide range of mixed mode angle. Experimental results were extracted with two methods and compared with outputs from numerical models.

In both cases, results agreed and the mixed mode angle from the simulation was associated with the corresponding experimental fracture energy. By this way, the interfacial fracture toughness curve can be determined for a given material combination.

The whole work allows the establishment of procedures to:  
measure experimentally the fracture toughness of a material and to determine its confidence interval,  
compare different materials from a reliability point of view,  
measure experimentally the interfacial fracture energy for a material combination and, in combination with the simulations, to determine the interfacial fracture toughness curve,  
introduce a crack in a mesh and to perform a fracture mechanics analysis, in a homogeneous material as well as at the interface between different materials  
simulate the crack propagation and represent the crack path.

**Based on these achievements, it is possible to study some design variations of a cracked component and to study their influence on the crack behaviour.**

However, this work needs to be completed and enhanced by further investigations in both domains.

Concerning cracks in homogeneous materials, one has to study the influence of parameters on the crack propagation such as the temperature, residual stresses, mixed mode conditions or cyclic fatigue.

In the case of interfacial cracks, the results presented here need to be confirmed and enhanced by other mixed mode angles. One needs to characterise other material combinations and the influence of surface treatment on the interfacial fracture toughness.

The work realised in the framework of this PhD-thesis allowed the installation of numerous tools and methods making the testing of

materials easier. These materials can contain a crack or not, which can be able to propagate itself under various loading conditions and to lead to the complete failure of components.

In the framework of the experimentation, new testing devices were designed and numerical models including original features were developed during this work. These features required overcoming problems linked to associated technical difficulties, even if all the results gathered during the work are not presented in this report.

A new industrial methodology can now be applied in the development of new components and numerous perspectives are already planned in the continuity of this work.



---

## REFERENCES

## References

[1913-Inglis]: C.E. Inglis, "Stresses in a plate due to the presence of cracks and sharp corners", Trans. Inst. Naval Arch., London, vol 40, 219-230, 1913

[1920-Griffith]: A.A. Griffith, "The phenomena of rupture and flow of solids", Phil. Trans. Roy. Soc. London, 1920

[1939-Westergaard]: H.M. Westergaard, "Bearing pressure and cracks", Journal of applied mechanics, vol 6, 49-53, 1939

[1954-Irwin]: G.R. Irwin, J.A. Kies, "Critical energy release rate analysis of fracture strength", Welding Research supplement, 193-198, 1954

[1955-Orowan]: E. Orowan "Energy criteria of fracture", Welding Journal. Res. Sup., vol 34(3), 157-160, 1955

[1957-Irwin]: G.R. Irwin, "Analysis of stresses and strains near the end of a crack traversing a plate", Journal of applied Mechanics, vol 79, 361-364, 1957

[1959-Barenblatt]: G.I. Barenblatt, "On the equilibrium cracks due to brittle fracture", Doklady AN SSSR, vol 127, 47-50, 1959

[1960-Dugdale]: D.S. Dugdale, "Yielding of steel sheets containing slits". J. Mech. Phys. Solids., vol 8, 100-104, 1960

[1961-Paris]: P.C. Paris, R.E. Gomez, W.E. Anderson, "A rational analytic theory of fatigue", Retrospect Fracture Mechanics, 199-204, 1961

[1968-Rice]: J.R. Rice, "A path independent integral and the approximate analysis of strain concentration by notches and cracks", Journal of applied mechanics, 379-386, 1968

[1969-Dundurs]: J. Dundurs, "Edge-bonded dissimilar orthogonal elastic wedges under normal and shear loading", Transaction of the ASME, 650-652, sept 1969

[1973-Kanninen]: M.F. Kanninen, "An augmented double cantilever beam model for studying crack propagation and arrest", Int. Journal of Fracture, vol 9, 83-92, 1973

[1975-Beaumont]: P.W.R. Beaumont, R.J. Young, "Failure of brittle polymers by slow crack growth, part I: Crack propagation in PMMA time-to-failure", Journal of materials science, vol 10, 1334-1342, 1975

[1975-Schapery]: R.A. Schapery, "A theory of crack initiation and growth in viscoelastic media, part I: theoretical development", Int.

---

---

Journal of Fracture, Vol 11, 141-159; "part II: Approximate methods of analysis", vol 11, 369-388; "part III: Analysis of continuous growth", vol 11, 549-562, 1975

[1980-Hertzberg]: R.W. Hertzberg, J.A. Manson, "Fatigue of Engineering Plastics", Academic Press, 1980

[1984-Schapery]: R.A. Schapery, "Correspondence principles and a generalised J Integral for large deformation and fracture analysis of viscoelastic media", Int. J. Fract., Vol 25, 195-223, 1984

[1984-Williams]: J.G. Williams, "Fracture mechanics of polymers", Ellis Horwood Ltd, 1984

[1987-Kausch]: H.H. Kausch, "Polymer fracture", 2<sup>nd</sup> edition, Springer Verlag, 1987

[1988-Rice]: J.R. Rice, "Elastic fracture mechanics concepts for interfacial cracks", Transaction of the ASME, vol 55, 98-103, 1988

[1988-Williams]: J.G. Williams, "On the calculation of energy release rates for cracked laminates", Int. Journal of Fracture, vol 36, 101-119, 1988

[1989-Charalambides]: P.G. Charalambides, J. Lund, A.G. Evans, R.M. McMeeking, "A test specimen for determining the fracture resistance of bimaterial interfaces", Journal of applied mechanics, vol 56, 77-82, 1989

[1989-He]: M.Y. He, J.W. Hutchinson, "Crack deflection at an interface between dissimilar elastic materials", Int. Journal of Solids and structures, vol 25(9), 1053-1067, 1989

[1990-Hutchinson]: J.W. Hutchinson, "Mixed mode fracture mechanics of interfaces", Acta Scripta Metallurgica, Proceeding series, vol 4, 295-306, 1990

[1990-Wang]: J.S. Wang, Z. Suo., "Experimental determination of interfacial toughness using brazil-nut-sandwich", . Acta Met., Vol 38, 1279-1290, 1990

[1991-Liechti]: K.M. Liechti, Y.-S. Chai, "Biaxial loading experiments for determining interfacial fracture toughness", Transaction of the ASME, Vol 58, 680-687, 1991

[1991-Shih]: C.F. Shih, "Cracks on bimaterial interfaces: elasticity and plasticity aspects", Materials Science and Engineering, Vol 143, 77-90, 1991

[1992-Liechti]: K.M. Liechti, Y.-S. Chai, "Asymmetric shielding in interfacial fracture under in-plane shear", Journal of applied mechanics, Vol 59, 295-304, 1992

[1993-Lawn]: B.R. Lawn, "Fracture of brittle solids", 2nd edition, Cambridge university press, 1993

---

## References

---

- [1994-Timbrell]: C. Timbrell, P. Claydon, G. Cook, "Application of Abaqus to analysis of 3D cracks and fatigue crack growth prediction", Abaqus user's conference, Rhode Island, USA, June 1-3, 1994
- [1995-Anderson]: T.L. Anderson, "Fracture mechanics: fundamentals and applications", 2nd ed. CRC Press, Inc., 1995
- [1996-Belytschko]: T. Belytschko, M. Tabbara, "Dynamic fracture using element-free galerkin methods" International Journal for Numerical Methods in Engineering, Vol 39, 923-938, 1996
- [1996-Belytschko-2]: T. Belytschko, Y. Krongauz, D. Organ, M. Fleming, P. Krysl, "Meshless methods: An overview and recent developments", Computer Methods in Applied Mechanics and Engineering, Vol 139, 3-47, 1996
- [1996-Gross]: D. Gross, "Bruchmechanik", 2. völlig neu bearbeitete und erweiterte Auflage, Springer Verlag, 1996
- [1996-Melenk]: J.M. Melenk, I. Babuska, "The Partition of unity finite element method: basic theory and applications", Seminar für angewandte Mathematik, Eidgenössische Technische Hochschule Zürich January 1996
- [1996-Organ]: D. Organ, M. Fleming, T. Terry, T. Belytschko, "Continuous meshless approximations for nonconvex bodies by diffraction and transparency"
- [1996-Turner]: M.R. Turner, A.G. Evans, "An experimental study of the mechanisms of crack extension along an oxide/metal interface", Acta Materialia, vol 44, 863-871, 1996
- [1997-Bootstrap]: A.C. Davison, D.V. Hinkley, "Bootstrap methods and their application", Cambridge University Press, 1997
- [1997-Chaboche]: J.L. Chaboche, R. Girard, A. Schaff, "Numerical analysis of composite systems by using interphase/interface models", Computational Mechanics, vol 20, 3-11, 1997
- [1997-Gaul]: L. Gaul, C. Fieder, "Methode und Berechnung in Statik und Dynamik - Einführung und Grundlagen der Randelementmethode", Vieger & Sohn Verlagsgesellschaft mbH, Braunschweig/Wiesbaden, Germany, 1997
- [1997-Fleming]: M. Fleming, Y.A. Chu, B. Moran, T. Belytschko, "Enriched Element free galerkin methods for crack tip fields", International Journal of numerical methods of engineering, Vol 40, 1483-1504, 1997
- [1997-Siegmund]: T. Siegmund, N.A. Fleck, A. Needleman, "Dynamic crack growth across an interface", Int. Journal of Fracture, vol 85, 381-402, 1997
- [1997-Mao]: S.X. Mao, A.G. Evans, "The influence of blunting on crack growth at oxide/metal interfaces", Acta Materialia, vol 45, 4263-4270, 1997
-

- [1998-Abou-Hamda]: M.M. Abou-Hamda, M.M. Megahed, M.M.I. Hammouda, "Fatigue crack growth in double cantilever beam specimen with an adhesive layer", Engineering Fracture Mechanics, vol 60, 605-614, 1998
- [1998-Diemer]: M. Diemer, "Benetzungsverhalten und mechanische Eigenschaften der Cu/Al<sub>2</sub>O<sub>3</sub>-Grenzfläche", Dissertation TU Darmstadt, 1998
- [1998-Hofinger]: I. Hofinger, M. Öchsner, H.-A. Bahr, M.V. Swain, "Modified four-point bending specimen for determining the interface fracture energy for thin, brittle layers", Int. Journal of fracture, vol 92, 213-220, 1998
- [1998-Ikeda]: T. Ikeda, N. Miyazaki, T. Soda, "Mixed mode fracture criterion of interface crack between dissimilar materials", Eng. Fract. Mechanics, Vol 59, 725-735, 1998
- [1998-Suresh]: S. Suresh, "Fatigue of materials", 2<sup>nd</sup> edition, Cambridge university press, 1998
- [1999-Astm]: ASTM D5045-99, "Standard test methods for plane-strain fracture toughness and strain energy release rate of plastic materials"
- [1999-Gaudette]: F.G. Gaudette, S. Suresh, A.G. Evans, "Effects of sulfur on the fatigue and fracture resistance of interfaces between  $\gamma$ -Ni(Cr) and  $\alpha$ -Al<sub>2</sub>O<sub>3</sub>", Princeton Materials Institute, PMI-99-13, 1999
- [1999-Sundararaman]: V. Sundararaman, S.K. Sitaraman, "Determination of fracture toughness for metal/polymer interfaces", Journal of electronic packaging, vol 121, 275-281, 1999
- [1999-Walrick]: J.-C. Walrick, "Contribution au développement d'une nouvelle méthodologie pour l'étude du délaminage dans les structures stratifiées composites: application a l'impact basse vitesse", Ph.D thesis, Université de Valenciennes, France, 1999
- [1999-Zahndarov]: S. Zahndarov, E. Pisanova, K. Schneider, "Adhesive pressure as failure criterion in micromechanical tests", Proceeding of the ICCM 12, 1999
- [2000-Chaboche]: J.-L. Chaboche, F. Feyel, "On the multiscale analysis o composite structures by using a FE<sup>2</sup> technique and fibre-matrix damage mechanics", Workshop on Continuous Damage and Fracture, Cachan (France), November 23-27, 2000
- [2000-Corigliano]: A. Corigliano, O. allix, "Some aspects of interlaminar degradation in composites", Computer methods in applied mechanics and engineering, vol 185, 203-224, 2000
- [2000-Coutellier]: D. Coutellier, P. Rozycki, "Multi-layered multi-material finite element for crashworthiness studies", Composite part A: applied science and manufacturing, vol 31, 841-851, 2000
- [2000-Davies]: P.Davies, Habilitation à diriger des recherches, 2000
-

[2000-Dollhofer]: J. Dollhofer, W. Beckert, B. Lauke, "Linear-elastic finite element analysis", Materialprüfung, Jahrgang 42(10), Carl Hanser Verlag, München, 2000

[2000-Pahn]: L.O. Pahn, Y.Y. Earmme, "Analysis of a short interfacial crack from the corner of a rectangular inclusion", Int Journal of Fracture, Vol 106, 341-356, 2000

[2000-Timbrell]: C. Timbrell, G. Cook, R. Chandwani, "3D crack analysis using MSC.Marc", 1<sup>st</sup> northern european technology conference, Manchester, England, June 7-8, 2000

[2000-Uhlig]: C. Uhlig, O. Kahle, B. Wieneke, and M. Bauer. "Optical crack tracing - a new method for the automatic determination of fracture toughness for crack initiation and propagation", Proc. 3rd International Micro Materials Conference, 618-629, Berlin, April 2000

[2000-Xiong]: Z. Xiong, A.A.O. Tay, "Modelling of viscoelastic effects on interfacial delamination in IC packages", IEEE Electronic Components and Technology Conference, 1326-1331, 2000

[2001-Auersperg]: J. Auersperg, E. Kieselstein, A. Schubert, B. Michel, "Interfacial fracture toughness test suited for reliability enhancements of advanced plastic packages", Transaction of the IEEE, Conference on Polymers and Adhesives in Microelectronics and Photonics, Postdam (Germany), 2001

[2001-Harries]: R. J. Harries, S. K. Sitaraman, "Numerical modelling of interfacial delamination propagation in a novel peripheral array package", IEEE Transactions on components and packaging technologies, Vol 24(2), 256-264, 2001

[2001-Leguillon]: D. Leguillon, C. Lacroix, E. Martin, "Crack deflection by an interface - asymptotics of the residual thermal stresses", Int Journal of Solids and Structures, Vol 38, 7423-7445, 2001

[2001-Molski]: K.L. Molski, "A crack between two dissimilar media", VIIth Summer school of fracture mechanic, university of technology Warsaw, 2001, Poland

[2001-Monerie]: Y. Monerie, M. Raous, "Fissuration tridimensionnelle des matériaux composites: rôle de l'interface fibre/matrice", Proceeding of the french "5<sup>e</sup> colloque national en calcul des structures", Giens, 2001

[2001-Reedy]: E.D. Reedy Jr, T.R. Guess, "Rigid square inclusion embedded within an epoxy disk: asymptotic stress analysis", Int Journal of Solids and Structures", Vol 38, 1281-1293, 2001

[2001-Stresscheck]: Stresscheck handbook, release 6.0, ESRD, Inc., 2001

[2001-Sundararaman]: V. Sundararaman, S. Sitaraman, "Interfacial fracture toughness for delamination growth prediction in a novel

---

peripheral array package", IEEE Transactions on Components and Packaging Technologies, vol 24(2), 265-270, 2001

[2001-Toth]: L. Toth, VII Summer school of fracture mechanics, Pkrywna, Poland, 2001

[2002-Chen]: Y.P. Chen, J.D. Lee, A. Eskandarian, "Dynamic meshless method applied to non-local crack problems", Theoretical and applied fracture mechanics, vol 38, 293-300, 2002

[2002-Cook]: G. Cook, C. Timbrell, M. Wiehahn, "Using Abaqus to analyse fatigue crack growth under the combined influence of residual stress and cycle external load", UK Abaqus user group conference, 2002

[2002-Dollhofer]: J. Dollhofer, "J-Q Theory for the fracture of elastically mismatched interfaces", Materialprüfung, Jahrgang 44(5), Carl Hanser Verlag, München, 2002

[2002-Qian]: Z.Q. Qian, "Stress behaviour at the interface junction of an elastic inclusion", Transaction of the ASME, Vol 69, 844-852, 2002

[2002-Wiederhorn]: S.M. Wiederhorn, A.D. Dretzke, J. Rödel, "Crack growth in soda-lime-silicate glass near the static fatigue limit", Journal of american ceramic society, vol 85(9), 2287-2292, 2002

[2002-Wittler]: O. Wittler, P. Sprafke, B. Michel, "Elastic and viscoelastic fracture mechanical analysis of cracks in polymer encapsulations" Conference from ESIS TC4 in Les Diablerets, Switzerland, 15-18 September 2002

[2003-Leblanc]: F. Leblanc, P. Sprafke, A. Zimmermann, D. Coutellier, "Analyse du comportement des fissures dans un composant encapsulé bimatériau", Transaction des JNC13, 869-878, 2003

[2003-Karihaloo]: B. L. Karihaloo, Q.Z. Xiao, "Modelling of stationary and growing cracks in FE framework without remeshing: a state-of-the-art review", Computers and Structures, Vol 81, 119-129, 2003

[2003-Leguillon]: D. Leguillon, "Failure of a metallic inclusion in a resin encapsulant under thermal loadings", 2003, submitted to Elsevier Preprint.

[2003-Rozycki]: P. Rozycki, D. Coutellier, "Improvement of the simulation tools dedicated to composite structures subjected to crash loads", Recent advances in Integrated Design and Manufacturing in Mechanical Engineering, Kluwer Academic Publishers, 105-116, 2003

[2003-Sukumar]: N. Sukumar, Z.Y. Huang, J.-H. Prévost, Z. Suo, "Partition of unity enrichment for bimaterial interface cracks", Int. J. Numer. Meth. Engng, vol 00, 1-44, 2003

[2003-Surcin]: L. Surcin, F. Lachaud, R. Piquet, O. Nemes, "Procédés de mise en oeuvre et délaminage des stratifiés en carbone/époxyde", Transaction des JNC13, 161-170, 2003

---

## References

---

[2003-Zencrack]: Zencrack user manual, v7.2, 2003

[2004-Abaqus]: Abaqus v6.4 handbook, Hibbit Karlson and Sorenson, 2004

[2004-Nist]: "NIST/SEMATECH e-Handbook of Statistical Methods", <http://www.itl.nist.gov/div898/handbook/>, 2004-06-21

[2004-Noda]: N.-A. Noda, "Stress intensity factors for three dimensional cracks in homogeneous and bonded dissimilar materials", Engineering Fracture Mechanics, vol 71, 1-15, 2004

[2004-Pirondi]: A. Pirondi, G. Nicoletto, "Fatigue crack growth in bonded DCB specimens", Engineering Fracture Mechanics, vol 71, 859-871, 2004

[2004-Sørensen]: B.F. Sørensen, T.K. Jacobsen, "Determination of cohesive laws by the J integral approach", Engineering Fracture Mechanics, vol 70, 1841-1858, 2003

[2004-Wittler]: O. Wittler, "Bruchmechanische Analyse von viskoelastischen Werkstoffen in elektronischen Bauteilen", PhD Thesis, Berlin, 2004

---

---

---

---

## Abstract

The work focuses on potting materials for electronic components. A methodology to analyse the behaviour of cracks initiated in homogeneous materials or at the interface between different materials is addressed. An experimental procedure is described in order to measure the critical stress intensity factor of a homogeneous material. This procedure is then used to compare the crack behaviour in a bimaterial structure and to determine the validity of the results. Hereafter a method is proposed to determine crack growth under subcritical loading conditions. In the case of a crack at the interface of bimaterials, a methodology has been developed to measure the energy release rate necessary to let the crack propagate. With the help of numerical simulations, the corresponding stress intensity factors are computed as well as the resulting mixed mode angle. The whole work realised experimentally and the developed numerical simulations allow us to propose a methodology to analyse the behaviour of a crack placed in a multi-material structure under thermo-mechanical loads.

**Keywords:** energy release rate, stress intensity factors, fracture toughness, interface, mixed mode angle, finite element method

## Zusammenfassung

Die vorliegende Arbeit befasst sich mit Vergussmassen für elektronische Erzeugnisse. Eine Vorgehensweise wird vorgeschlagen, um das Verhalten von initiierten Rissen in homogenen Materialien oder entlang der Grenzschicht zwischen verschiedenen Materialien zu analysieren. Ein experimenteller Verfahrensschritt wird beschrieben, um den kritischen Spannungsintensitätsfaktor von homogenen Materialien zu messen. Dann wird dieser Verfahrensschritt benutzt, um das Rissverhalten in verschiedenen Materialien zu vergleichen und um das Ergebniskonfidenzintervall festzulegen. Danach wird eine Methode vorgeschlagen, um das Risswachstum des betrachteten Materials unter subkritischer Belastung festzulegen. Im Fall eines Grenzschichtrisses wird eine Vorgehensweise entwickelt, um die Energiefreisetzungsrates zu messen, die benötigt wird, um den Riss sich ausbreiten zu lassen. Mit Hilfe von numerischen Simulationen werden die entsprechenden Spannungsintensitätsfaktoren und die Modusmischungswinkel ermittelt. Die komplette experimentelle Arbeit und die entwickelte numerische Simulationen führen zu einer Methodologie, um das Verhalten von einem Riss Verbundwerkstoffen und Bauteilen unter thermischen und mechanischen Belastungen zu beurteilen.

**Schlüsselwörter:** Energiefreisetzungsrates, Spannungsintensitätsfaktoren, Bruchzähigkeit, Grenzschicht, Modusmischungswinkel, Finite Elemente Methode

## Résumé

Ce travail s'articule autour de l'étude de matériaux coulés pour des composants électroniques. Une méthodologie est proposée pour analyser le comportement de fissures initiées dans des matériaux homogènes ou à l'interface entre différents matériaux. Une procédure expérimentale est décrite afin de mesurer le facteur d'intensité de contrainte critique d'un matériau homogène. Cette procédure est ensuite appliquée dans la comparaison du comportement d'une fissure d'un bimatériau et à la détermination du degré de validité des résultats. Une méthode est ensuite proposée pour déterminer la propagation de fissures dans les différents matériaux sous des chargements sous-critiques. Dans le cas d'une fissure à l'interface de bimatériaux, une méthodologie a été développée pour mesurer le taux de restitution d'énergie nécessaire à la propagation de la fissure. Les facteurs d'intensité de contraintes correspondants sont calculés à l'aide de simulations numériques, ainsi que l'angle de mode mixte résultant. L'ensemble des travaux expérimentaux réalisés et des simulations numériques développées permet de proposer une méthodologie d'analyse du comportement d'une fissure située au sein d'un composant multimatériau sollicité sous chargement thermo-mécanique.

**Mots clés:** taux de restitution d'énergie, facteurs d'intensité de contraintes, ténacité, interface, angle de mode mixte, méthode éléments finis

---